The detection and analysis of wave slamming from full-scale ship measurements

by

Clinton Frederick Wood Saunders

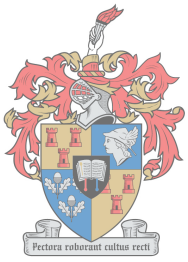

UNIVERSITEIT
iYUNIVESITHI
STELLENBOSCH
UNIVERSITY

Thesis presented in partial fulfilment of the requirements for the degree of Master of Engineering (Mechanical) in the Faculty of Engineering at Stellenbosch University

Supervisor: Prof. A. Bekker

Co-supervisor: Dr. J. Muiyser

December 2018

Stellenbosch University https://scholar.sun.ac.za

Declaration

By submitting this thesis electronically, I declare that the entirety of the work contained therein is my own, original work, that I am the sole author thereof (save to the extent explicitly otherwise stated), that reproduction and publication thereof by Stellenbosch University will not infringe any third party rights and that I have not previously in its entirety or in part submitted it for obtaining any qualification.

Date: .....

Copyright © 2018 Stellenbosch University
All rights reserved.

Stellenbosch University https://scholar.sun.ac.za

UNIVERSITEIT·STELLENBOSCH·UNIVERSITY
jou kennisvennoot • your knowledge partner

Plagiaatverklaring / Plagiarism *Declaration*

1 Plagiaat is die oorneem en gebruik van die idees, materiaal en ander intellektuele eiendom van ander persone asof dit jou eie werk is.
Plagiarism is the use of ideas, material and other intellectual property of another's work and to present is as my own.

2 Ek erken dat die pleeg van plagiaat 'n strafbare oortreding is aangesien dit 'n vorm van diefstal is.
I agree that plagiarism is a punishable offence because it constitutes theft.

3 Ek verstaan ook dat direkte vertalings plagiaat is.
I also understand that direct translations are plagiarism.

4 Dienooreenkomstig is alle aanhalings en bydraes vanuit enige bron (ingesluit die internet) volledig verwys (erken). Ek erken dat die woordelikse aanhaal van teks sonder aanhalingstekens (selfs al word die bron volledig erken) plagiaat is.
Accordingly all quotations and contributions from any source whatsoever (including the internet) have been cited fully. I understand that the reproduction of text without quotation marks (even when the source is cited) is plagiarism.

5 Ek verklaar dat die werk in hierdie skryfstuk vervat, behalwe waar anders aangedui, my eie oorspronklike werk is en dat ek dit nie vantevore in die geheel of gedeeltelik ingehandig het vir bepunting in hierdie module/werkstuk of 'n ander module/werkstuk nie.
I declare that the work contained in this assignment, except where otherwise stated, is my original work and that I have not previously (in its entirety or in part) submitted it for grading in this module/assignment or another module/assignment.

Studentenommer / *Student number*	**Handtekening / *Signature***
Voorletters en van / *Initials and surname*	**Datum / *Date***

Stellenbosch University https://scholar.sun.ac.za

Abstract

The detection and analysis of wave slamming from full-scale ship measurements

C.F.W. Saunders

Department of Mechanical and Mechatronic Engineering,
University of Stellenbosch,
Private Bag X1, 7602, Matieland, South Africa.

Thesis: MEng (Mechanical)

December 2018

Bow and stern wave slamming has proven to be a persisting and concerning problem on the S.A. Agulhas II. Various full-scale vibration measurements have been conducted over several voyages in the Southern Ocean. Past research has concluded that vibration has reached levels where damage was possible in the stern and is probable in the bow during open water navigation (Soal, 2014). In order to better understand the drivers behind slamming, an algorithm was developed to detect and count slamming events in full-scale signals. Detection was done in the time domain using acceleration peaks, as well as the frequency domain using a wavelet transform. Statistical thresholds were then determined using a median absolute deviation. The data in the frequency domain proved most accurate for counting slams. Slamming counts were then compared with environmental and operational variables for the voyages. It was determined that these variables have a significant effect on the frequency of slamming events.

Stellenbosch University https://scholar.sun.ac.za

Uittreksel

Die opsporing en analise van branderklap vanaf volskaalse skip metings

C.F.W. Saunders

Departement Meganiese en Megatroniese Ingenieurswese,
Universiteit van Stellenbosch,
Privaatsak X1, 7602, Matieland, Suid Afrika.

Tesis: MIng (Meganies)

Desember 2018

Skeepslag op die boeg en agterstewe van ’n skip is ’n aanhoudende en kommerwekkende probleem op die S.A. Agulhas II. Verskeie volskaalse vibrasie metings is al geneem op die skip tydens verskeie reise in die Suidelike Osean. Vorige navorsing het bewys dat die vibrasie wat ervaar word skade kan aanrig in die agterstewe en waarskynlik in die boeg wanneer die skip op die oop see vaar (Soal, 2014). Om beter te verstaan wat skeepslag veroorsaak, is ’n algoritme ontwikkel om branderklap in die vibrasie sein te identifiseer en te tel. Skeepslag is geindentifiseer in die tyd domein deur middel van versnellingspieke, asook in die frekwensie domein deur middel van golfomskakeling. Statistiese drempels is dan bepaal deur van ’n mediaan absolute afwyking gebruik te maak. Daar is gevind dat die data in die frekwensie domein meer akuraat is om skeepslag gevalle te identifiseer en te tel. Skeepslag is ook vergelyk met omgewingsfaktore sowel as operasionele faktore vir die reise. Daar is vasgestel dat beide omgewings en operasionele faktore ’n beduidende uitwerking het op die frekwensie van skeepslag.

Stellenbosch University https://scholar.sun.ac.za

Acknowledgements

This thesis was made possible by the grace of God, without whom I would not have had the strength to persist. The opportunity to be part of this project and travel to Antarctica is something that will shape the rest of my life. I met my wife on the S.A. Agulhas II during a voyage to Antarctica for this project. I also had the opportunity to meet and befriend many wonderful people along the way.

I would like to thank the following parties for there support; My supervisor, Prof. Annie Bekker, for her support and friendship throughout the project, it wasn't always easy but her wisdom and enthusiasm was always encouraging. My co-supervisor, Dr. Jacques Muiyser, for his support, and always being there to bounce ideas off of. The National Research Foundation, for the funding for the project. The Department of Environmental Affairs, for the cooperation and opportunities to be part of the research voyages and to have access to the vessel for measurements. The South African Weather Service, for sea state data collected during voyages. Captain Knowledge Bengu, Captain Gavin Syndercombe and their crew members for their professionalism and hard work, it was always a pleasure being on-board. Hannes Swart, Rosca de Waal and Keith Soal for all the advice, debates and great times during measurement voyages, your friendship and support is greatly appreciated. My dad, Trevor; brothers Greg, Philip and Ross; mother-in-law, Estelle and sister-in-law Linda for their continued support. Last but not least, my wife Alta, without whom this thesis would not been completed. Her continued support and encouragement got me through this project.

Stellenbosch University https://scholar.sun.ac.za

Dedication

This thesis is dedicated to my late brother, Mark and late mother, Marianne

Stellenbosch University https://scholar.sun.ac.za

Table of Contents

Stellenbosch University https://scholar.sun.ac.za

Stellenbosch University https://scholar.sun.ac.za

Stellenbosch University https://scholar.sun.ac.za

List of Figures

Stellenbosch University https://scholar.sun.ac.za

Stellenbosch University https://scholar.sun.ac.za

Stellenbosch University https://scholar.sun.ac.za

Stellenbosch University https://scholar.sun.ac.za

List of Tables

Stellenbosch University https://scholar.sun.ac.za

Stellenbosch University https://scholar.sun.ac.za

Nomenclature

Variables:

b	MAD multiplication factor
g	Gravity
H_{swell}	Swell height
i	Index of the sampled data
j	Index of the time interval
k	Threshold multiplication factor
M	Median
n	no. of samples
Q_3	Upper quartile limit
T	Threshold vector
T_{swell}	Swell period
t	Time
X	Complex wavelet coefficient matrix
x	Sampled data value
α	Wavelet function scale
z	Slam count

Stellenbosch University https://scholar.sun.ac.za

β	Wavelet function translation
$\phi_{incident}$	Incident swell angle
μ	Sample data mean
v_{ship}	Speed of the ship
ψ	Wavelet function

Stellenbosch University https://scholar.sun.ac.za

Acronyms

AIC Akaike information criterion

AMSOL African Marine Solutions

ANN Artificial neural network

AR Antarctic relief

BNC Bayonet Neill-Concelman

CFD Computational fluid dynamics

CMU Central measurement unit

DEA Department of environmental affairs

DNV Det Norske Veritas

FFT Fast Fourier Transform

FN False negative

FP False positive

FPR False positive rate

GLM General linear model

GPS Global positioning satellite

MAD Median absolute deviation

Matlab Matrix laboratory

Stellenbosch University https://scholar.sun.ac.za

MCR Maximum continuous rating

MIZ Marginal ice zone

MLP Multi-layer perception

MRU Motion response unit

NMISA National Metrology Institute of South Africa

PC Polar class

PCA Principle component analysis

PPV Positive predictive valve

PSD Power spectral density

PSRV Polar supply and research vessel

r.m.s. Root mean square

r.p.m. Revolutions per minute

ROC Receiver operator curve

SAAII S.A. Agulhas II

SANAE South African National Antarctic Expedition

SANAP South African National Antarctic Program

SAWS South African Weather Service

SCADAS Supervisory control and data acquisition system

SDS Scientific data System

SHM Structural health monitoring

SOG Speed over ground

SVRG Sound and vibration research group

SYNOPS Surface synoptic observation

Stellenbosch University https://scholar.sun.ac.za

TN True negatives

TP True positives

TPR True positive rate

UTC Universal time coordinated

WC Winter Cruise

Stellenbosch University https://scholar.sun.ac.za

Chapter 1

Introduction

The S.A. Agulhas II (SAAII) is a state-of-the-art polar supply and research vessel (PSRV), designed and build by STX Finland. These types of vessels are created for the transportation of scientists and cargo while also serving as a floating science platform. She is the work horse of the South African National Antarctic Program (SANAP), and allows South Africa to maintain a scientific presence in the Antarctic and Southern Ocean regions. SANAP operates bases on Antarctica, Marion Island and Gough Island. The SAAII has the responsibility of resupplying these bases and providing scientists with access to these areas.

The seas in the Southern Ocean are notorious for being some of the worst seas on earth. That, together with the ice fields surrounding Antarctica mean that the SAAII needs a unique design compared to many commercial vessels seen in harbours today. She was designed and built in accordance with the Det Norske Veritas (DNV) ICE-10 and Polar Class 5 (PC-5) (Suominen *et al.*, 2013). These classifications mean that she should have the strength and operational capability for year-round operation in medium first-year ice (ice which has formed in the last twelve months) that may contain older ice inclusions (O.C.I.M.F., 2014).

To this end the SAAII was designed with a rounded or "spoon" bow (see Figure 1.1. This allows her to push up on top of and break the ice in bending, as opposed to compression. At the stern, she has a raised and extended transom to allow ice to pass between the propellers and hull of the vessel while giving extra scientific deck space (Omer, 2016). These hull design aspects, while beneficial

Stellenbosch University https://scholar.sun.ac.za

in ice, are thought to be the source of the severe wave slamming experienced by the SAAII. Wave slamming can be defined as the exposure of a vessel structure to large forces as a result of wave impacts over a very short period of time (Kapsenberg, 2011). It can be classified as either bow, stern or bottom slamming.

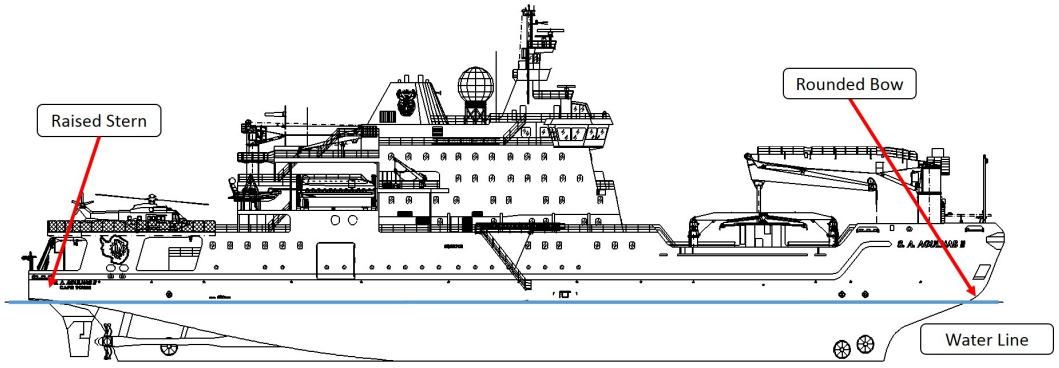

Figure 1.1: Profile of the SAAII

This thesis focuses on the wave slamming phenomenon, to best understand slam characteristics as well as the frequency with which these events occur. The application area for this study is sea fairing vessels, in particular, the SAAII. She experiences excessive slamming at the bow in head seas and at the stern when stationary in following seas. Slamming has been known to cause damage to the vessel and scientific equipment as well as affect the comfort of passengers and crew on-board (Omer, 2016).

The aims of this project are to:

- Detection of wave slamming events in full-scale vibration data.
- Count slamming events over a period of time and compare them with environmental and operational variables around the vessel.

The issue of slamming on-board the SAAII has become of particular interest to the Department of Environmental Affairs (DEA), the vessel owner, and African Marine Solutions (AMSOL), vessel operations and maintenance contractors. This phenomenon could be causing a dynamic response, shorting the vessel's life span due to fatigue loading. AMSOL, on behalf of the DEA, has been in dispute

Stellenbosch University https://scholar.sun.ac.za

with the ship builders, STX Finland, about the warrantee claim for the vessel as the research is showing that aspects of the vessel's design are at fault.

Due to the unpredictable nature of slamming events and the crew's constant efforts to avoid slamming conditions, the full-scale measurement of the structural response to slamming is not always possible. This promotes the need for continued measurement, as well as methods of event detection, in the hopes that more conclusive data can be collected. The research from this slamming project will form part of an international pool of structural response knowledge. This can contribute to preserving the longevity of one of South Africa's most prized national research assets along with other vessels like her that are yet to come.

The objectives needed to be accomplished upon the completion of this thesis are:

- Collect full-scale vibration and environmental data while on-board the SAAII.
- Develop an algorithm for the detection and counting of slamming events.
- Test the algorithm using selected vibration case studies.
- Apply the algorithm to the vibration data from a complete voyage and compare the results with environmental and operational data.

This thesis discusses; literature pertaining to wave slamming, detection of events as well as measurements on a full-scale were completed. The collection of the data is then presented with regards to the equipment used and decisions made for recording the data. The manner in which the data is handled and the detection algorithm development is then discussed. The testing of the algorithm using case studies is then conducted. The tested algorithm is then applied to long term data and compared with environmental and operational inputs at the time. Lastly the thesis is concluded and recommendations are made for future work.

Stellenbosch University https://scholar.sun.ac.za

Chapter 2

Literature review

The review of literature begins by looking at the slamming phenomena and discussing the origins of its investigation and its uniqueness. Full-scale measurements of slamming occurring on vessels will be reported and important parameters will be discussed. Lastly, a variety of methods for detecting slams in large datasets will be looked at. Statistical outlier analysis and neural networks will also broadly be discussed.

The SAAII is not the only vessel to experience adverse slamming. Slamming is a phenomenon that plagues sea fairing vessels all around the world and has resulted in large maritime accidents. In 1994 the ferry MV Estonia sank in the Baltic Sea when heavy slamming tore her bow visor from its mountings and caused damage to the watertight front door (Figure 2.1a and 2.1b). This caused the vessel to fill with water and capsize (Haward *et al.*, 2009). In 2007 the container ship MSC Napoli was caught in bad weather in the English Channel. She experienced structural failure in the form of a large crack in the engine room (Figure 2.1c) through which water flooded and she was abandoned at sea (Figure 2.1d). It was concluded that there were no deficiencies in the construction or material of the hull and that this structural failure was as a result of slamming-induced whipping, or transient structural vibration in the hull (Dessi & Ciappi (2013);M.A.I.B (2008)).

Stellenbosch University https://scholar.sun.ac.za

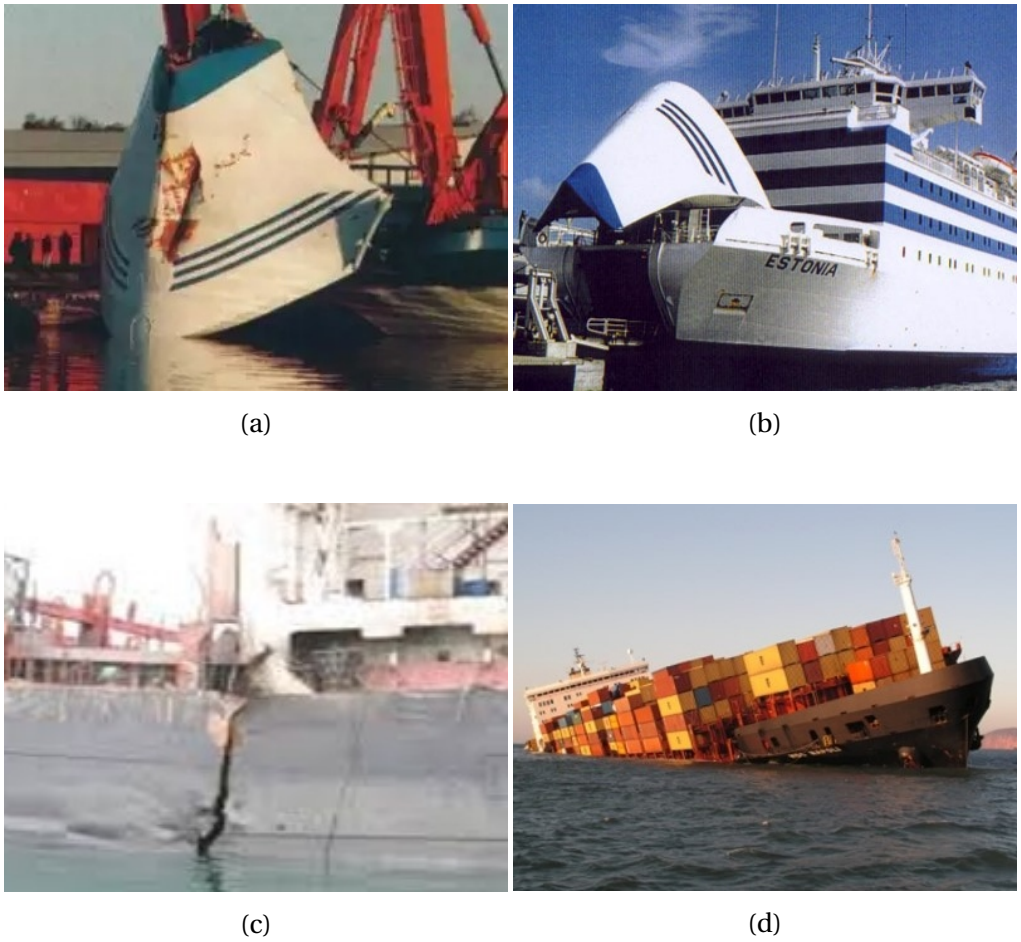

(a) (b)

(c) (d)

Figure 2.1: Slamming accidents; (a) Detached bow visor of the MV Estonia. (b) MV Estonia with her bow visor raised. (c) Crack in the hull of MSC Napoli. (d) MSC Napoli listing to the starboard side.

2.1 Slamming phenomenon

A body or structure experiences a slamming event when a sudden high force is exerted on it over a short period of time (Kapsenberg, 2011), thus being impulsive in nature. von Karman (1929), was the first to take interest in the slamming phenomenon when he published on it in 1929. The investigation focused on predicting the forces exerted on the floats of a sea plane when landing on the surface of the ocean. The impact force of these floats upon landing can be described as sudden and short, thus fitting the description of a slam. In the context of sea fairing vessels Figure 2.2 shows the moment before slamming takes place, when a

Stellenbosch University https://scholar.sun.ac.za

vessel re-enters the water with a small relative angle between the vessel hull and the surface of the ocean (Kapsenberg, 2011).

Figure 2.2: Sea fairing vessel right before a slam

It has been shown that there is a correlation between this relative angle and the impact pressure on the hull. The impact force thus increases with a decrease in the relative angle. Figure 2.3a shows what is meant by deadrise angle in terms of a section of a ship hull. This deadrise angle is also referred to as the bow flare of a hull (the deadrise angle of the bow of the ship). Experimental results from Lloyd & Andrew (1977) are presented in Figure 2.3b, where peak pressure coefficients ($\kappa = p/(1/2\rho v^2)$) are given as a function of the deadrise angles. The experiment was conducted with various shapes, spheres (crosses), ellipsoids (open circles), curved wedges (open triangles), two-dimensional wedges (open squares), cones (asterisks). The solid line represents Wagner's theor. A dashed line shows the best fit for the experimental data.

When looking at Figure 2.3b it can be seen that for deadrise angles under 5° the slamming phenomena is more complicated. It is theorized that at these angles air is being compressed underneath the hull in the moments before impact (air entrapment). There is an increase in pressure which causes a depression in the surface of the water. This causes the hull to make contact with the fluid on its outer edge during these moments, which encloses a volume of air. The compression of this air, now trapped underneath the hull, plays a role in the impact pressure experienced at these deadrise angles. In the next stage the trapped air

Stellenbosch University https://scholar.sun.ac.za

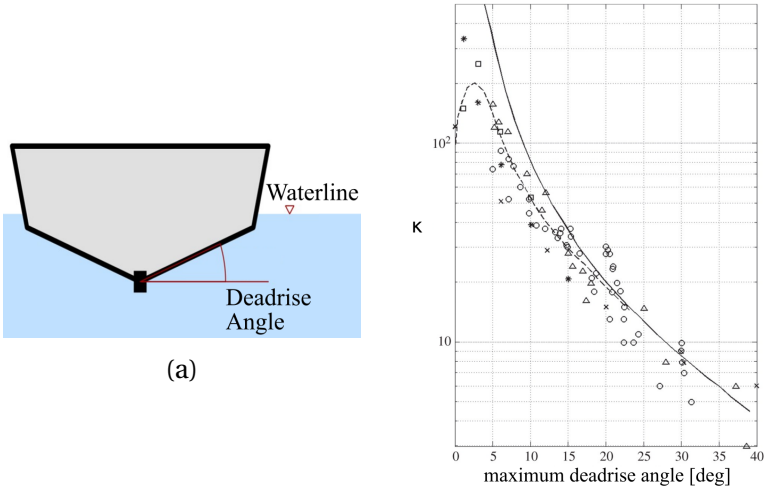

Figure 2.3: Results from scale impact test; (a) Visualization of the deadrise angle. (b) Experimental results of the impact pressure as a function of deadrise angle (Lloyd & Andrew, 1977).

will escape and the hull will come into contact with the water. The compressibility of the fluid could play a role in the impact pressure. The local response of the hull must also be considered during these impacts. There have been studies to suggest that the dynamic response of a flat stiffened plate under these impacts could induce local cavitation (Faltinsen, 1996). This would explain the very high pressures on the hull surface.

It is suggested, at this stage, that the SAAII is experiencing severe slamming impacts due to her rounded bow and flat raised stern. These design aspects give the hull a small deadrise angle at the bow and stern, this leads to the high pressures upon impact with the ocean surface. The exact deadrise angles at these locations on the hull are unknown as that is preparatory information kept by the designers. The information up to this point also demonstrates the importance of detecting and counting these events in order to monitor the condition of the structure.

Stellenbosch University https://scholar.sun.ac.za

2.2 Full-scale measurement

2.2.1 Structural measurements

Full-scale measurements, aimed at the investigation of slamming, started as early as 1956. It was soon discovered that full-scale measurements required complicated and expensive measurement systems as well as bad weather. This combination was not always readily available, forcing measurements campaigns to run over several years. The instruments used in these early days were custom-made and measured the strain at various points throughout the vessel (Warnsinck & Saint Denis, 1957). These measurements were then used to determine the wave-induced midship bending stresses or hogging moment. Later efforts implemented automated measuring and recording systems with pressure gauges mounted in the bottom of the vessel in order to measure the slamming pressures (Wheaton *et al.*, 1970).

A full-scale study was conducted, by Aalberts & Nieuwenhuijs (2006), on a vessel having a small deadrise angle. They looked at whipping, transient vibrations in the structure, and its contribution to the vertical bending moment in the midship section. The higher frequency component of the bending moment, from slamming-induced whipping, was found to contribute significantly to fatigue damage on the vessel. More recent publications on full-scale measurements are either, still being carried out or remain outside of the public domain for confidentiality reasons (Kapsenberg, 2011).

Thanks to early measurement campaigns, the impact that slamming has on a vessel structure was demonstrated and evaluated. Although full-scale measurements are still becoming more useful to the investigation of slamming, long-term measurements on a single vessel are proving less useful. Long term measurement campaigns across vessels have shown that either, slamming conditions are not encountered every year or crews learn to avoid slamming of their vessels (through ballasting, speed control and heading adjustment) (Kapsenberg, 2011). This is great for comfort and longevity of the vessel but detrimental to the measurement of slamming responses.

Stellenbosch University https://scholar.sun.ac.za

The need for full-scale measurements lies in measuring and predicting the full-scale stresses. Doing this with modelling and controlled experiments is a very complex matter as scaling laws cannot yet account of the air entrapment phenomenon. A possible solution, to predict full-scale responses, is a full-scale computational fluid dynamics (CFD) model. This model would require full-scale measurements for validation of accuracy. This allows the simulation of various ocean conditions without repeated exposure of the vessel to possibly dangerous circumstances.(Kapsenberg, 2011).

2.2.2 Sea state information

Measuring the vessel response is not the only measurement deemed important. During the early full-scale measurements the need for concurrent sea state information was quickly realised (Bledsoe *et al.*, 1961). Sea state information refers to the swell direction, speed, height and frequency as well as wind speed and direction. This information would allow a comparison to be made between the vessel response (output) and the sea state information (input) (Bledsoe *et al.*, 1961). This cause and effect relationship could be the basis for a vessel operating procedure.

The environmental information is normally estimated and catalogued by a vessel's crew. Wheaton *et al.* (1970) reported on slamming measurements and sea state information gathered in this way. It was shown that head-on sea conditions were the worst in terms of the number of bow slams experienced. The relative wave speed could be estimated at the moment of impact based on the pressure signal that was measured during an impact event. Considerable simplifications were required, but considering the uncertainties a correlation was found between the speed of the impact and the peak of the pressure signal (Kapsenberg, 2011).

Various measurements were carried out by Aertssen (1968). The diagram in Figure 2.4 was created in order to visualise the relationship between the measured parameters. This diagram shows the vessel speed as a function of the Beaufort number (an accepted maritime classification, relating wind speed and wave height) for different ship power levels. Solid lines show the different power set-

Stellenbosch University https://scholar.sun.ac.za

tings, dotted lines show the maximum wave stress and maximum whipping stress. The dashed line shows the pitch angle, the dashed-dotted line shows probability of propeller emergence and the light dotted line, the probability of slamming.

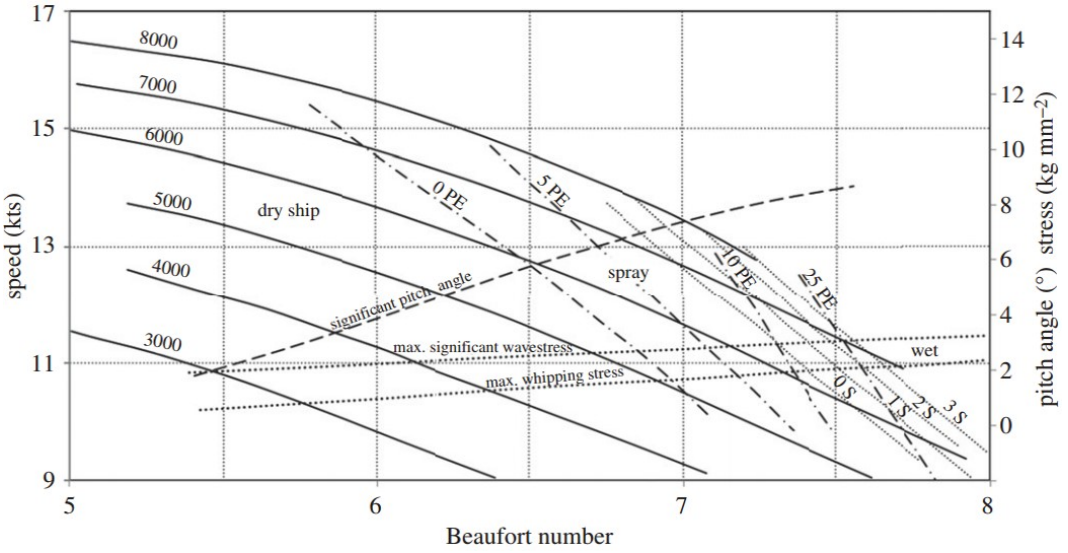

Figure 2.4: Performance diagram of cargo liner Jordaens (Aertssen, 1968).

As alluded to above, the wave height is of particular interest for slamming incidence. Within physical oceanography, the significant wave height (H_s) is typically defined as the average wave height of the highest third of waves heights, or as four times that of the standard deviation in the surface elevation (Battjes & Groenendijk, 2000).

As mentioned above, visual observations by the crew is a way of determining sea state information for the duration of a voyage. Other, autonomous, devices used for the determination of sea state will be discussed further. Over the last 30 years wave rider buoys (wave buoys) have been used for the routine measurement of sea state (Krogstad *et al.*, 1998). Wave buoys are buoyant devices that make use of accelerometers and tilt sensors to determine significant wave height and swell direction (Reichert *et al.*, 1999). The data collected by these devices has frequently been used to validate the measurements from the other devices yet to be discussed (Nieto-Borge *et al.*, 1999). A limitation of the wave buoy is that it is most often used in moored, or stationary platform applications (Carrasco *et al.*, 2017).

Stellenbosch University https://scholar.sun.ac.za

Since the late seventies sea state measurements have been determined by exploiting rough surface microwave scattering theories (Nieto-Borge *et al.*, 1999). Another method for determining the state of the ocean is by using satellite mounted radar altimeters. These operate in the Ku and C frequency bands (Scharroo *et al.*, 2016). These devices are able to determine the average height of the ocean surface, surface roughness, the geoid and the wave height (Rufenach &Alpers, 1978). Ocean surface roughness is found to cause the leading edge of the returning pulse to stretch. This stretching of the return pulse is a direct measure of the ocean wave height (Brown, 1977). Older technology, such as the satellite Geos-3 were able to offer a spacial resolution of ±23 km (Rufenach & Alpers, 1978). Newer satellites such as the Jason-3 are capable of a spacial resolution of approximately seven km, with satellites like Sentinel-6 having an approximate 300 m resolution (Scharroo *et al.*, 2016). A disadvantage of data like this is it lacks time resolution while also being limited to certain paths.

Sea state is also being determined using short range nautical radar, this radar is operated in the, longer wavelength, X-band frequency range (Nieto-Borge *et al.*, 1999). A noise signal, refereed to as sea clutter (Figure 2.5), is usually received when using these radars. Analysis, of this normally suppressed signal, generates a 3-D evolution of the sea surface in space and time (Young *et al.*, 1985). This technology can be used on moving vessels, moored platforms or at shore-based sites (Reichert *et al.*, 1999).

The wave height measurements from this technology shows to be reliable when compared to measurements from wave rider buoys (Nieto-Borge *et al.*, 1999; Reichert *et al.*, 1999). That said, there is still uncertainty in the wave height estimation. This is as a result of the wave having small wavelets caused by local wind fields (Kapsenberg, 2011). Thornhill & Stredulinksky (2010) proposed combining the radar measurement with ship motion measurements in order to correct or calibrate the wave height estimation. In fact, wave radar systems today, such as the Miros Wavesytem 200 and WaMoS II (MIROS, 2009; OceanWaveS, 2006), incorporate a motion response unit (MRU) that is able to account for the ship motion by equation(2.1).

$$\frac{Measured}{Predicted} \cdot H_{s_{waveradar}} = H_{s_{corrected}} \tag{2.1}$$

Stellenbosch University https://scholar.sun.ac.za

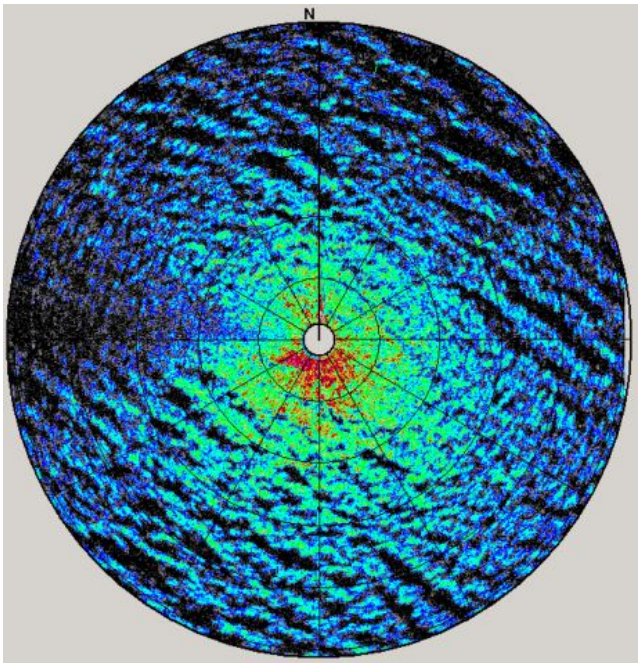

Figure 2.5: An example of sea clutter on a radar image (OceanWaveS, 2006)

Where $Measured$ is the actual response of the vessel. $Predicted$ is the predicted vessel response based on the radar image. $H_{s_{waveradar}}$ is the original calculated wave height and $H_{s_{corrected}}$ is the new corrected wave height (Thornhill & Stredulinksky, 2010).

2.3 Slamming detection algorithm

A vital aspect of the full-scale measurements is the processing and analysis of data after it has been recorded. A measurement campaign could span months or years. It would be beneficial to have an algorithm that could search applicable sections of data in order to identify desirable events. This could be done according to a signature or characteristic signal that is known. As can be seen in Figure 2.6, the characteristic of a slamming event is defined by an impulsive response followed by transient vibration (whipping). Transience refers to the fact that the response signal exists for a limited time before dying out (Brandt, 2011). Elements of these characteristics can be used in identifying this event in a large data set.

Stellenbosch University https://scholar.sun.ac.za

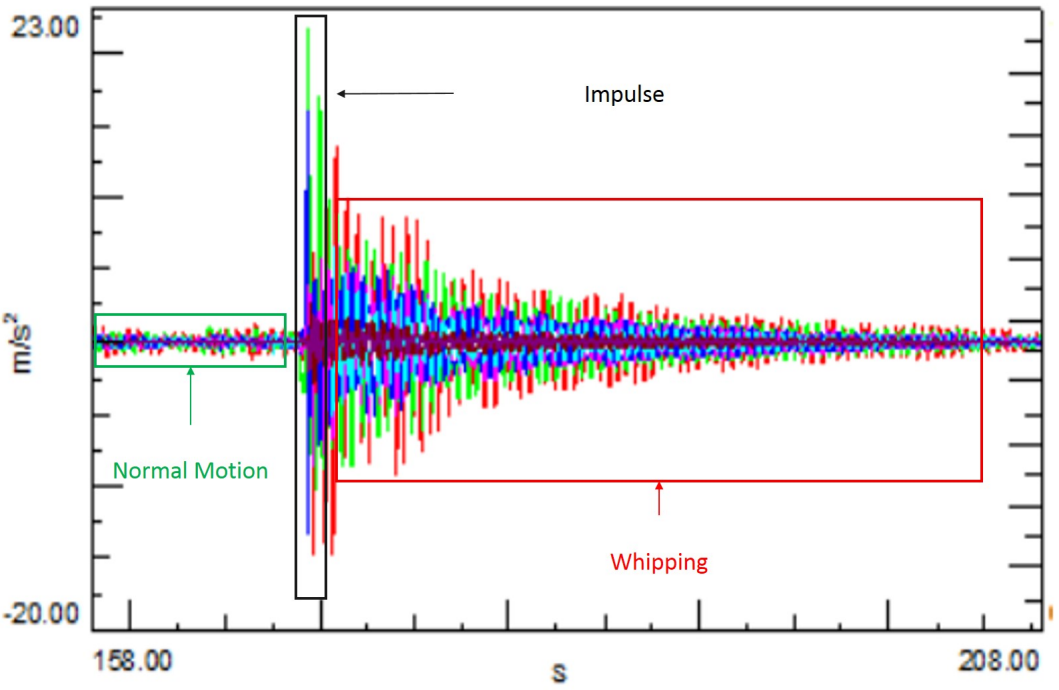

Figure 2.6: Typical slamming signature in a dataset.

Kapsenberg (2011) refers to several bulk carriers having a monitoring system on board the vessel in order to monitor fatigue damage and crack growth. What is referred to here is a structural health monitoring (SHM) system. These systems operate according to;

- Level 1: detection of damage,
- Level 2: locating where in the structure the damage is,
- Level 3: estimating the extent of the damage,
- Level 4: predicting the time left to failure (Omenzetter *et al.*, 2003; Worden *et al.*, 2003).

An algorithm for detecting slamming events in a data set would be based on the concept of a SHM system, level 1. Instead of determining if damage has occurred, the algorithm would search for desired characteristics and identify an event in the time history. Omenzetter *et al.* (2003) conducted analysis on data from a multi-channel SHM system installed on a major bridge structure. In order to differentiate between abrupt and slow changes, the strain data was analysed us-

Stellenbosch University https://scholar.sun.ac.za

ing a discrete wavelet transform. The wavelet coefficients were then processed using a statistical outlier analysis to find the data that is significantly different to the remainder.

Dessi (2014), discusses identifying slamming on vessels, using the transient, broad-frequency response caused by the impulse. This "whipping criterion" looks at the global effects as a result of the local impact response. In order to do this wavelet analysis an envelope extraction with the Hilbert transform was used. It was concluded that wavelet transforms were effective and show well shaped, broad band frequency peaks after a slam. According to Dessi (2014) it is important to look at the whipping response when identifying a slam. In the case of closely occurring slams, the phasing between the global response and the subsequent slam should be investigated.

A laboratory experiment, on a simulated aircraft wing, was conducted by Worden *et al.* (2003) in which they looked to identify increasing levels of structural damage. Three methods were used; outlier analysis, a neural network approach and kernel density estimation. All three showed they could successfully detect damage, with varying success. The outlier analysis and neural network showed the most sensitivity in detecting damage. These two methods will be discussed further. This forms part of level 1 of a SHM system, and methods discussed here could be applied to identifying slamming events in large datasets.

Outlier analysis gives an indication of a data point's inconsistency with the remaining data. An outlier is believed to result from different mechanisms to the other data points. A common measure of outliers is a discordance test, this gives an indication of the extent of inconsistency (Barnett & Lewis, 1994). A measure of discordancy can be determined by;

$$Z = \frac{|Y - \mu|}{\sigma} \tag{2.2}$$

where Z and Y are vectors of discordancies and inputs respectively. μ and σ are the input's mean and standard deviation respectively. These discordances are compared to some threshold in order to determine if the corresponding data point was an outlier. This threshold was determined using extreme values from

Stellenbosch University https://scholar.sun.ac.za

a Monte Carlo method (Worden *et al.*, 2000).

A neural network, or artificial neural network (ANN) is a form of machine learning that is designed to mimic the human brain. An ANN consists of an input, output and hidden layers (Figure 2.7a). There may be as many hidden layers as deemed necessary for a particular problem. A single node in a hidden layer will receive the outputs from the nodes in the previous layer as inputs (Karn, 2016).

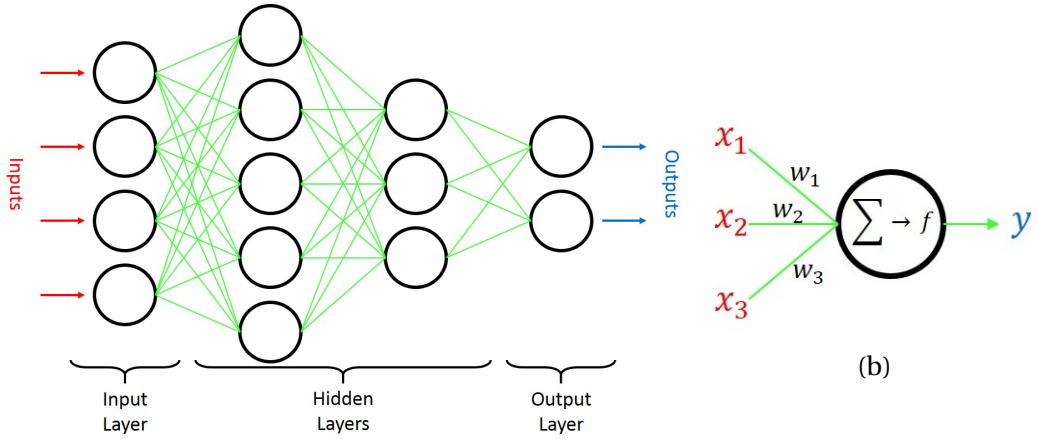

Figure 2.7: Example of a neural network structure; (a) Visualization diagram of an ANN. (b) Visualization diagram of a single ANN node.

Each connection or input to each node has a random initial associated weight (Figure 2.7b). Upon entering the node, the weighted inputs are summed;

$$s' = \sum_{k=1}^{N} (x_{j,k} w_{j,k}) \tag{2.3}$$

Where j is the number of the node in any particular layer, k is the identification number of the input to the node and N is the number of nodes in the previous layer. The sum of the weighted inputs, s', is then the input to the activation function, f, (Eq (2.4)). There are many different activation functions to suit the type of problem. The purpose of an activation function is to introduce non-linearity into the output (Karn, 2016). Typical activation functions include the sigmoid (Eq (2.5)) and hyperbolic tangent functions (Eq (2.6)).

Stellenbosch University https://scholar.sun.ac.za

$$y = f(s') \tag{2.4}$$

$$f(s') = \frac{1}{1+\exp(-s')} \tag{2.5}$$

$$f(s') = \tanh(s') \tag{2.6}$$

The ANN employs feed forward multi-layer perception (MLP) (Worden *et al.*, 2003). This basically means that the network has multiple hidden layers and outputs are produced by moving information forward through the network (Haykin, 1994). The network is then trained using back-propagation of errors. This is a supervised learning technique, which trains on labelled training data. Essentially, the network is able learn from its own mistakes. For the first training run of the network outputs are compared with what is expected. The error is then "propagated" back through the layers and the connection weights are adjusted. This is repeated until the output error approaches zero. The ANN is then considered trained and can be run with "new" data (Mantri, 2013).

Stellenbosch University https://scholar.sun.ac.za

Chapter 3

Measurement methods

The data used for this thesis was recorded during the Antarctic relief voyage 2016 /2017, and winter cruise 2017. Full-scale measurements were carried out on-board the SAAII. This allowed the structural vibration response of the vessel to be recorded, while she was under way. Ship operational data, as well as environmental data, along the two voyage paths were also collected. All of this data was used to form a holistic picture of the structural behaviour of the vessel dependent on the variety of environmental and operational input factors.

3.1 The vessel

The SAAII (Figure 3.1) was built by STX Finland in Rauma, Finland. Her keel was laid in January of 2011 and she was completed and delivered to Cape Town, South Africa in May of 2012 (Det Norske Veritas, 2017).

The vessel's classifications fulfil a number of roles while in service. She is able to carry passengers, cargo, bunker flammable liquids and achieve scientific research goals, owing to the laboratories and equipment installed on-board, while also being able to access the polar regions, due to her PC-5 classification. The vessel was designed with the strength and operational capability for year-round operation in medium first-year ice containing multi-year ice inclusions. According to the requirements concerning PC-5, the hull material thickness of the ves-

Stellenbosch University https://scholar.sun.ac.za

Figure 3.1: The SAAII, stern raised above the water line.

sel gradually decreases from bow to stern. The opposite is true for the spacing of stiffening frames, the distance between frames increases from bow to stern (Polar Class, 2011). This makes her extremely heavy in the bow of the vessel. Table 3.1 shows main characteristics of the vessel, as supplied by the manufacturer and measured during voyages. The modal frequencies are very sensitive to the changing mass and mass distribution throughout the vessel.

Table 3.1: The main characteristics of the SAAII

Physical Characteristics		**Frequency Characteristics**	
Length	121.80 m	Shaft frequency at MCR	2.33 Hz
Beam	21.70 m	Blade pass frequency	9.33 Hz
Draught	7.65 m	Diesel engines	12.50 Hz
Gross tonnage	12 897 ton	1st bending mode	2.23 Hz
Deadweight tonnage	4 780 ton	2nd bending mode	3.87 Hz
Max. Speed	14 kn	3rd bending mode	5.25 Hz

Stellenbosch University https://scholar.sun.ac.za

3.2 Measurement method

The following section presents and discusses the equipment and system setup used during both measurement voyages. Not all of the equipment and locations mentioned below were used for this thesis. The entire set-up forms part of an assortment of projects that make use of the structural vibration response data from the vessel.

3.2.1 Measurement equipment

The measurement equipment used during this voyage is presented in Table 3.2.

Table 3.2: Equipment used to measure vibrational response

Equipment:
3 x LMS SCADAS
Fibre optic cables
12 x DC PCB accelerometers, 20,4 mV/(m/s^2)
12 x DC signal conditioner
15 x ICP PCB accelerometers, 10,2 mV/(m/s^2)
3 x Seismic PCB accelerometers, 1019,4 mV/(m/s^2)
Coaxial cables
LMS Test.Lab 11A Turbine Testing software
Laptop computer

The three SCADAS were set up in a master-slave configuration using fibre optic cables. The SCADAS have built-in low-pass, anti-aliasing filters. The sample rate for the entire voyage was 2048 Hz. This sample rate was chosen in accordance with BS ISO2631-1:1997, so that this data could also be used for human whole body vibration projects. The DC signal conditioners supplied 12 V DC to the DC PCB accelerometers and connected them to the SCADAS. All accelerometers used for the measurement were calibrated by the National Metrology Institute of South Africa (NMISA) in accordance with ISO 9001. Accelerometer calibration values can be found in Appendix A.1. Before each measurement voyage the drift of the accelerometers was checked using a SVANTEK vibration calibrator. The procedure for this process can be found in Appendix A.2.

Stellenbosch University https://scholar.sun.ac.za

Environmental and operational data (Table 3.3) was gathered in order to compare with the structural vibration response recordings. This data was recorded by the crew and permanently installed sensors on the ship. Data from the ship's scientific data system (SDS) was recorded at UTC time. The swell observations come from the ship's logbook which was recorded local time. The South African Weather Service (SAWS) synoptic observations (SYNOPs) were also conducted at UTC.

Table 3.3: Environmental and operational parameters used in the study

Measured data	**Visual observations**
Longitude & Latitude (SDS)	Swell height (Logbook)
GPS speed over ground (SDS)	Swell direction (Logbook)
Ship heading (SDS)	Swell period (SAWS)
Wind speed (SDS)	
Wind direction (SDS)	

3.2.2 Measurement set-up

In order to simplify the measurement set-up the vessel was divided into two sections, the hull and the superstructure. The hull, being deck four and below and the superstructure, being deck five and above. The hull was instrumented with 22 accelerometers while the superstructure contained eight accelerometers. Sensor distribution, seen in Figure 3.2, was chosen for the following reasons:

- Sensors placed in the bow and stern, of the hull, measure the wave slamming response in open water, as well as ice impact response while in sea ice.
- Sensors in the cargo hold, engine store room and stern thruster room (hull, midships), were installed in order to study global bending modes as well as the global structural response as a result of slamming.
- Sensors placed on the bridge, and throughout the rest of the superstructure, captured responses used to evaluate human comfort as a result of structural vibration.

Stellenbosch University https://scholar.sun.ac.za

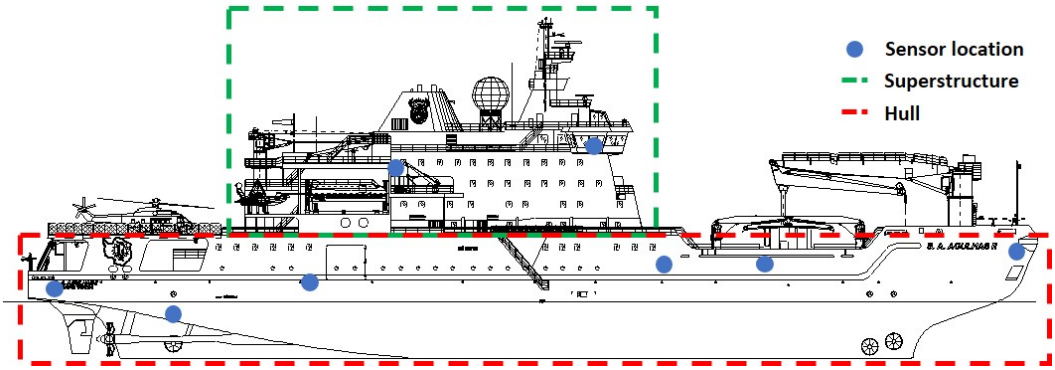

Figure 3.2: Sensor locations for the Antarctic relief and winter cruises

The measurement axis convention was set up so that the positive X direction points to the bow, the positive Y direction points to port and the positive Z direction points upwards. Sensor orientations, seen in Figure 3.3, were chosen for the following reasons:

- Z-axis measurements, for the hull, were recorded on the port and starboard sides to study the bending and torsional modes of the structure, as well as the presence of slamming events through the length of the vessel.
- Y-axis measurements, for the hull, were recorded to study the transverse bending response.
- X-axis measurements, for the superstructure, were recorded to study human whole body vibration and any bending response consisting of fore and aft motion.
- Y-axis and Z-axis measurements, for the superstructure, were recorded to study transverse and torsional bending respectively, as well as human whole body vibration.

For the purposes of this study only sensors on the z-axis were considered as they provided most sensitive during slamming events. Figure 3.4 shows the starboard locations of the six sensors used during this slamming study. These sensors are spaced as evenly along the length of the vessel as possible, while also being as close to in-plane as possible.

Stellenbosch University https://scholar.sun.ac.za

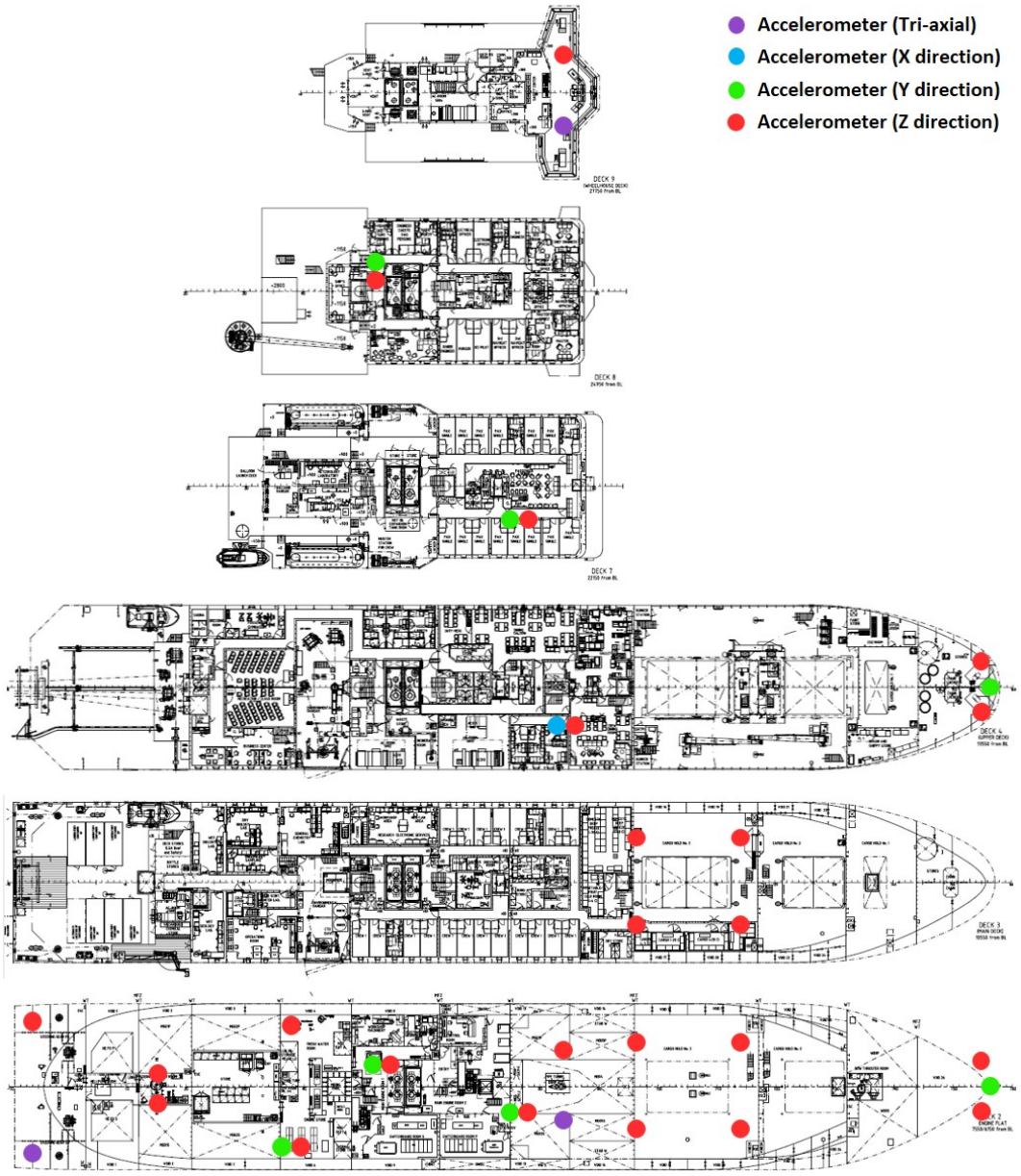

Figure 3.3: Sensor orientations for the locations on each deck where they were installed.

A stand alone laptop controlled the measurement system, housed inside the central measurement unit (CMU) cabinet (Figure 3.5a). LMS Test.Lab 11A Turbine Testing software allowed continuous recording for the duration of the voyages at UTC. This software saved data in consecutive five minute files.

Stellenbosch University https://scholar.sun.ac.za

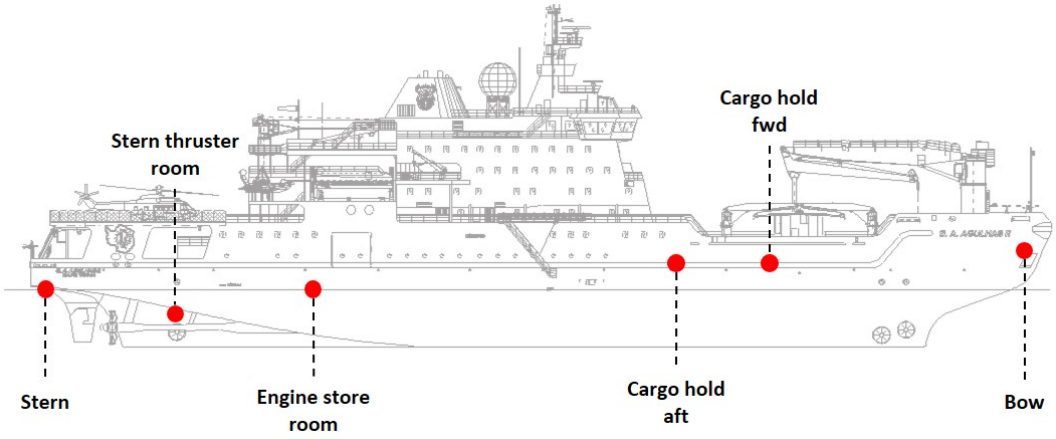

Figure 3.4: The sensors used for the source of data for the thesis.

Fibre optic cables were used to configure two of the SCADAS (Figure 3.5b), at the CMU, with the third one in the stern of the vessel. Shielded cables running to each measurement location, as in Figure 3.3, converge at the CMU to allow for synchronized recording. Accelerometers were super glued to rigid structural members. This ensured that the vessel's global response was recorded. When mounting accelerometers (Figure 3.5c and 3.5d), all excess cable was secured using duct tape and cable ties, to minimize the effect a moving cable could have on the measurement.

3.3 Data pre-processing

This section is a short description of the pre-processing done on all of the data before being looked at further. Data collected was first detrended in order to remove any DC off-sets in the signal. DC accelerometers were constantly measuring local gravity while measuring other perturbations. Certain sensors had to be mounted in a negative direction due to the availability of mounting locations on the vessel. The orientations of these sensors were corrected by multiplying their signals by negative one. Given that the sample frequency for the voyages was set at 2048 Hz, a down sample step was also included into the pre-processing of the data. A sample rate of 1024 Hz was deemed sufficient in order to still capture the detail of an impulse with out clipping the peaks. A band width of 512 Hz

Stellenbosch University https://scholar.sun.ac.za

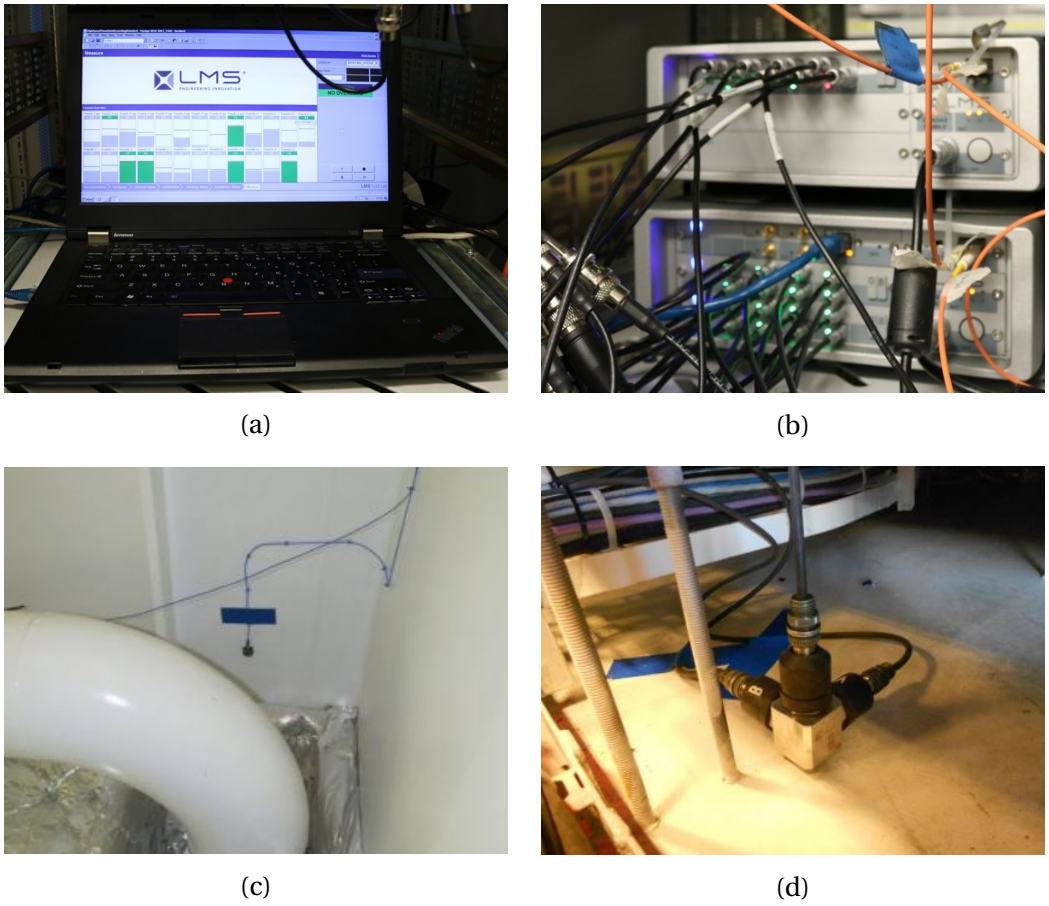

(a) (b)

(c) (d)

Figure 3.5: Equipment used for measurement. (a) Stand-alone recording laptop. (b) Master and slave SCADAS at the CMU. (c) DC accelerometer mounted on a rigid I-beam. (d) Seismic accelerometers mounted under the floor on the bridge.

was satisfactory for the continuation of this study, as the modal responses and machinery excitation are all relatively low frequency. Given the shear size of the data set, down sampling the data to 1024 Hz also saved on storage space as well as processing time later on. Further processing of the data will be detailed in the Chapters 4 and 5.

Stellenbosch University https://scholar.sun.ac.za

3.4 Voyage description

3.4.1 Antarctic relief 2016/2017

The Antarctic relief 2016/2017 voyage took place over 70 days, from December 2016 to February 2017. The purpose of this cruise was to resupply the SANAP base in Antarctica, with the vessel completing various research objectives along the way. The measurement system recorded for the duration of the voyage, apart from unforeseen stoppages and the vessel standing stationary on standby at RSA Bukta in Antarctica. A track of the global positioning system (GPS) coordinates for the voyage can be seen in Figure 3.6.

Figure 3.6: The Antarctic relief voyage 2016/2017 cruise track (Natural Earth, 2018).

The Antarctic relief 2016/2017 voyage was broken down as follows:

- The SAAII departed Cape Town harbour on the 1st of December 2016 and headed South West to the Greenwich Meridian, at which point she headed due South. During this time the vessel stopped multiple times, for scientific stations.

Stellenbosch University https://scholar.sun.ac.za

- The ice field was reached on the 7th of December 2016 and the vessel proceeded on to RSA Bukta, arriving on the 10th of December 2016, where she went onto standby.
- She then navigated West, along the Antarctic coastline, to Akta Bukta, arriving on the 23rd of December 2016.
- The 2nd leg of the voyage then began by sailing back to RSA Bukta for standby operations during construction at the SANAE Base, arriving on the 30th December 2016
- She remained on standby at the ice shelf until 24th of January 2017, departing for South Georgia, arriving on the 31th January 2017. She then departed to Cape Town on the same day.
- Arrived back in Cape Town on the 13th of February 2017.

This voyage was fairly eventful in terms of slamming occurrences. There were multiple times when the vessel would stop for a scientific station and probability of stern slamming would be high. There was a single large storm, near to South Georgia, where swell heights reached 10 metres. It would be dangerous to stop during this time so the vessel continued ahead with her bow to the swell. During such times the probability of bow slamming was highly likely.

3.4.2 Winter cruise 2017

The winter cruise 2017 voyage took place over 16 days, during June and July 2017. The purpose of this cruise was to study the marginal ice zone (MIZ) during the winter period, while also completing various research objectives along the way. The measurement system recorded for the duration of the voyage, apart from unforeseen stoppages. A GPS coordinate track for the voyage can be seen in Figure 3.7.

The winter cruise 2017 was broken down as follows:

- The SAAII departed Cape Town harbour on the 28th of June 2017 and headed South East, in search of the beginning if the sea ice extent around Antarc-

Stellenbosch University https://scholar.sun.ac.za

Figure 3.7: The winter cruise 2017, cruise track (Natural Earth, 2018).

tica. During this leg the vessel stopped multiple times, for scientific stations.

- The ice field was reached in the early hours of the 4th of July 2017. The vessel proceeded with various scientific activities, leaving the ice again in the early hours of the 5th of July 2017.
- The vessel then navigated due North, along the 30 degree east longitude line, stopping for various oceanographic stations along the way.
- She then proceeded back to Cape Town, arriving on the 13th of July 2017.

This voyage was very eventful in terms of slamming occurrences. The winter months in the Southern Ocean are notorious for large swell conditions, in excess of 12 metres. This resulted in a lot of slamming activity throughout the voyage. During this time the vessel found itself in the middle of large storm system, the size of Southern Africa, which made for interesting slamming data.

Stellenbosch University https://scholar.sun.ac.za

3.5 Challenges of the measurement voyages

Measurement voyages came with their own set of challenges for collecting the data. The following occurrences hindered the collection of data;

- The vessel faced power outages, or power surges would cause the measurement system to reset.
- The environmental and operational data was collected by a variety of other systems on board that were also subject to power outages as well as human error in observing the measurement accurately.
- Due to multiple other electronic systems on board the vessel, signal interference was an issue that would cause abnormalities in the data from time to time. The faults would be investigated and the cables would be changed or isolated to remove the interference.
- As eluded to in the literature review, the crew on the SAAII would endeavour to avoid slamming conditions at every possible chance.

Stellenbosch University https://scholar.sun.ac.za

Chapter 4

Analysis methods

Algorithms developed here will make it possible to detect slamming events based on known features in the signal, as discussed in Section 2.3. The identification of the impulsive slamming signal proves to be difficult. This particular signal has the following characteristics, that make its detection challenging;

- Impulsive
- Non-periodic
- Random peak magnitudes
- Non-stationary over time
- Introduces and variable noise floor

Attempting to account for these challenges, the algorithms will make it possible to easily count the number of slams over a given time period. This work aims to improve the accuracy and efficiency of visually, or manually inspecting data in order to identify and locate slamming events. This chapter develops ideas in order to achieve the detection of slamming events. Some basic metrics will be determined in order to construct a broad overview of all the data collected from the voyage. Thereafter, the unfiltered acceleration signal will be looked at to determine its influence. By using distributions of the data, thresholds will be calculated for the intermittent outputs. Finally, algorithms, in both time and frequency domain will be developed and explained.

Stellenbosch University https://scholar.sun.ac.za

4.1 Broad overview representation

While at sea many observations were made around the times that slamming occurred. These observations were performed by participating passengers and crew on-board the vessel. It was observed that, the likelihood of bow slamming increases greatly when moving forward in larger swell conditions, with the bow into the swell. The captain would many times be forced to sail with the bow into the swell to minimise the rolling motion of the vessel, for increased passenger comfort in rough seas. The probability of slamming at the stern increased greatly when the vessel was moving slowly, or was stopped in any type of swell conditions. Stern slamming was most prevalent when the stern was orientated towards oncoming swells.

In order to apply the above observations, the bow and stern sensor data was used to get an indication of overall vibration levels. A root-mean-square (r.m.s.) (Eq. 4.1) and an absolute maxima value (Eq. 4.2) were determined for 1 minute intervals over the duration of the vibration data. These absolute maxima values will also be referred to as peak values. Where x_i is the sampled data and n is the total number of data points recorded in one minute. The subscript j is the index for the time intervals. These metrics were used as features to describe the data over time due to the non-stationarity in the signal (Subsection 4.3.1 will expand on this).

$$r.m.s._j = \sqrt{\frac{\sum_{i=1}^{n}(x_i^2)}{n}} \tag{4.1}$$

$$peak_j = max(|x_i, x_{i+1}, ..., x_n|) \tag{4.2}$$

Both r.m.s. and absolute maxima values were plotted concurrently with the environmental parameter, swell height (H_{swell}) and operational parameters; ship speed (v_{ship}) and incident swell angle ($\phi_{incident}$). The $\phi_{incident}$ is the heading of the oncoming swell, relative to the bow of the ship (Figure. 4.1). The range is from 0 to 180 degrees on an absolute scale, because the ship is symmetrical about its longitudinal plane. The arrow shows the direction from which the swell

Stellenbosch University https://scholar.sun.ac.za

front is approaching.

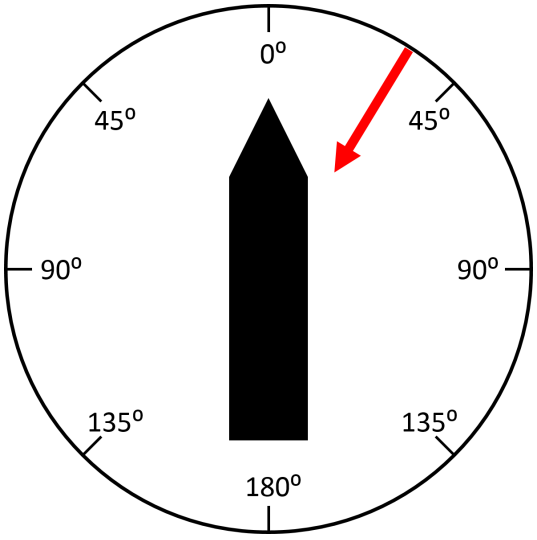

Figure 4.1: Diagram representing incident swell angle.

Figure 4.2 shows data describing the first six days of the winter cruise 2017. Blue dots represent the features for the bow data, and green dots represent the features for the stern data. It can be seen here that the H_{swell}, (black line) v_{ship}, $\phi_{incident}$, (red and purple lines respectively) influence the vibration data. In Figure 4.2a, encircled section 1, shows that when the ship is moving forward (v_{ship} remains constant) the r.m.s. level, at the bow and stern increase with an increase in H_{swell}. Here, $\phi_{incident}$ also shows that during raised r.m.s. levels the vessel was heading into the swell. During other periods of time (encircled section 2) the H_{swell} remains constant if not decreases, yet the vibration levels increase due to an increase in v_{ship} and change in $\phi_{incident}$.

In Figure 4.2b, encircled section 1, shows that in large H_{swell} the peak values show local increase on the bow and stern. While in encircled section 3, when v_{ship} decreases the peaks show local increase on the stern only. These local increases in Figure 4.2b strongly suggest the presences of slamming events at these times. The trends seen in the data confirm what is descried by passengers and crew on board the vessel.

A normalised axis was used in order to represent the data on the same set of axis, while keeping the scale between variables the same. The data plotted on the y-

Stellenbosch University https://scholar.sun.ac.za

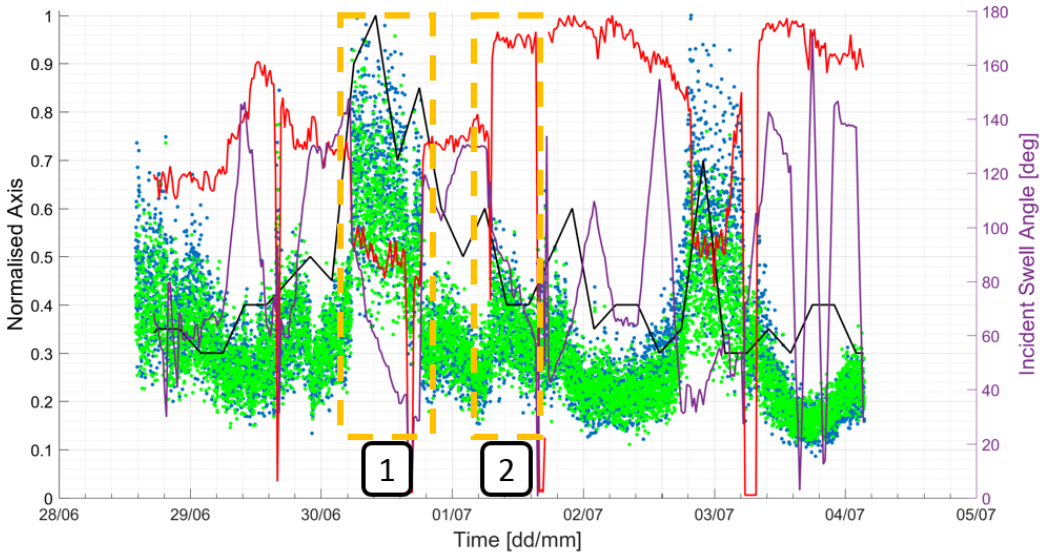

(a)

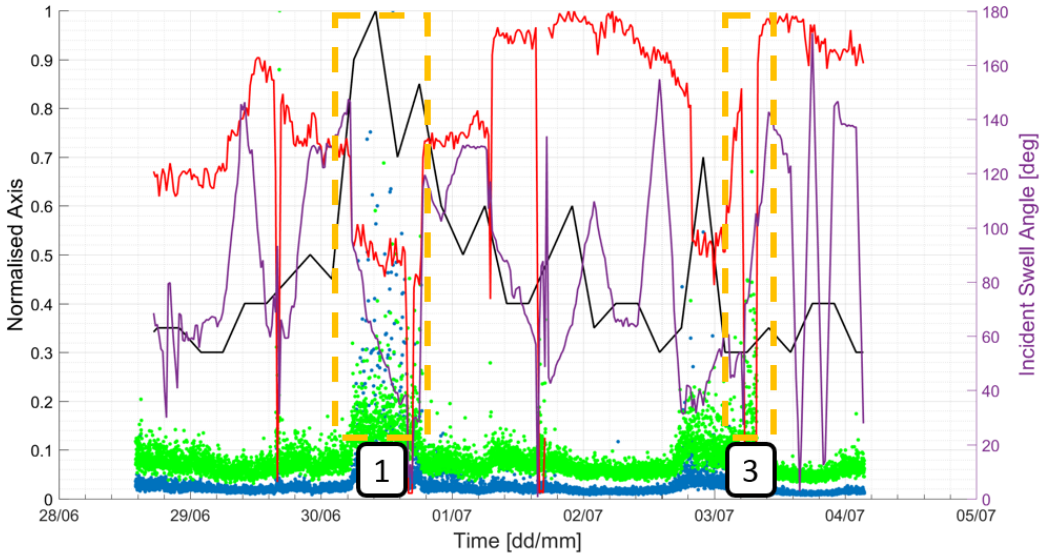

(b)

Figure 4.2: Example of overview data spanning the first 6 days of the winter cruise 2017; (a) ● bow r.m.s., ● stern r.m.s., — H_{swell}, — v_{ship}, — $\phi_{incident}$. (b) ● bow peaks, ● stern peaks, — H_{swell}, — v_{ship}, — $\phi_{incident}$.

axis on the left hand side was normalized with reference to the respective variable maximums. These maximums can be seen in Table 4.1 below.

Stellenbosch University https://scholar.sun.ac.za

Table 4.1: Normalization reference values.

Data set	Maximum value	Unit
Bow r.m.s.	0.273	[g]
Stern r.m.s.	0.196	[g]
Bow peak	9.742	[g]
Stern peak	2.810	[g]
H_{swell}	10	[m]
v_{ship}	17.60	[knots]

4.2 Unfiltered signal

The accelerometers used for these measurements have varying frequency ranges, the DC accelerometers are able to measure down to 0 Hz. The ICP accelerometers cannot accurately measure under 1 Hz. Therefore when looking at the unfiltered signal, data from the DC accelerometers was used. Figure 4.3 shows a bow signal from the winter cruise 2017, it is plain to see that this signal contains a low frequency component, on top of which the higher frequency content has been superimposed. This low frequency component is the rigid body motion of the vessel. Rigid body motion refers to the first modal frequency of the structure.

It was noted in early observations, slamming events seem to occur when the bow or stern of the vessel is moving downwards. Using double differentiation between displacement and acceleration, a crest in low frequency acceleration signal corresponds to a trough in the displacement signal, being the end of the range for movement in the negative direction. The signal shown in Figure 4.3 contains slamming events (however big or small) as can be seen by the presence of impulsive peaks marked by asterisks. In most places, just before the crest of the low frequency component in the raw unfiltered acceleration time signal. The impulsive peaks seen in the low frequency troughs on the bow are a reaction to impulsive peaks initiated at the stern.

4.2.1 Frequency content

A power spectral density (PSD) was determined for five time periods each, five minutes in length, picked from throughout both voyages. All frequency spectra

Stellenbosch University https://scholar.sun.ac.za

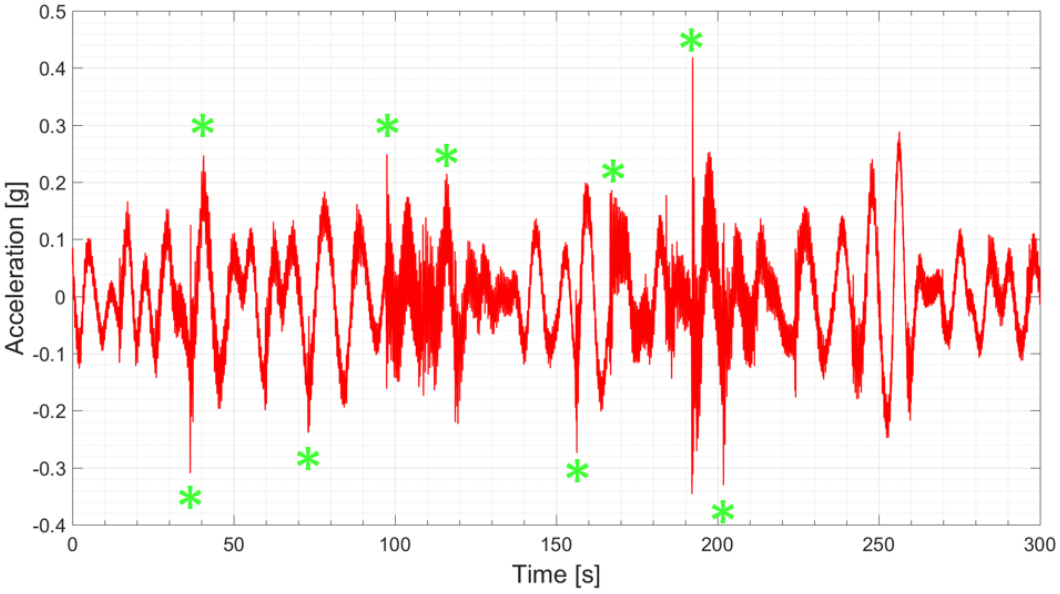

Figure 4.3: Unfiltered acceleration vs. time signal at the bow of the vessel, during winter cruise 2017.

show the similar behaviour. Figure 4.4 shows the PSD for the bow acceleration signal above. In the PSD it can be seen that there are a number of dominant frequencies under 5 Hz, correlating with the frequencies reported in Table 3.1. Both a rectangular and Hanning window were plotted to observe any influence in the frequency shift, but the rigid body frequency remained consistent for both windows over a range of window sizes. It was therefore decided to make use of the rectangular window in order to obtain the rigid body frequencies in the data. This was also done since there are impulsive events of interest in the signal. A Hanning window would loose detail of the peak. The sample frequency for the data was 1024.

Table 4.2 shows the lowest dominant (rigid body) frequencies for the five samples of selected data, spanning both voyages, encapsulating a variety of environmental and operational conditions. From this data it can be seen that the rigid body frequency remains between 0.1 - 0.2 Hz. This corresponds with previous measurements on the SAAII done by (Soal (2014))

Stellenbosch University https://scholar.sun.ac.za

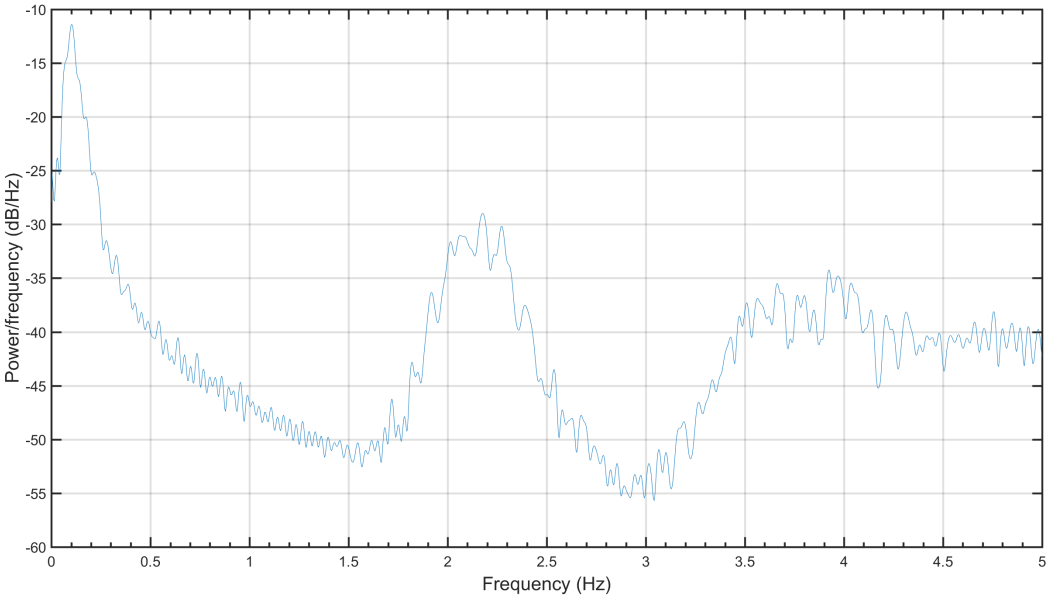

Figure 4.4: Bow Acceleration Signal Power Spectral Density.

Table 4.2: Sample rigid body frequencies and when they were recorded.

Sample	Date	$f_{\text{rigid body}}$	Voyage
1	26 Jan 2017	0.125 Hz	Antarctic relief 2016
2	28 Jan 2017	0.133 Hz	Antarctic relief 2016
3	02 Jul 2017	0.152 Hz	winter cruise 2017
4	28 Jun 2017	0.102 Hz	winter cruise 2017
5	05 Jul 2017	0.121 Hz	winter cruise 2017

4.2.2 Filtering

Due to the frequency content of the signal, it was decided that a filter would be applied to the data to remove the rigid body motion. The data was filtered in order to exclude frequencies lower than 0.7 Hz. This cut-off was chosen as the rigid body frequencies are all under 0.2 Hz, and the next modal / significant frequency in the signal is at ±2.2 Hz. The filter was designed using a fifth order high pass Butterworth filter. Figure 4.5a shows the attenuation curve for the filter, at 0.2 Hz the signal is attenuated by ±55 dB, and by 1 Hz the signal has no more attenuation. Figure 4.5b shows a PSD of the now filtered signal to confirm that the low frequency component has been attenuated.

Stellenbosch University https://scholar.sun.ac.za

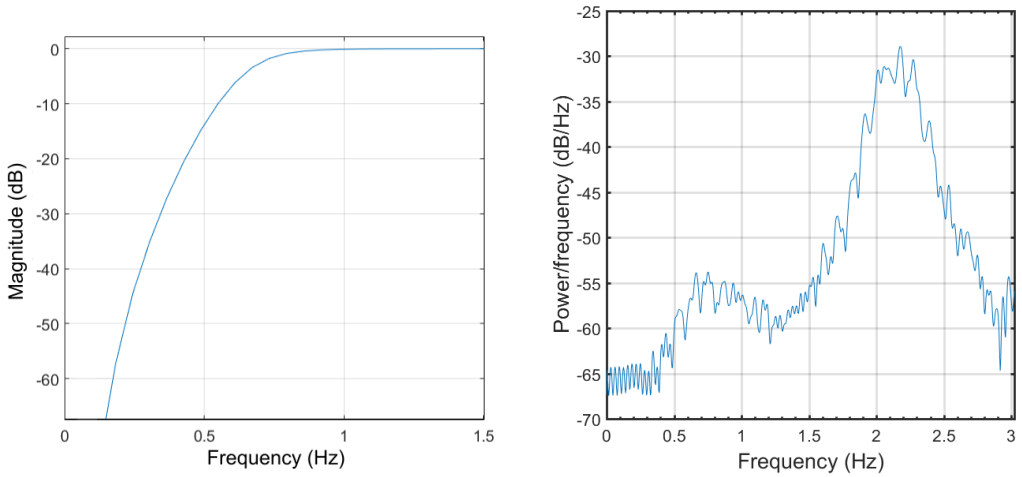

(a) (b)

Figure 4.5: (a) 5^{th} order Butterworth filter with a 0.7 Hz cut-off frequency, (b) Filtered signal power spectral density.

Figure 4.6 shows a high pass filtered signal from Figure 4.3. It is clear to see that the low frequency component of the signal has been filtered out. The impulsive events in the signal now become clearer to see.

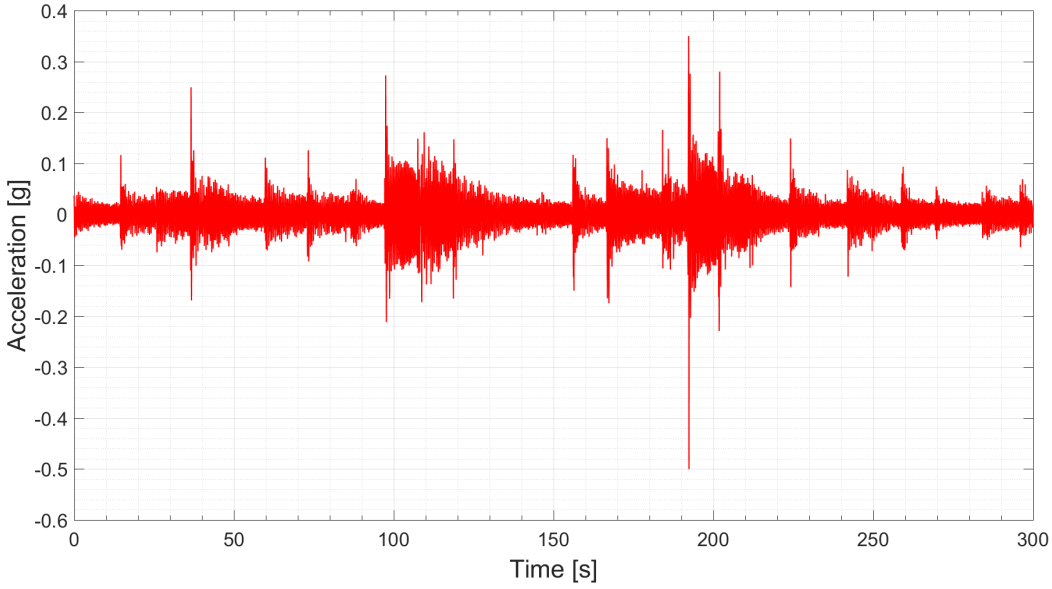

Figure 4.6: Filtered acceleration vs. time signal at the bow of the vessel (f_{cut} = 0.7 Hz), during winter cruise 2017.

Stellenbosch University https://scholar.sun.ac.za

4.3 Thresholding

This section will detail thresholds for slamming events to be detected. The algorithms that are to be developed need to be benchmarked against values in order to identify a slam. Thresholds will be determined for the data in the time domain initially. Thresholds in the frequency domain will be determined much in the same way as described for the time domain, only using data that has been transformed into the frequency domain. These thresholds will then be used for the detection and counting of slams during analysis. The thresholding was done using the high pass filtered data, using the sensors introduced in Figure 3.4.

4.3.1 Interval selection

As eluded to in Section 4.1 the vibration data is represented using features (r.m.s. and peak) for individual time intervals. This is because the signal is non-stationary in nature, making the data features dependant on the duration and interval over which they are calculated. This is attributed to the fact that during the measurements the vessel speed and swell conditions were constantly changing. To prove this in the data a simple equality, seen in equation 4.3, was applied. If this equality is true for any arbitrary time intervals, t_1 and t_2, the signal is considered stationary (Brandt, 2011). For the data being considered this equality is not true.

$$r.m.s(x(t_1)) = r.m.s.(x(t_2)) \tag{4.3}$$

Due to the non-stationarity of the signal it is not possible to represent the data using a metric spanning to long a time. The data was thus divided into representative time intervals. The duration of the intervals was based on multiple factors;

- Allow enough resolution to identify multiple slams within a rigid body period, on an average of eight seconds (Table 4.2),
- Ensure that two slamming events are not captured in the same time interval,
- Allow for multiple oscillations of the first elastic mode at (2.2 Hz),

Stellenbosch University https://scholar.sun.ac.za

A time interval of two seconds was selected based on the factors mentioned above. This is short enough to allow for the possibility of multiple slams over an eight second period, as well as only capturing a single slam per interval, while still being long enough to capture at least four oscillations of the first elastic mode. The selection of this time interval will be scrutinised further in Section 5.5.

4.3.2 Data distribution (time domain)

An absolute maxima value was extracted for two second intervals across the combination of the Antarctic relief 2016/2017 and Winter 2017 cruises. This was done using Eq. 4.2, where n is now the number of data points in two seconds. The histograms of these values were plotted for the bow of the vessel initially. From the densities in Figure 4.7 (x axis range is limited to 0.2 g for viewing purposes) it can be seen that the distributions of the maximums has a long right hand tail. The same can be said for the other five sensor positions (Appendix B.2).

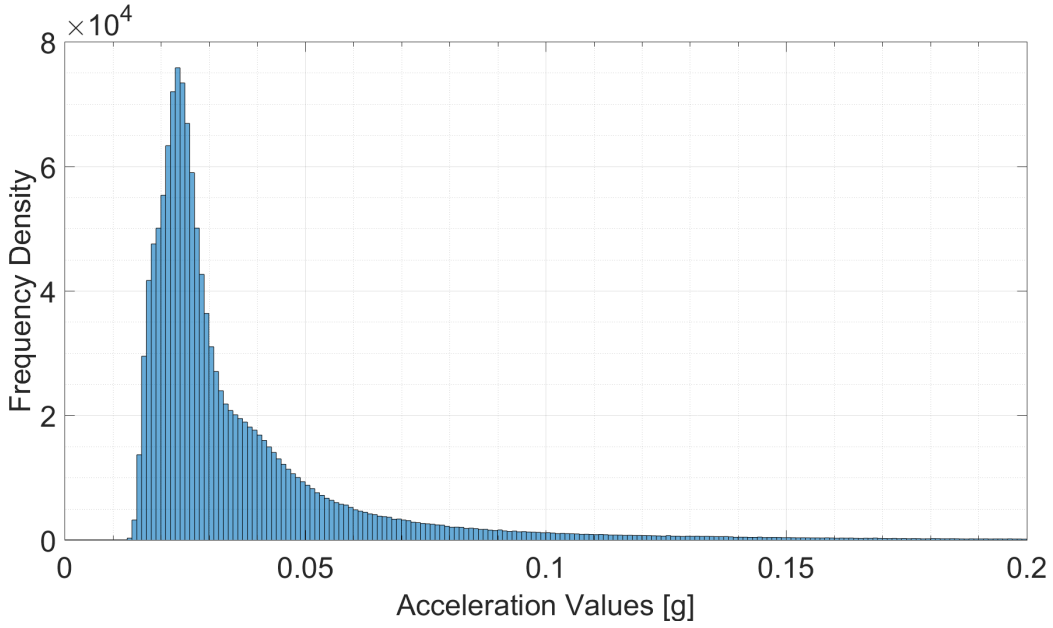

Figure 4.7: Histogram of bow peak values across two voyages in the time domain (for two second intervals).

This shows that there are a number of high valued outliers, or extreme values in these data sets. A commonly used distribution model fitted when considering

Stellenbosch University https://scholar.sun.ac.za

data of this nature is the Weibull distribution (Pimentel *et al.*, 2014). This distribution has been used when considering peak slamming forces on a hull (Kapsenberg, 2011), or maximum bending moments during slamming events (Tuitman, 2010), and even ice-induced impact loads on a ships hull (Suominen & Kujala, 2014). This is because the Weibull distribution can be classified as a extreme value distribution (Pimentel *et al.*, 2014), making it suitable to describe the data in this data set. The assumption here is that these extreme values exist as a result of wave slamming, due to the fact that this data only represents open water navigation and not ice.

In order to determine the length of tail that contains these outlying or extreme peaks, a distance of the mean plus three standard deviations ($\mu + 3\sigma$) is commonly suggested (Pimentel *et al.*, 2014). However, this presents a few problems; firstly, it assumes that the data is normally distributed, which this data set is not. Secondly, both the mean and standard deviation of a data set are strongly influenced by outliers (Leys *et al.*, 2013), which this data set contains a lot of. A median value, on the other hand, offers the advantage of being insensitive to extreme values in the data set. As an alternative, Huber (1981), presents the Median Absolute Deviation (MAD), defined by equation 4.4.

This forms part of extreme values statistics, where $M(\mathbf{x})$ is the median of the data set set, x_i is each peak's values in the set. Then, $M(|x_i - M(\mathbf{x})|)$ is the median of the absolute difference vector of each data point minus the data median. Lastly, b can be calculated as $1/Q_3$, where Q_3 is the upper quartile of the underlying distribution ($Q_3 = 1.39$), in this case the Weibull distribution. This MAD was calculated for each sensor and applied in the thresholding process for determining outlying impulses.

$$MAD = b\, M(|x_i - M(\mathbf{x})|) \tag{4.4}$$

Table 4.3 shows the mean and standard deviation for the bow data set in Figure 4.7. Looking at the spread of these statistics the effect of the outliers on the mean and standard deviation are plain to see, with $\mu + 3\sigma$ being an order of magnitude higher than the thresholds calculated in Table 4.4.

Stellenbosch University https://scholar.sun.ac.za

Table 4.3: Outlier analysis statistics for normal distribution assumption, in the time domain (bow peaks value as in Figure 4.7).

Statistic	**Peak [g]**
Mean (μ)	0.0393
Standard Deviation (σ)	0.0600
$\mu + 3\sigma$	0.2193

The threshold values are now determined using the median and MAD values by equation 4.5. Where k is a somewhat subjective multiplier chosen to represent the stringency of the threshold. In an effort to not falsely detect slams, $k = 3$ is used for the determination of the threshold in the time domain (T_3). The selection of this k multiplier will be evaluated later, in Section 5.5.

$$T_k = M(x) + kMAD \tag{4.5}$$

A breakdown of the metrics leading to the threshold for each sensor is presented in Table 4.4. Vibration values above these peak levels therefore have a better chance of being in the presence of a slamming event. The sensor thresholds cater to the definition of a local slamming event. In order to cater for the global definition of slamming one has to consider the movement of the vibration along the length of the hull. This will be described in the development of the algorithm in Section 4.4.1.

Table 4.4: Threshold peak values along the length of the vessel in the time domain.

Sensor	**Data median [g]**	**Data MAD [g]**	T_3 **[g]**
Bow	0.0274	0.0069	0.0423
Cargo Hold FWD	0.0100	0.0050	0.0208
Cargo Hold AFT	0.0288	0.0090	0.0483
Engine Store	0.0350	0.0066	0.0493
Stern Thruster	0.0227	0.0094	0.0430
Steering Gear	0.0482	0.0160	0.0828

Stellenbosch University https://scholar.sun.ac.za

4.3.3 Data distribution (frequency domain)

The vibration data was transformed into the frequency domain. This was done in order to compile a distribution of data in this domain. This was done by making use of the wavelet transform, as is further discussed in Subsection 4.4.2. This data is presented here as it forms part of the thresholding of the algorithm. Much like the analysis outlined in Subsection 4.3.2, the frequency data was divided into two second time intervals and absolute two second maxima were determined. Figure 4.8 shows the distribution of the bow frequency data peaks. The frequency data distribution for the remaining sensors can be found in Appendix C.1.

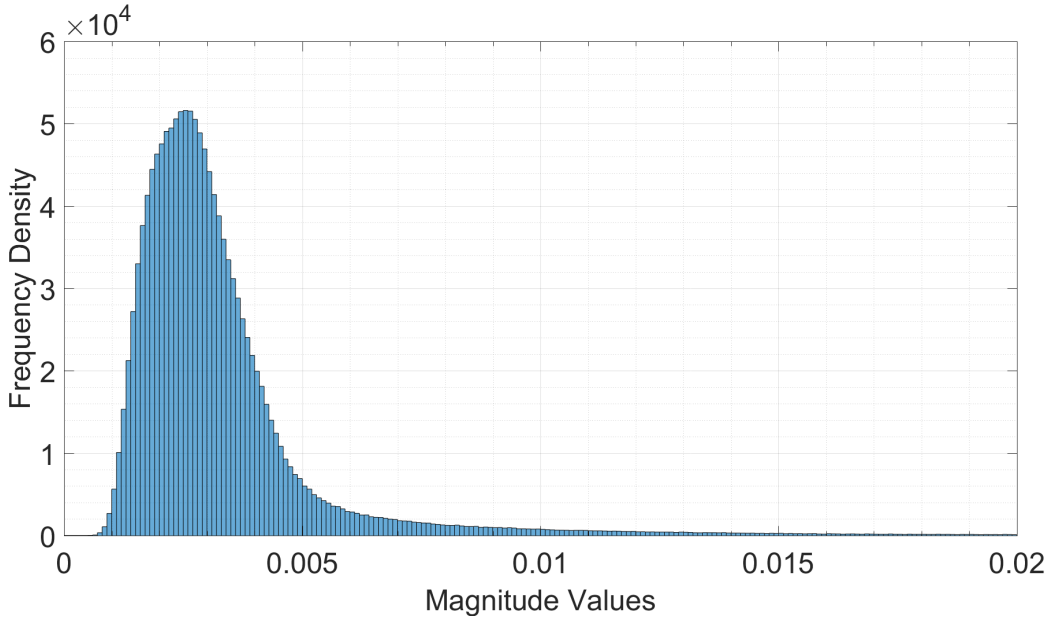

Figure 4.8: Histogram of bow peak values across two voyages in the frequency domain (for two second intervals).

Much like the distributions in the time domain, these distributions in the frequency are also right tailed. This lends itself to theory, as applied above, that the data contains a number of extreme values. Again the Weibull distribution can be used to explain this extreme value data set. Remembering that the extreme values in the data would bias the mean and standard deviation, the MAD (Eq 4.4) will be used in order to determine thresholds for the data in the frequency domain.

Stellenbosch University https://scholar.sun.ac.za

Table 4.5 shows the mean and standard deviation for this bow data set in Figure 4.8. Looking at the spread of these statistics the effect of the outliers on the mean and standard deviation can be seen, with $\mu + 2\sigma$ being approximately two and half times higher than the thresholds calculated in Table 4.6.

Table 4.5: Bow signal outlier analysis statistics under normal conditions for the frequency domain.

Statistic	**Peak [g]**
Mean (μ)	0.0034
Standard Deviation (σ)	0.0032
$\mu + 2\sigma$	0.0098

Table 4.6 shows the frequency domain limit values for the six locations along the length of the vessel. These limit values are then to be applied to the processed data in Subsection 4.4.2. The threshold multiplier for the frequency domain was selected at to be $k = 2$. The reason for this is to account for the smaller slams. These smaller slams may not have the same energy at this frequency, therefore the threshold is lowered slightly in order to detect them. The selection of this k multiplier will be re-evaluated later in Section 5.5.

Table 4.6: Threshold peak values along the length of the vessel in the frequency domain.

Sensor	**Data median**	**Data MAD**	T_2
Bow	0.0028	0.000752	0.0039
Cargo Hold FWD	0.0017	0.000834	0.0029
Cargo Hold AFT	0.0015	0.000310	0.0019
Engine Store	0.0031	0.000692	0.0041
Stern Thruster	0.0013	0.000354	0.0018
Steering Gear	0.0055	0.001400	0.0075

4.4 Algorithm development

In this section the details of the algorithm for identifying and counting the slamming events will be presented. In order to achieve these two aims, the two important aspects of a slamming signal will be addressed. Firstly the data will be

Stellenbosch University https://scholar.sun.ac.za

processed in a way to highlight the extreme or impulsive values in the data set. Secondly, these extreme values will be aligned in time across the sensors to address the global response induced by the slamming event. As eluded to above the data will be handled in two domains, time domain and frequency domain. This is in order to compare two methods of highlighting extreme values. The slam counting component of the algorithm will remain the same for both domains. A comparison will be drawn between the two domains in order to determine which of the two is better for the representation and ultimate identification of slamming events in the vibration data.

4.4.1 Time domain approach

Time domain refers to the same domain in which the data was recorded. Handling the data in this manner is thought to be the simplest and best starting point for an algorithm for slamming detection. This approach aims to utilise the impulsive, or extreme vibration levels seen across all sensors during a slamming event. Slamming is an event that spans multiple seconds therefore, as mentioned previously, data is grouped into two second intervals. For each time interval the absolute two second maxima were determined.

A peak value shows the maximum vibration experienced in the each of the time intervals. These values were gathered simply by determining the absolute maximum value in each of the two second time intervals. Figure 4.9 shows the peak values over time for the sample signal from Figure 4.6. From the graph it can be seen that the peaks highlight distinct events over the intervals. Peak interval data handling will thus be used further in the application of the algorithm.

4.4.2 Frequency domain

The handling of data here refers to the transformation of data into the frequency domain and the interpretation of that data. A wavelet transform converts the data into the frequency domain. This is a form of frequency-time analysis. This approach aims to utilise the broadband frequency excitation characteristic associated with the impulse in the slamming signal. In order to interpret the wavelet

Stellenbosch University https://scholar.sun.ac.za

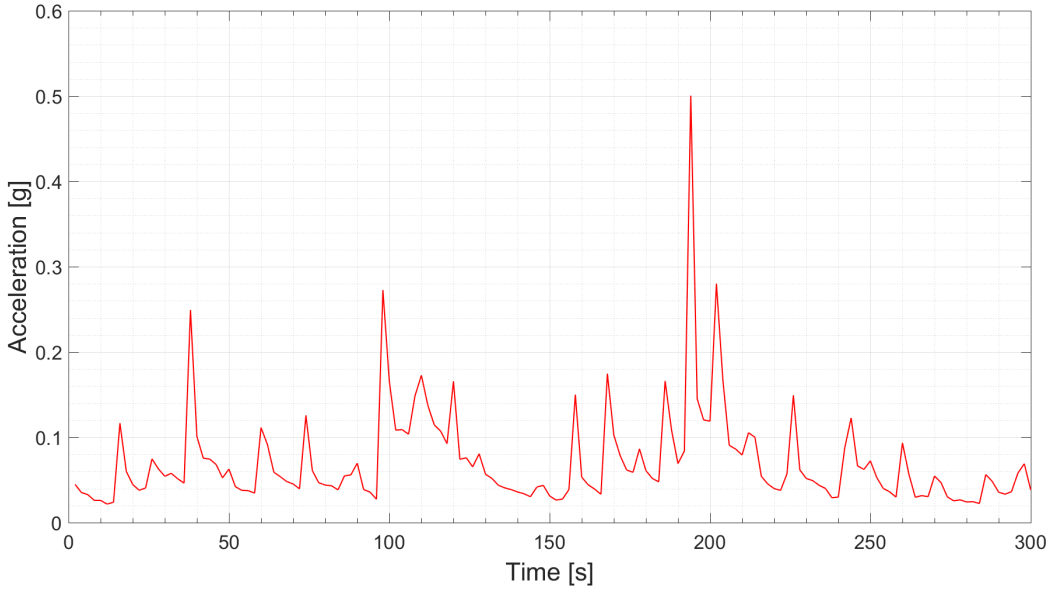

Figure 4.9: The absolute peak values, representing the sample signal in the time domain, for two second time intervals.

transform data, a fine scale analysis was conducted. This makes use of a single frequency band over time.

Wavelet transform

In order to transform the data into the frequency domain a wavelet transform was used. The output from the wavelet transform is a matrix of complex coefficients that are indexed by their scale and translation. Equation 4.6 shows the transform, where; α represents scale and β represents translation. The time signal to be transformed is $x(t)$ and $\psi^*_{\alpha,\beta}(t)$ is the analysing or wavelet function. The α and β for this function are varied to "stretch" and "place" this function in order to best approximate the original signal. Translation (β) is directly proportional to time, while scale (α) can be related to frequency through an inverse exponential curve dependent on the wavelet function.

$$X(\alpha,\beta) = \frac{1}{\sqrt{\alpha}} \int_{-\infty}^{\infty} x(t)\, \psi^*_{\alpha,\beta}(t)\, dt \tag{4.6}$$

For this analysis the built-in Matlab function "cwt" was used. Inputs were; the

Stellenbosch University https://scholar.sun.ac.za

vibration data to be transformed, wavelet function choice (Morlet wavelet) and the data sample frequency (1024 Hz). The wavelet function is chosen according to the features in the time signal that want to be captured. Therefore a wavelet function with an impulsive shape should be chosen in order to capture impulsive events in the original signal (Yang & Ren, 2004). Dessi (2014), makes use of the Morlet wavelet when trying to isolate slamming events in a measured signal. Yang & Ren (2004), also states that because of the Morlet wavelet's ability to approximate an impulse it is an ideal function for the extraction of impulses from mechanical signals.

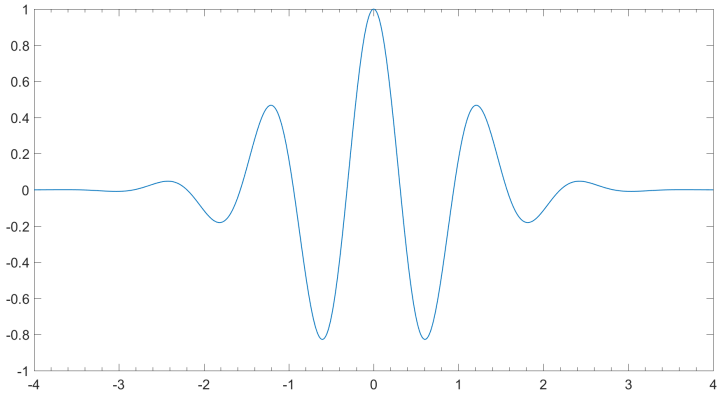

Figure 4.10: Morlet wavelet function used in the wavelet transform

A graphical representation of the continuous wavelet transform (CWT) of the data is shown in Figure 4.11. The output of the transform (X) is then the complex matrix of coefficients, with as many rows as there are frequency bins and as many columns as there are data points. In this case the frequency spectrum divided the signal bandwidth into the 250 bins. The number of columns was equal to the length of the signal in seconds multiplied by 1024 Hz.

As can be seen in Figure 4.11, the straight vertical lines (cones of influence) represent the broadband frequency excitation at various times in the data sample. Straight horizontal lines represent operation frequencies from the vessel, such as the shaft line rotational frequencies or water pumps. Previous vibration measurements conducted on board the vessel have revealed the majority of these operational and modal frequencies as presented in Table 3.1.

Stellenbosch University https://scholar.sun.ac.za

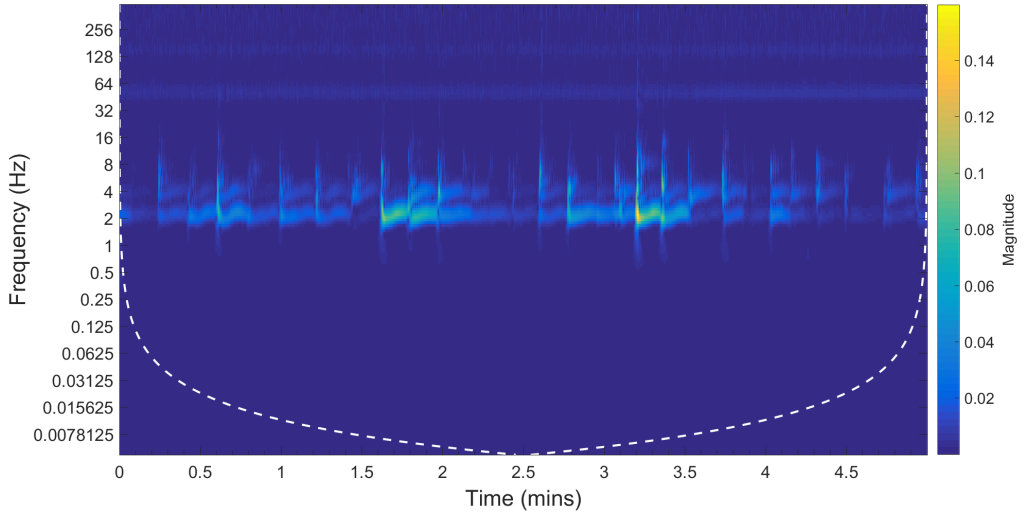

Figure 4.11: Scalogram representing wavelet transform of the sample data.

Fine scale analysis

In this analysis the "fine scale" refers to selecting a single frequency band, or scale (α) from the complex coefficient matrix to use for analysis. This also represents the data on a two-dimensional plane that can be processed and compared with results from the other algorithm. The logic behind this technique is that an impulsive event activates a broad spectrum of frequencies. Therefore, if the selected frequency band is free of operational and modal frequencies, the only reason for a peak in magnitude at said frequency would be as a result of an impulsive event (Yang & Ren, 2004), i.e. slamming.

It is required that the frequency band be selected that is clear of modal responses and machinery excitation, as per the approach of Yang & Ren (2004). In order to do this, the frequency spectrum of the vibration data was considered as per Table 3.1. Taking into account the vessel has a variable speed on its main shaft line, with a maximum rotational speed of 140 rpm or 2.33 Hz. This pushes the blade pass frequency to 9.33 Hz (seen in Table 3.1). Given the other, lower modal frequencies, the safest frequency band to select is higher than 9.33 Hz. An average Fast Fourier Transform (FFT) for the six sensors, at five time periods across both voyages, is presented in Figure 4.13. This provides a visualisation of the spectrum of frequencies already activate on the vessel. Between 10 and 12 Hz would be ideal, because it is low enough to still contain enough energy and miss

Stellenbosch University https://scholar.sun.ac.za

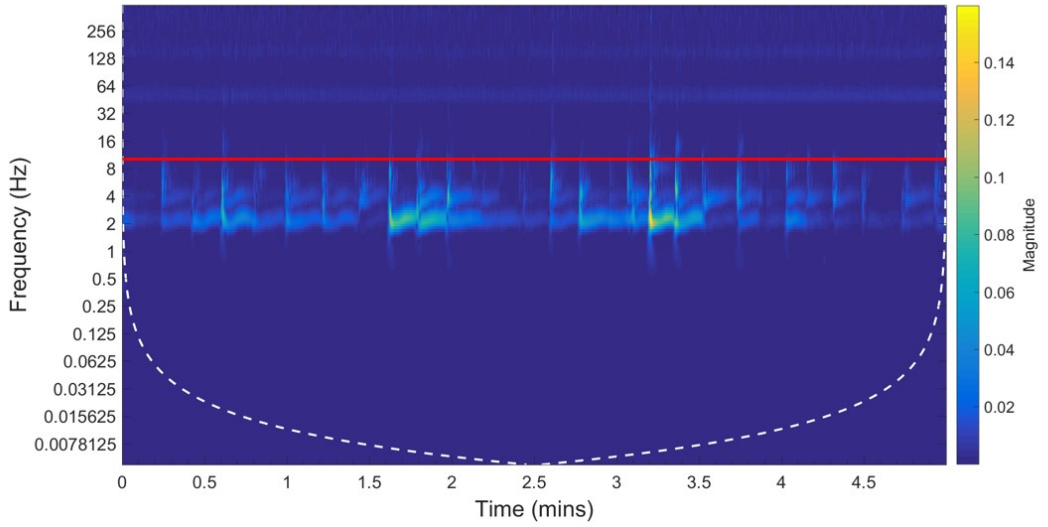

Figure 4.12: Scalogram representing wavelet transform of the sample data, with selected "fine scale" frequency band for analysis.

the diesel engines rotation frequency. Yet, it is high enough to miss the blade pass frequency for the propeller. From the plot (Figure 4.13) it can be seen that the energy around these frequencies shows to be decreasing, meaning that impulsive energy would be even more pronounced.

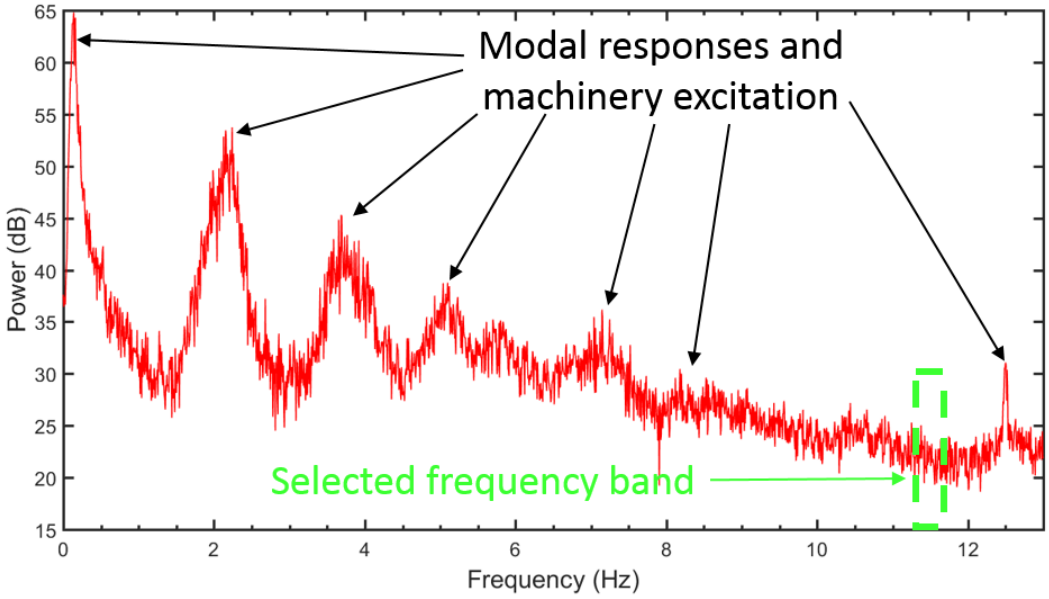

Figure 4.13: The average FFT across six sensors for five time intervals spanning both voyages.

Stellenbosch University https://scholar.sun.ac.za

The continuous wavelet transform output was plotted in the form of a scalogram in Figure 4.11. When looking at the data in this way it can be seen that the 11.5 Hz frequency band is clear (Figure 4.12) of other modal responses and machinery excitation frequencies, making it an ideal frequency band for this analysis.

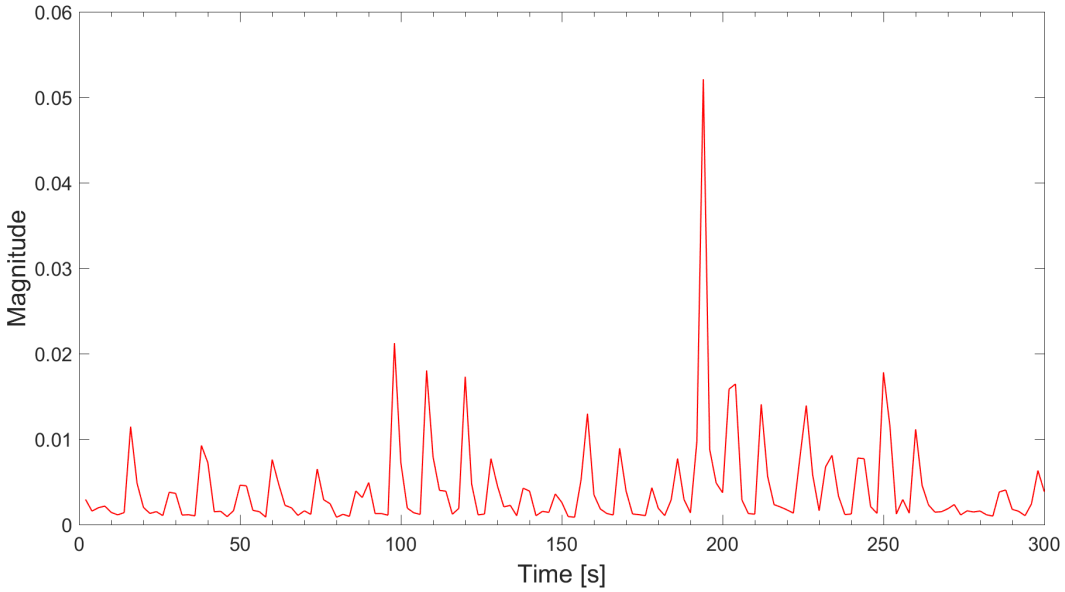

Figure 4.14: The fine scale absolute peak values, representing the sample signal in the frequency domain at 11.5 Hz, for two second time intervals.

Figure 4.14 shows the result of the fine scale operations described above, for the sample data in Figure 4.6. As can be seen in the graph there are many distinguishable peaks for the 2 second intervals. Given that these peaks appear in the otherwise "quiet" 11.5 Hz frequency band, the deduction is that they are as a result of impulses in the original signal. Proof of no other phenomenon exciting this frequency band can also be seen. Outside of the impulsive peaks, correlating with those in Figure 4.14 and 4.9, the magnitude remains low in the remaining time intervals. These peaks look to be more distinguishable than the peaks seen in Figure 4.9 for the time domain analysis. Comparing the location of peaks in Figure 4.14 with the impulses seen in Figure 4.6 it can be seen that they do look to line up in time.

Stellenbosch University https://scholar.sun.ac.za

4.4.3 Slam counting

For both the time and frequency domains the data analysis was performed in order to highlight the raised level of vibration during a slamming event. This section will explain how the thresholds are applied to the analysed data, as well as how slamming events will be counted using the global definition of slamming. The algorithm caters to the global definition for slamming by making use of the six sensors along the length of the hull on the starboard side, as described in the measurement set-up in Subsection 3.2.2.

$$\begin{bmatrix} 0 & 0 & 1 & 1 & \dots & 1 \\ 0 & 0 & 0 & 1 & \dots & 1 \\ 0 & 1 & 0 & 1 & \dots & 0 \\ 0 & 0 & 0 & 1 & \dots & 0 \\ 0 & 0 & 1 & 1 & \dots & 1 \\ 0 & 0 & 1 & 1 & \dots & 0 \end{bmatrix} \tag{4.7}$$

$$\begin{bmatrix} 0 & 1 & 3 & 6 & \dots & 3 \end{bmatrix} \tag{4.8}$$

The slam counting begins by creating a zero matrix of dimension, six by the number of time intervals. Each row of this matrix, one to six, corresponds to a sensor position on the vessel, bow to stern, respectively. The algorithm searches each sensor's analysed data and determines for which indices that sensor exceeds its threshold. The corresponding indices in the zero matrix are then made equal to one (Eq. 4.7). Each column of the matrix is now summed, giving a new row vector one times the number of time intervals, with the number of sensors that exceeded their respective threshold in each of the time intervals (Eq. 4.8).

For the purposes of accounting for the global effect, the row vector is then searched for where all six sensors exceeded their thresholds. These time intervals will be counted as slamming events in the data. The index of the vector corresponds to the time at which the event took place.

The chapters that follow will investigate the application of the algorithms described above and assess their performance. Algorithm results for the time and

Stellenbosch University https://scholar.sun.ac.za

frequency domains will be compared with one another, in order to determine which is more accurate for the identification of slamming events.

Stellenbosch University https://scholar.sun.ac.za

Chapter 5

Case studies

In the previous chapter an algorithm was developed using two different analysis methods, one in the time domain and one in the frequency domain. This chapter will investigate the performance of these algorithms on five independent case studies. The selection of these case studies is based on their high probability of containing slamming events. The case studies will then be searched visually in order to subjectively identify slamming events contained within them. The slams visually identified in these case studies will then be used to benchmark and validate the outputs from the algorithm.

5.1 Case study selection

The source data originates from roughly 80 days at sea, recording full-scale vibration data. This section details the selection process followed to narrow down the data and choose case studies. These case studies should clearly demonstrate local impacts with global excitation. It was decided to limit the case studies to a length of five minutes. This allows for easy visual verification of the algorithm results. The data used in order to select the case studies was the raw unfiltered signal, filtered after the selections were made.

Stellenbosch University https://scholar.sun.ac.za

5.1.1 Visual selections

The representation of voyage data in Figure 4.2 provides a good indication of what the ship structure was experiencing during various days of a cruise. By using the environmental and operational conditions around and for the vessel, an informed selection can be made of periods of time where slamming events are most probable. The correlation plot in Figure 5.1 shows a positive Pearson's Correlation of 0.75 and 0.71 between bow r.m.s. and stern r.m.s. level and the swell height respectively. The other variables don't have quite as strong correlations. The Pearson's correlation gives an indication of the extent to which two variables are linearly related (McKillup, 2012). The correlation between r.m.s. and H_{swell} is what is expected based on the trends seen in Figure 4.2a. The correlation between peaks for the bow and stern with respect to ship speed is not as was expected, based on the trends seen in Figure 4.2b.

It was expected to see a strong positive correlation between the bow peak values and ship speed. While it was expected to see a notable negative correlation between the stern peak values and the ship speed. The correlation between the bow and stern peaks with wave height was positive but not high enough to be significant. The reason for this could be that the expected correlation only exists for excessive swell heights. That said, the wave height seems to be the most significant variable in terms of its influence on the vibration levels. Similar correlations could be seen in the high-pass filtered data.

A total of 21 selections, for 24 hour or less time periods, were made visually using the above described observations to select periods of time for probable slamming. Bow and stern vibration data, from the starboard sensors, for these times were then compiled. These sections of data were designated "visual selections". The time signals were then plotted in order to visually identify the presence of local impacts with global tendencies.

Figures 5.2 and 5.3 present a visual selection made on 03/07/2017, during the winter cruise 2017. This data was extracted from a time during a scientific station, when the ship was stationary. Impacts at the stern can be seen by the impulsive vertical green lines in Figure 5.3. The zoomed in window shows definite impulses reaching 1 to 1.5 g, followed by exponential decay. Correspondingly,

Stellenbosch University https://scholar.sun.ac.za

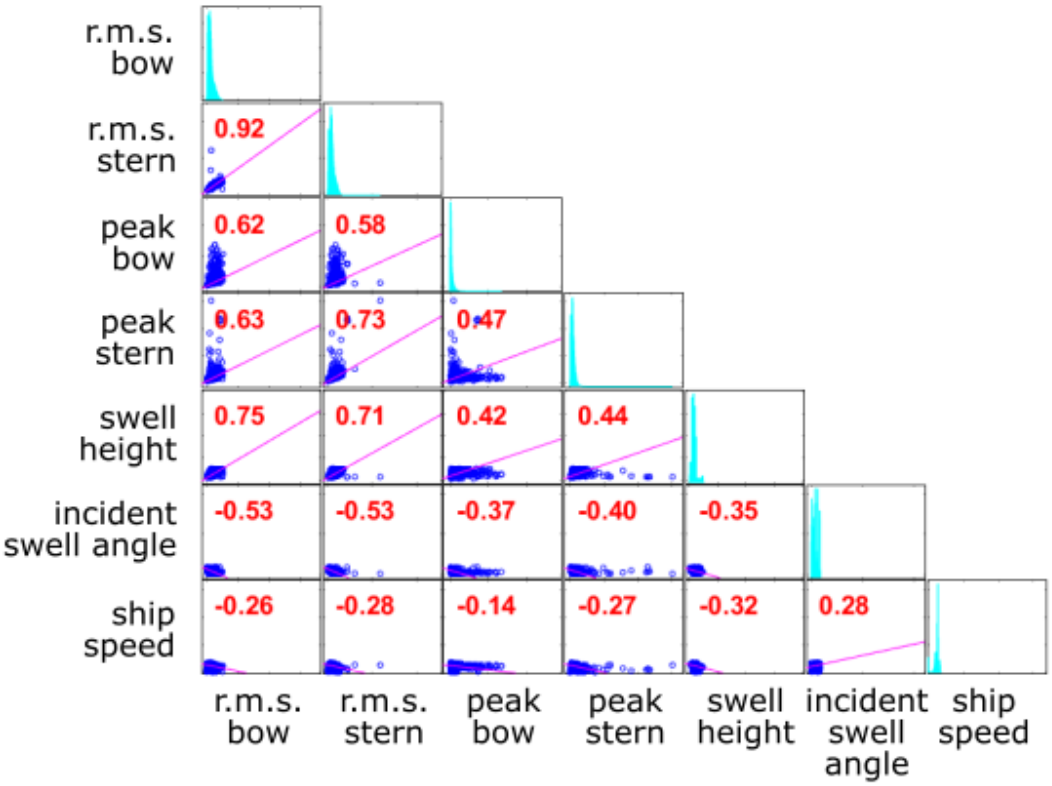

Figure 5.1: Correlation matrix between variables r.m.s. bow and stern, peak bow and stern, swell height, incident swell angle and ship speed.

Figure 5.2 also contains impulsive vertical blue lines recorded at the bow (120 m away). This provides an indication that these impacts are demonstrating a global response in the structure. The zoomed in section in Figure 5.2 shows the now typical impulsive peak, with the peak being 50% less than the stern peak for the same time range. The magnitude of the vibration at the stern, coupled with the fact that the ship is stationary, gives a good indication as to the location of the impact site. From these 21 selections of data, narrower sections of time were selected. This was done by inspecting the signals as described above.

Stellenbosch University https://scholar.sun.ac.za

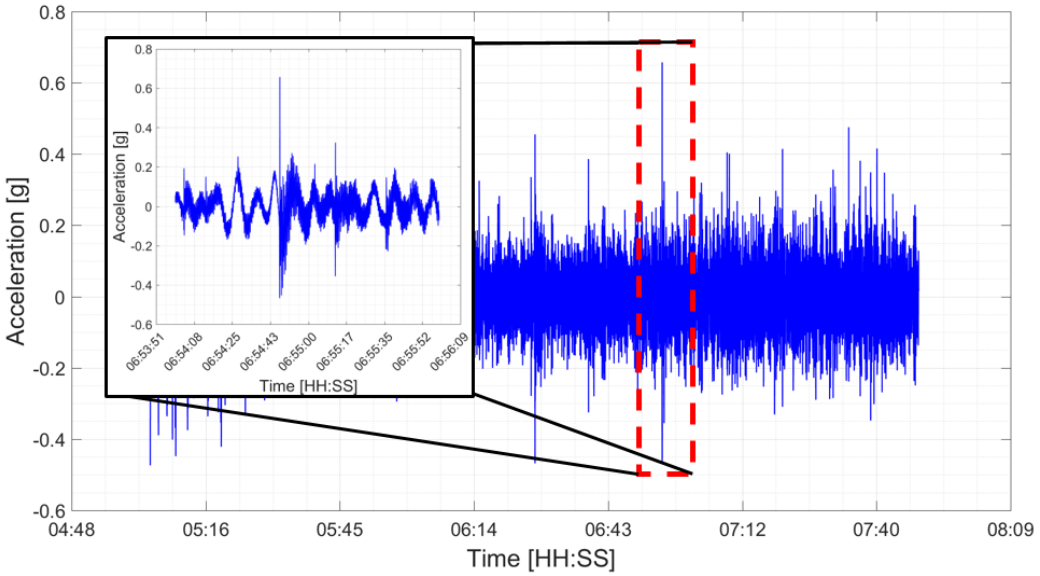

Figure 5.2: A visual selection of possible slamming data (03/07/2017), using bow acceleration

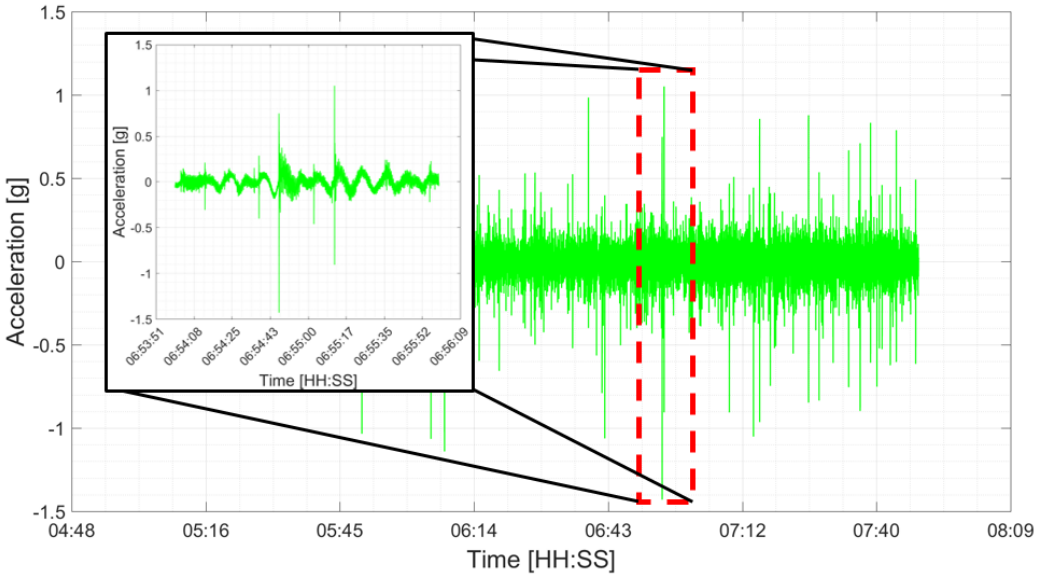

Figure 5.3: A visual selection of possible slamming data (03/07/2017), using stern acceleration

Stellenbosch University https://scholar.sun.ac.za

5.1.2 Possible case studies

The narrower time sections selected above, spanned no longer than one hour. For these selections, data along the length of the vessel was used, bow to stern, for six sensors in the hull. Based on observations from Section 4.1 it was seen that the ship's heading to the swell was not always 0 degrees. Because of this, the data from both port and starboard sensors were plotted to capture the impact signals, making it 12 sensors in total (six locations along the length of the hull, both port and starboard). These data sets were designated "possible case studies".

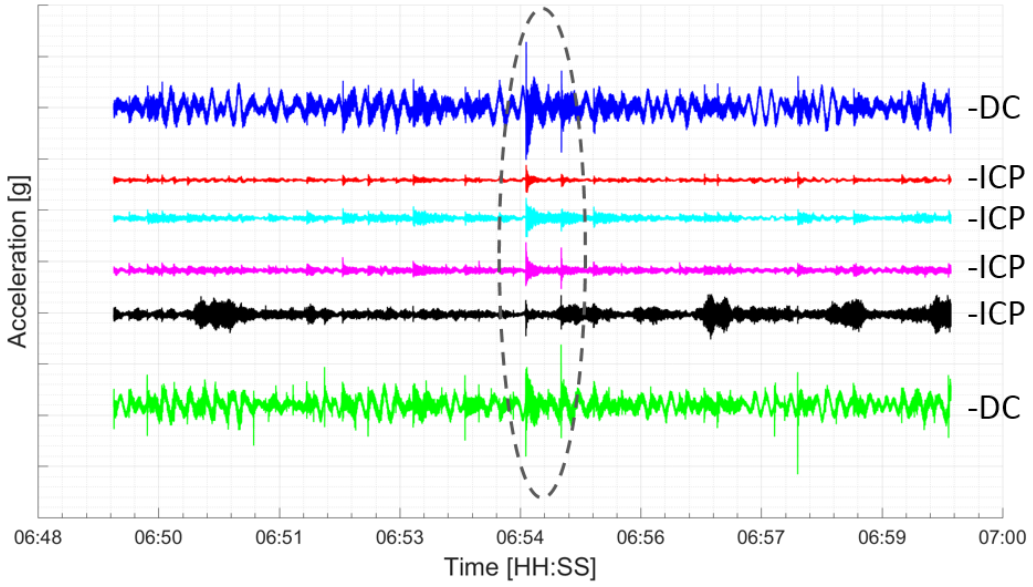

Figure 5.4: Port signals for a possible case study from 03/07/2017; bow cargo hold fwd cargo hold aft fresh water room stern thruster room stern.

Figure 5.4 is the vibration data for the port side of the vessel and Figure 5.5 is the vibration data for the same time on the starboard side of the vessel. These time signals were plotted in order to identify a local impact, but also important here, the global response seen along the length of the vessel. The global response can be seen by the impulse followed by an exponential decay at all locations from bow to stern. The circled features in Figures 5.4 and 5.5 clearly show how the local responses from each sensor align in time to demonstrate the structural global

Stellenbosch University https://scholar.sun.ac.za

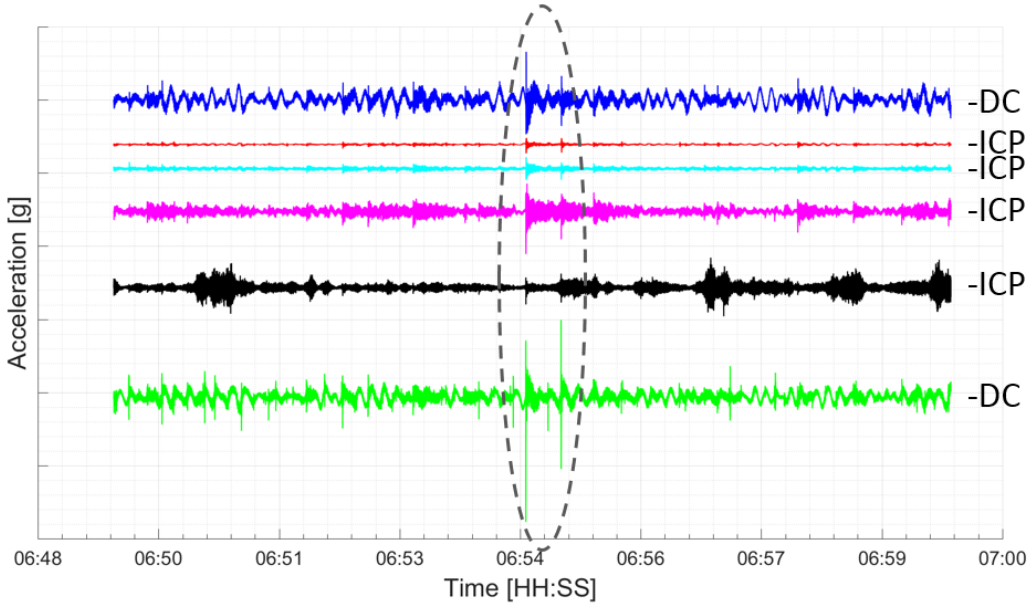

Figure 5.5: Starboard signas for a possible case study from 03/07/2017; bow cargo hold fwd cargo hold aft fresh water room stern thruster room stern.

response of the vessel. Here it could be seen that the structural response data from port to starboard does not typically vary much. The magnitudes may vary slightly between port and starboard depending on the incident angle of the impact. The characteristics that are trying to be detected and counted, however do not vary. Therefore for the purposes of achieving the aims of this project, to identify and count slamming events, data from only the starboard side of the vessel will be used further.

5.1.3 Case studies

The final selection of case studies was also made visually. Selections from the above "possible case studies" were made based on identifiable local impacts, global responses as well as the maximum number of slams that could be captured in a five minute time period. It was decided to select five, five minute case studies. This should capture a range of different slamming events, which would allow the algorithm to see slams under a range of varying conditions. These data sets were now designated "case studies" and would be used to validate the algo-

Stellenbosch University https://scholar.sun.ac.za

rithm.

Table 5.1 shows where each of the chosen case studies came from. It was decided to use slamming cases from both the Antarctic relief 2016/2017 and winter cruise 2017. In order to view the case studies in perspective with the environmental and operational data, Table 5.2 shows this data for each case study.

Table 5.1: Chosen case studies

Case Study	**Duration**	**Date**	**Start time (UTC)**
Case study 1	5min	26 Jan 2017	09:58:00
Case study 2	5min	28 Jan 2017	20:39:00
Case study 3	5min	02 Jul 2017	19:42:30
Case study 4	5min	29 Jun 2017	16:22:00
Case study 5	5min	05 Jul 2017	01:10:30

Table 5.2: Summary of the environmental and operational conditions during each of the case studies.

Case Study	H_{swell}	T_{swell}	v_{ship}	$\phi_{incident}$
Case study 1	6.5 m	6 s	9.5 kn	3.6 deg
Case study 2	- m	- s	- kn	- deg
Case study 3	5.0 m	10 s	14.0 kn	41.4 deg
Case study 4	4.3 m	8 s	0.4 kn	15.0 deg
Case study 5	6.2 m	9 s	7.4 kn	25.6 deg

The case studies were selected dependent on the clearest slamming events that could be identified. Given that the systems collecting data on the environmental and operational conditions were independent of the vibration data collection, loss of data was an unfortunate occurrence. This is the reason case study 2 has no environmental and operational statistics. This was the nature of long term full-scale measurements.

Figure 5.6 shows an example of a selected case study (case study 2). Slams can clearly be seen to occur on top of the low frequency oscillations. As discussed previously the algorithm will use data that has been high pass filtered. This is because the low frequency magnitude will impact the magnitude of an impulsive peak. Figure 5.7 shows the filtered case study 2, as can be seen, the impulses become a lot more pronounced without the presence of rigid body motion.

Stellenbosch University https://scholar.sun.ac.za

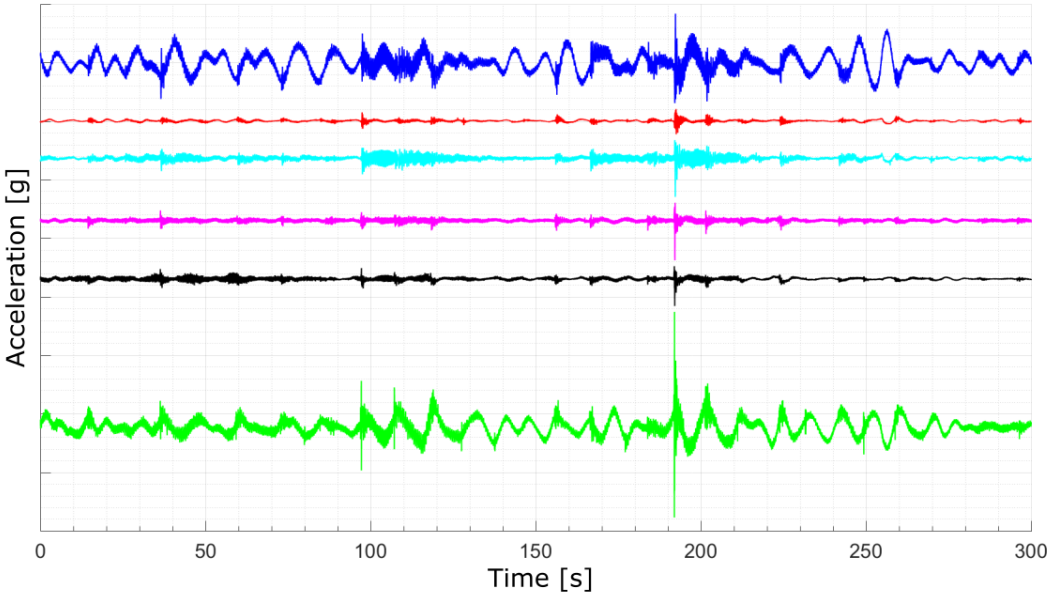

Figure 5.6: Unfiltered signals for case study 2; bow cargo hold fwd cargo hold aft fresh water room stern thruster room stern.

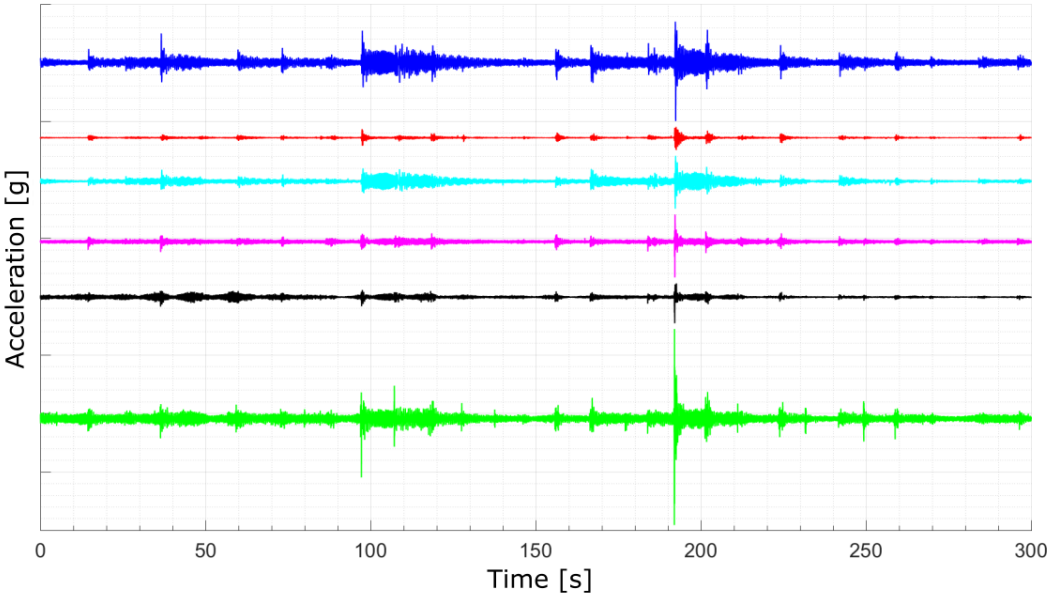

Figure 5.7: Filtered signals for case study 2; bow cargo hold fwd cargo hold aft fresh water room stern thruster room stern.

Stellenbosch University https://scholar.sun.ac.za

5.2 Manual counts

As a starting point for analysing the case studies, a subjective manual slamming count was performed. This was done through visual inspection of the acceleration vs. time signals. This was based on the technique used in a previous study by Omer (2016), and therefore will be used to benchmark the slam counts for the case studies. Slams in the case studies were counted by investigating the impact site for impulsive events at either the bow or stern (position one in Figure 5.8). The structural response along the length of the vessel was then looked for (position two in Figure 5.8).

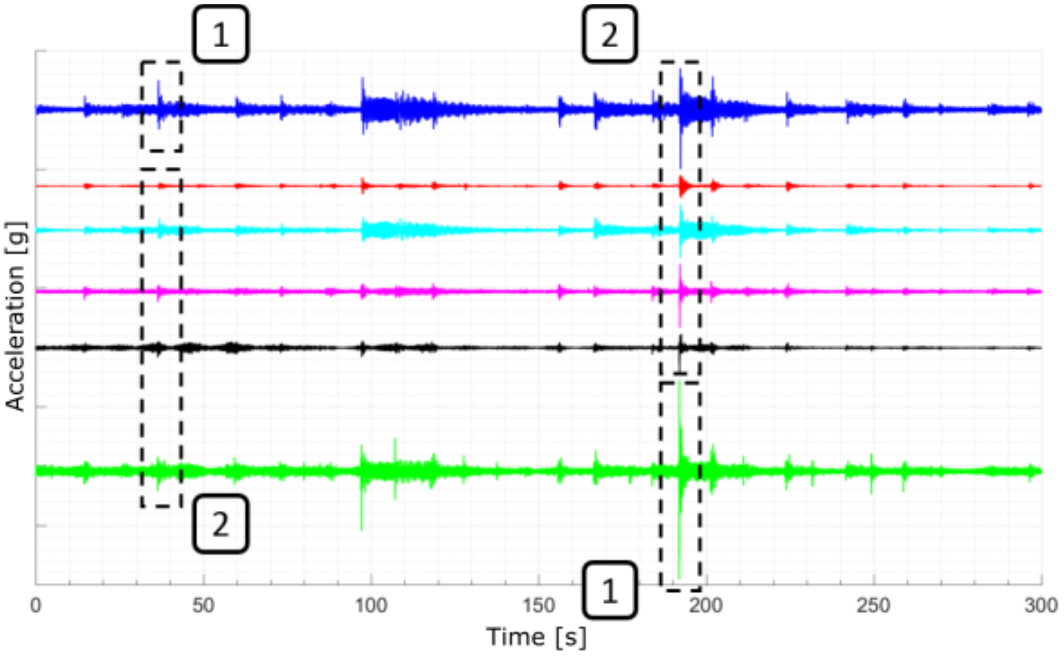

Figure 5.8: Explanation of manual counting on case studies; bow cargo hold fwd cargo hold aft fresh water room stern thruster room stern.

A structural response, in this case, was defined as a distinct disturbance from equilibrium seen across all five of the sensors marked by position two in Figure 5.8. These perturbations should line up vertically in time with the impulse registered at either the bow or stern. Therefore six out of the total six sensors should register a disturbance. The stringency of this selection criteria is in order to be

Stellenbosch University https://scholar.sun.ac.za

conservative in the detection of an event. Table 5.3 shows the slam counts for each case study.

Table 5.3: Manually counted slams for case studies.

Case study	$\mathbf{z_{manual}}$
Case study 1	14
Case study 2	18
Case study 3	15
Case study 4	19
Case study 5	16

5.3 Testing the algorithms

In this section the case studies will be discussed in the context of the algorithms developed in Section 4.4. The case studies will be run through the two objective algorithms and the results examined. First, the algorithm was applied in the time domain and then applied in the frequency domain. The algorithm should highlight extreme events in the signal, which are indicative of impulsive events. It then searches over multiple sensors to look for extreme events that occur in the same time interval, identifying these events as slamming events. This seeks to mimic the manual process described in Section 5.2.

5.3.1 Time domain

The application of the algorithm in the time domain refers to Subsection 4.4.1. Here the absolute peak values in the data are collected for every two second interval. Using the sample case study in Figure 5.8, the output from the analysis is shown in Figure 5.9. The interval peaks for the case studies can be seen to typically align in time, as represented by the encircled data in the figure. This is expected from what was seen in the original case study data.

The slam counting section of the algorithm was run on the case study interval peaks to locate slams and count them. The time domain thresholds, from Table 4.4, are applied to each sensor. This could prove tough, looking at Figure 5.9 there

Stellenbosch University https://scholar.sun.ac.za

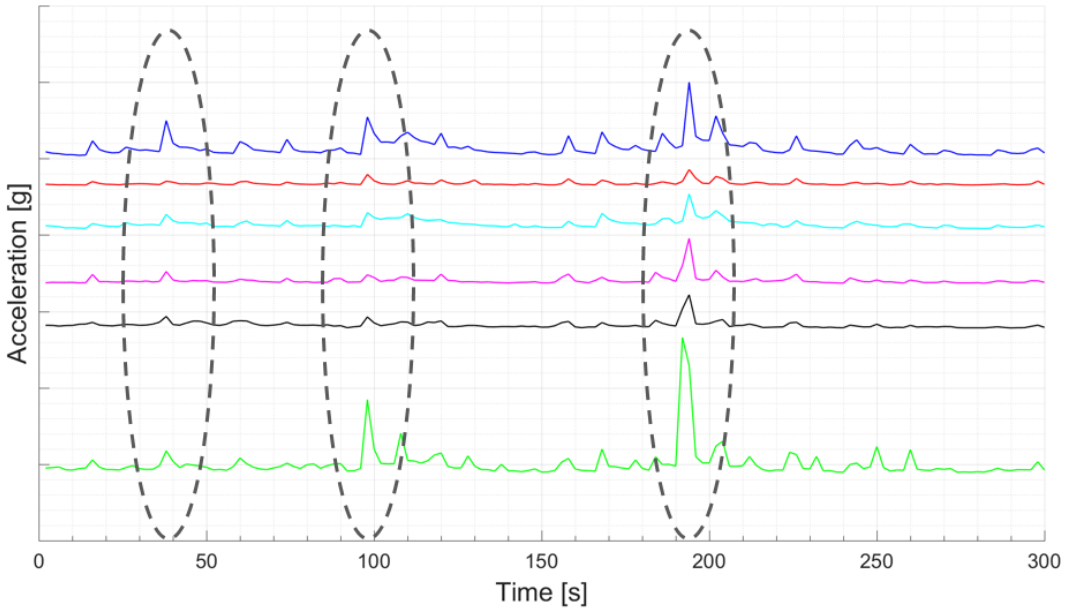

Figure 5.9: Time domain representation of the sample case study; bow cargo hold fwd cargo hold aft fresh water room stern thruster room stern.

are clear peaks rising and falling to and from a base line. Other peaks rise and do not fall back to the same base line before rising again. These are considered times of large and frequent slamming events where the vibration is so large in nature that the level does not return under the threshold before another slam occurs. This may result in the algorithm counting the same event more than once. The counting of slams was given the same condition as in Section 5.2, with the manual counts. All six of the sensors must register a breach in threshold in order to be counted as a slamming event. The number of slams counted in the time domain, per case study can be seen in Table 5.4, where z is the counted number slams.

Table 5.4: Time domain algorithm slam counts for case studies.

Case study	$\mathbf{z_{time\ domain}}$
Case study 1	8
Case study 2	18
Case study 3	22
Case study 4	10
Case study 5	20

Stellenbosch University https://scholar.sun.ac.za

5.3.2 Frequency domain

For this application of the algorithm the data is transformed into the frequency domain, as described in Subsection 4.4.2. Here peak values in the data are again collected for every two second interval. Using the sample case study introduced above, the output from the analysis is shown in Figure 5.10. The peaks seen here all correspond to the 11.5 Hz frequency band of the case study data. The peaks in the data can also be seen to align in time, which points to the presence of a global event.

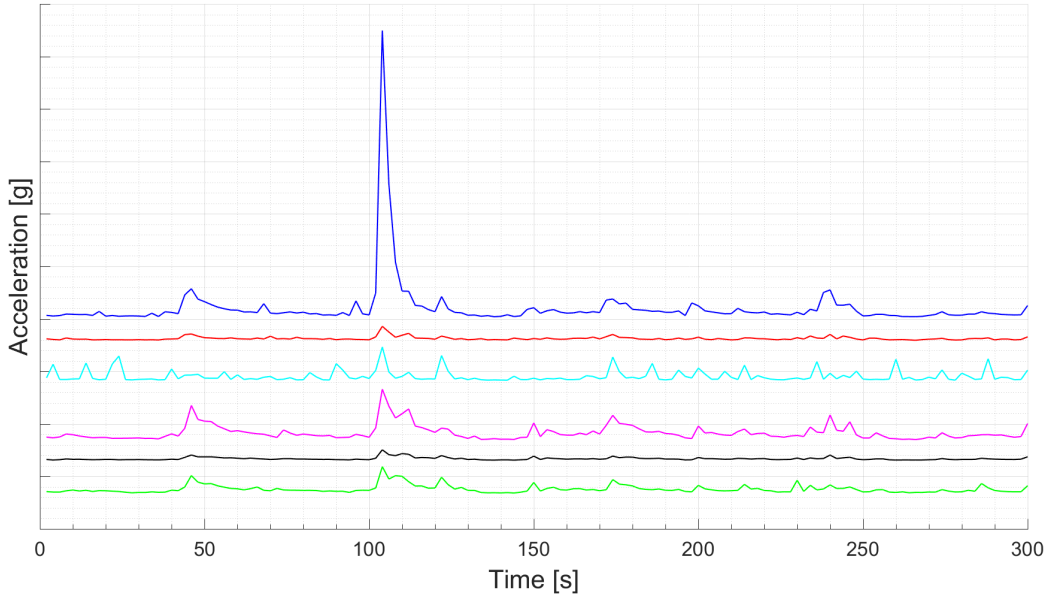

Figure 5.10: Frequency domain representation of the sample case study; bow cargo hold fwd cargo hold aft fresh water room stern thruster room stern.

The slam counting section of the algorithm was run on the frequency domain case studies to locate slams and count them. The values, from Table 4.6, are used as thresholds for each sensor. The counting of slams was given the same pass criteria as in Section 5.2, with the manual counts. All six sensors must register a breach in threshold in order to be counted as a slamming event. Table 5.5 presents the slams counted by this algorithm, where z is the counted slams. All results will be summarized in the following Section 5.4.

Stellenbosch University https://scholar.sun.ac.za

Table 5.5: Frequency domain algorithm slam counts for case studies.

Case study	$z_{\text{frequency domain}}$
Case study 1	18
Case study 2	50
Case study 3	20
Case study 4	15
Case study 5	26

5.4 Results

This section will discuss the results from the detection and counting of slamming events in the selected case studies. The slam counts for the case studies using both the time and frequency domain algorithms are shown in their respective sections above. Below, Table 5.6 summarizes all of the slamming counts. This table shows the slam counts using the manual count, of an experienced observer, as a benchmark for the algorithm outputs. A true positive (TP) is the number of slams that were located and counted by both methods. A false positive (FP) is the number of slams detected by the algorithm that were not detected in the manual count. A false negative (FN) is the number of slams that were detected in the manual count but not by the algorithm. True negatives (TN) were not considered in the presentation of the results. This is because the aim of the algorithm is concerned with the positive detection of slamming events. The number of non-events is not of importance, therefore to keep the presentation of the results as simple as possible the true negatives are omitted.

The total number of slams counted by the manual count can then be seen as $TP+FN$. The total number of slams counted by the respective algorithms can be seen as $TP+FP$. As a performance criteria for the algorithm the true positive rate (TPR) and the positive predictive value (PPV) are introduced. The TPR of the algorithm can be determined by $TP/(TP+FN)$. This is the percentage of slams detected out of the total number of slams manually counted. The PPV of the algorithm can be determined by $TP/(TP+FP)$. This is the percentage of correctly identified slamming events contained within the slams detected by the algorithm.

Looking at the results for each of the case studies it can been seen that there is a

Stellenbosch University https://scholar.sun.ac.za

Table 5.6: Slamming detection results for case studies using two second intervals.

Time domain				**Frequency domain**				
		TPR	**PPV**			**TPR**	**PPV**	
TP = 6	FP = 2	43%	75%	TP = 9	FP = 9	64%	50%	**Case study 1**
FN = 8				FN = 5				
TP = 9	FP = 9	50%	50%	TP = 17	FP = 33	94%	34%	**Case study 2**
FN = 9				FN = 1				
TP = 12	FP = 10	80%	55%	TP = 9	FP = 11	60%	45%	**Case study 3**
FN = 3				FN = 6				
TP = 8	FP = 2	42%	80%	TP = 11	FP = 4	58%	73%	**Case study 4**
FN = 11				FN = 8				
TP = 8	FP = 12	50%	40%	TP = 13	FP = 13	81%	50%	**Case study 5**
FN = 8				FN = 3				

lot of variation. The variation can exist for multiple reasons. There could be bigger slams triggering higher levels of vibration at one time over another, causing a higher peak to "leak" into the adjacent time interval. Looking at the environmental and operational data for each case study (Table 5.2), the H_{swell} is not notably different for each case study. A difference does come in with a higher T_{swell} and v_{ship} for case study 3, particularly. The T_{swell} could play a roll in spacing slams further apart, making them easier to isolate and detect, causing TPR to be higher. While an increase in v_{ship} would cause higher vibration levels, causing more peak "leakage" to adjacent time intervals, causing the PPV to decrease.

The time domain implementation of the algorithm shows that on average only 53% of the slamming events will be detected, according to the TPR. The PPV value shows that on average 60% of the total number of slams detected by the algorithm are accurately identified. In comparison, the frequency domain implementation of the algorithm shows that on average 71.5% (TPR) of the slamming events will be detected. While, the PPV shows that on average 50.5% of the total number of slams detected by the algorithm are accurately identified. The performance of the algorithm is dependant on the maximisation of the TPR and PPV.

Stellenbosch University https://scholar.sun.ac.za

5.5 Algorithm evaluation

The performance of the algorithms above needs to be maximised, to this end the TPR and PPV metrics are to be evaluated. Two subjective choices were made in order to analyse the data thus far. Namely; the threshold multiplication factor, k, in equation 4.5 for the threshold calculation and the interval size selection in Subsection 4.3.1, referred to here as t. Using Figure 5.11 various time intervals and k values were evaluated with regards to their influence on algorithm TPR and PPV values. Figure 5.11a shows the performance of the algorithm in the time domain, while Figure 5.11b shows the performance of the algorithm in the frequency domain. The various time intervals are colour coded, while TPR and PPV are represented by the solid and broken line respectively.

What is noticeable here is that, overall, the TPR is inversely proportional to both t and k. PPV, on the other hand is directly proportional to both t and k. It makes sense that for a lower k there is a better possibility of detecting more of the total slams, but there is an increased uncertainty as to whether the detected slams are TP. The opposite is true for higher k values. The similar trend seen for varying values of t also makes sense when considering the phenomenon described in Section 5.4, peak "leakage" due to elevated levels of vibration. Based on the data presented here, a point of intersection between the TPR and PPV lines, for a single value of t, would give the most effective variables for the algorithm.

While generating these results it was noted that, for $t = 6$ s, there were occurrences when two slams were separated by less than six seconds. This would be an undesirable inaccuracy in the algorithm that can easily be avoided by keeping t below this level. Not all of the points of intersection are visible in Figure 5.11, therefore the approximate location of these points can be inferred based on the trends in the data. Evaluating the remaining data it can be seen that the most effective point of intersection lays in Figure 5.11b, where $t = 4$ s. Therefore, in order to most effectively proceed with this algorithm, the analysis should be done in the frequency domain with $t = 4$ s and $k = 2.5$. These variables should then lead to highest TPR and PPV values possible.

Stellenbosch University https://scholar.sun.ac.za

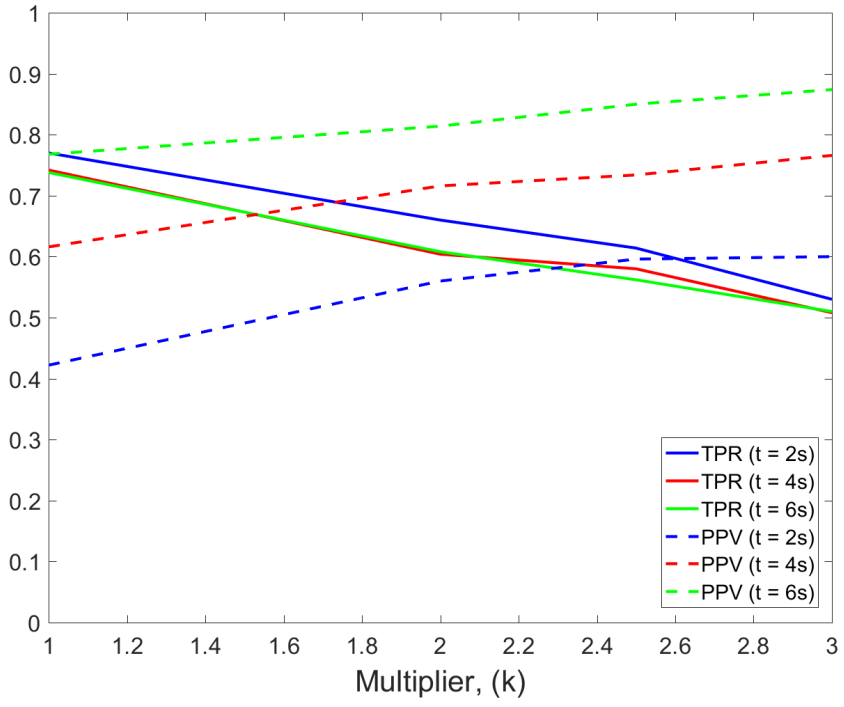

(a)

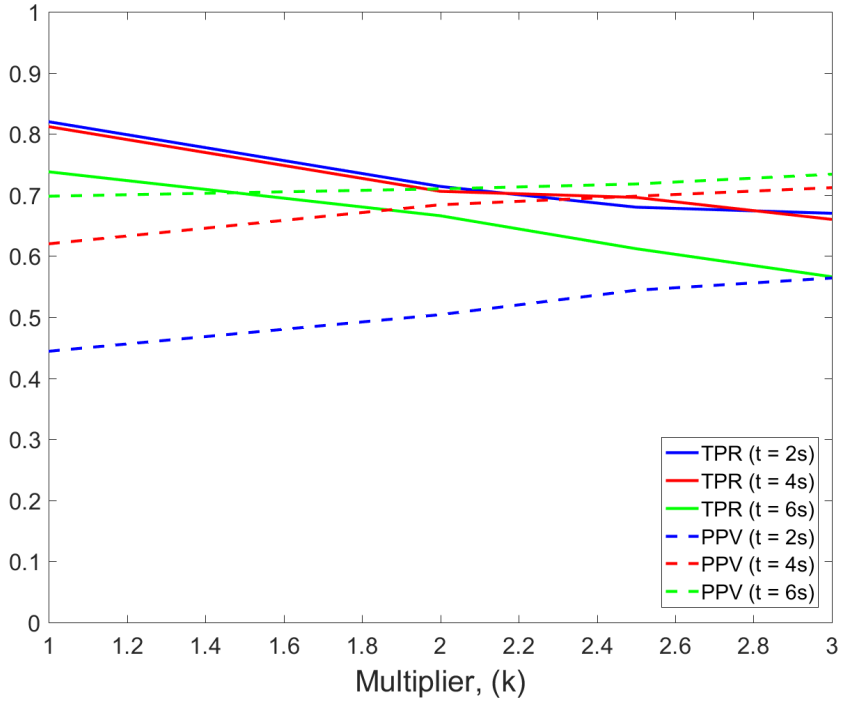

(b)

Figure 5.11: Subjective variable influence on algorithm performance: (a) Evaluation of subjective variables in the time domain, (b) Evaluation of subjective variables in the frequency domain.

Stellenbosch University https://scholar.sun.ac.za

Chapter 6

Winter cruise 2017

The need now exists to implement the algorithm using a larger data set, to represent a more practical scenario. The case studies that were used before served the purpose of benchmarking and refining the slamming detection algorithm. This chapter will observe the implementation of the algorithm on a larger data set, namely the entire Winter cruise 2017 data set (as described in Subsection 3.4.2). This data set has no benchmark with which to compare the outcome, and would be typical of a practical implementation of the algorithm with no supervision. The outputs from this analysis will be compared with the environmental and operational variables from the cruise. Using this comparison the performance of the algorithm can be evaluated based on what is already known about slamming.

6.1 Analysis

Based on the discussion in Section 5.5 the detection and counting algorithm used in this chapter was implemented in the frequency domain. As was demonstrated, the best compromise between the TPR and PPV of the algorithm can be achieved by dividing the fine scale, wavelet transform data into four second time intervals, while applying a threshold with a k multiplier equal to 2.5.

The Winter cruise 2017 is of particular interest because of the harsh weather encountered during this voyage. From the on-broad accounts, slamming was con-

Stellenbosch University https://scholar.sun.ac.za

sistently present throughout the voyage, making this data set a good candidate for detecting slamming events. The data from the Winter cruise was collected over a period of 16 days, and spans 350 hours of recording time. This data was recorded at 2048 Hz and down sampled to 1024 Hz for the purposes of this algorithm. This data was run through the wavelet transform and fine scale analysis, as described in Section 4.4.2, extracting 11.5 Hz frequency band.

The results for the slamming detection algorithm are presented below and will show the relationship between the frequency of detected slamming events, environmental and operational variables.

6.2 Results

The data was run through the algorithm using the above mentioned parameters in order to refine the algorithm. This slamming detection and count resulted in 11 931 slamming events being detected, 3.8% of the voyage. That is more or less 13.5 hours of consistent slamming. There is no way of looking at this number in isolation and evaluate the performance of the algorithm for this data. For this reason the detected slams are summed into 10 minute batches. This generates a count density over time, and allows the detected slams to be plotted against the environmental and operational variables.

6.2.1 Visual deductions

Figure 6.1 shows the results for the slamming detection algorithm for the Winter cruise voyage. The upper most panel shows the slam counts for 10 minute intervals. Moving downwards the next panel is wave height, then ship speed, then incident swell angle (as defined in Section 4.1) and finally, swell period in the last panel. The data shown is synchronised over time and covers 11 days during the cruise. This section of time is plotted for explanation purposes. The full voyage plot can be found in Appendix D. In Figure 6.1 there are encircled sections of time labelled one to four. These time sections will be used to point to features in the results in order assess the performance of the algorithm.

Stellenbosch University https://scholar.sun.ac.za

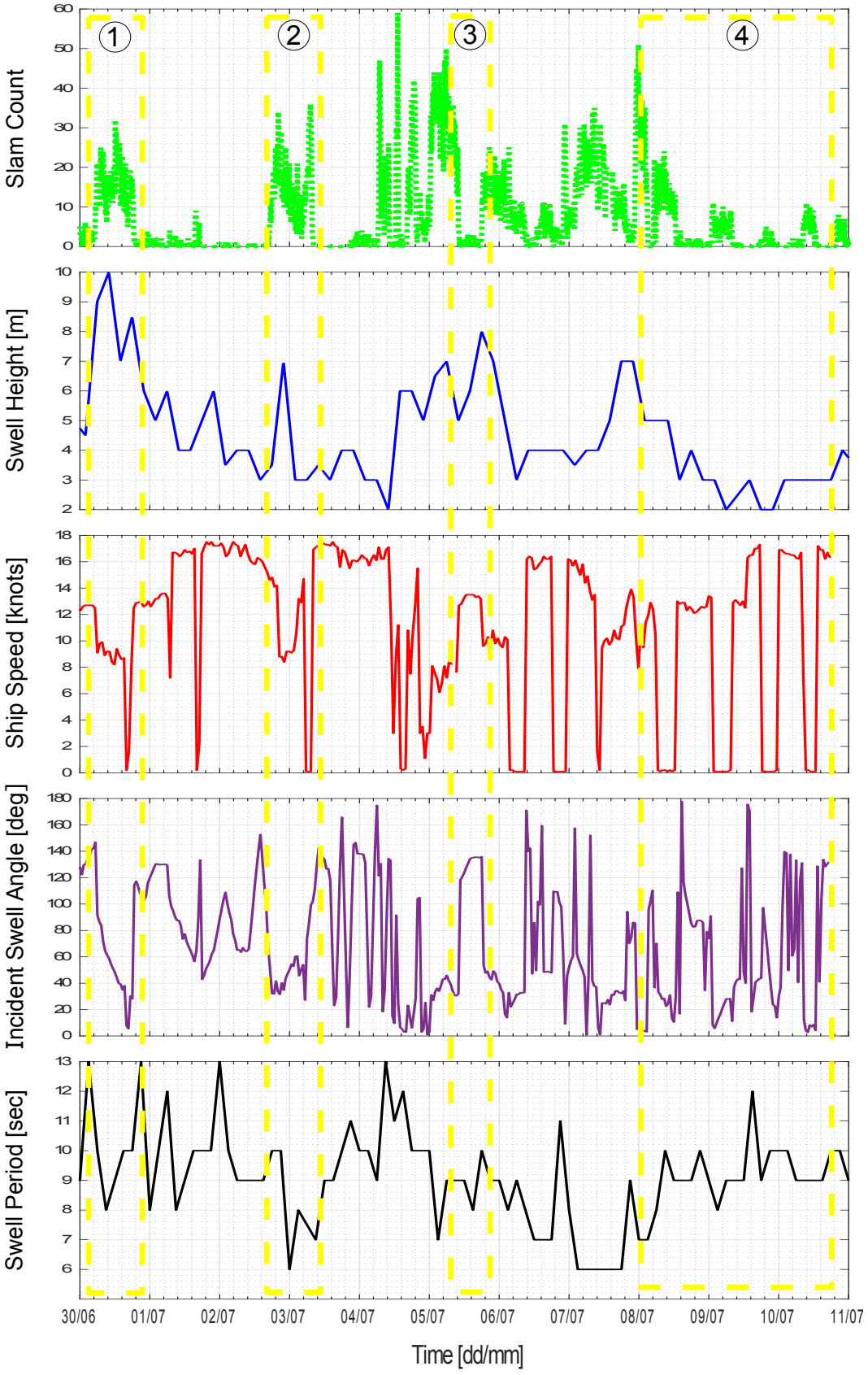

Figure 6.1: Result of slamming counts over a section of the Winter cruise 2017 voyage, compared with the environmental and operational variables from the same time.

Stellenbosch University https://scholar.sun.ac.za

In a general view of all of the data over time the slams counts do seem to follow trends in the other variables. This is already an indication of the algorithm detecting slams as would be expected. Upon closer inspection, in highlighted section 1, the swell height reaches a maximum of 10 m for the cruise. The slam count for the same time can be seen to elevate as high as 30 slams per 10 min batch. The slam count remains elevated until the swell subsides again. The slam count is then significantly less during the subsequent smaller swell state.

There are also odd occurrences, seen typically in highlighted section 4, during seemingly calm swell, where the slam count peaks. These peaks are not explained by large swell, therefore there must be another driver other than swell height. During these peaks the ship speed decreases to zero. This seems to explain the presence of the peaks seen in slam counts. Unfortunately the algorithm does not yet cater for categorizing slams as either bow or stern. However, from what is known about slamming conditions these slam counts have a high probability of being stern slams.

The elevated slam counts seen in highlighted section 1, for example, occur while the ship is moving forward. The swell height for the same time is also elevated. This points to a high probability of the ship experiencing bow slamming. A reduction in speed during highlighted section 1 is also proof of the crew's efforts to avoid harsh slamming during large swell states. During highlighted section 3 it can be seen that there is an increase in ship speed as well as swell height, yet the slam count remains low. This does not fit the trends seen until now.

Not all of the trends seen in the slam counts can be accounted for by the swell height and ship speed alone. In highlighted section 3 it can be seen that the incident swell angle increases, meaning that the swell is effectively coming from behind the vessel. As long as speed is maintained at this swell angle the vessel seems to avoids a high slam count during this time. At other times the slam counts can be seen to increase in frequency as the vessel is changing its incident swell angle (near vertical purple lines). This is typically when the vessel is forced to maintain a certain course for navigation or scientific activities. Highlighted section 3 though, is typical of another time where the crew would maintain a heading (not necessarily on course) in order to avoid harsh slamming conditions and increase the level of human comfort on-board.

Stellenbosch University https://scholar.sun.ac.za

During the testing of the algorithm on the case studies it was seen that the swell period could have an effect on the detection of slams. The last panel in Figure 6.1 show the swell period over time. From this data it can be seen that the period remains between 8 and 10 seconds for the majority of the voyage. During times of increased or decreased period there is no visible causality between swell period and slams counted.

What is noticeable is that during elevated swell heights, the swell period seems to decrease. This could have an effect on slam counts based on the fact that, with the increase in swell frequencies (decrease in swell period) there should be an increase in slamming count. By looking at the ship speeds though, the crew do seem to compensate for this effect by decreasing ship speed. This keeps the vessel's rigid body frequency more consistent during the voyage, instead of increasing or decreasing with the period of the swell itself.

The algorithm is tuned in order to give a TPR and PPV of 70%. Meaning, there still exists a certain level of unknown in the results of the algorithm, pertaining to slam counts. The periods of time during the voyage when slam counts increase and decrease are considered to be accurate. The actual number of slam counts can be considered valid within a 70% certainty, this is dictated by the limitations of the algorithm.

6.2.2 Multivariate statistics

A principal component analysis (PCA) was used to determine relationship between all variables and the number of slam counts detected by the algorithm. Slam counts were again determined for every 10 minutes and all measured environmental variables were averaged for every 10 minutes. In order to ensure that the variance of the measured variables in the dataset was uniform, the data for each variable was scaled about their respective mean values before the PCA was done.

The first four components of the PCA explained more than 90% of the variability with a fifth component having a minimal contribution. Component one explains 33% and component two cumulatively explains 56% (Table 6.1). Based on the

Stellenbosch University https://scholar.sun.ac.za

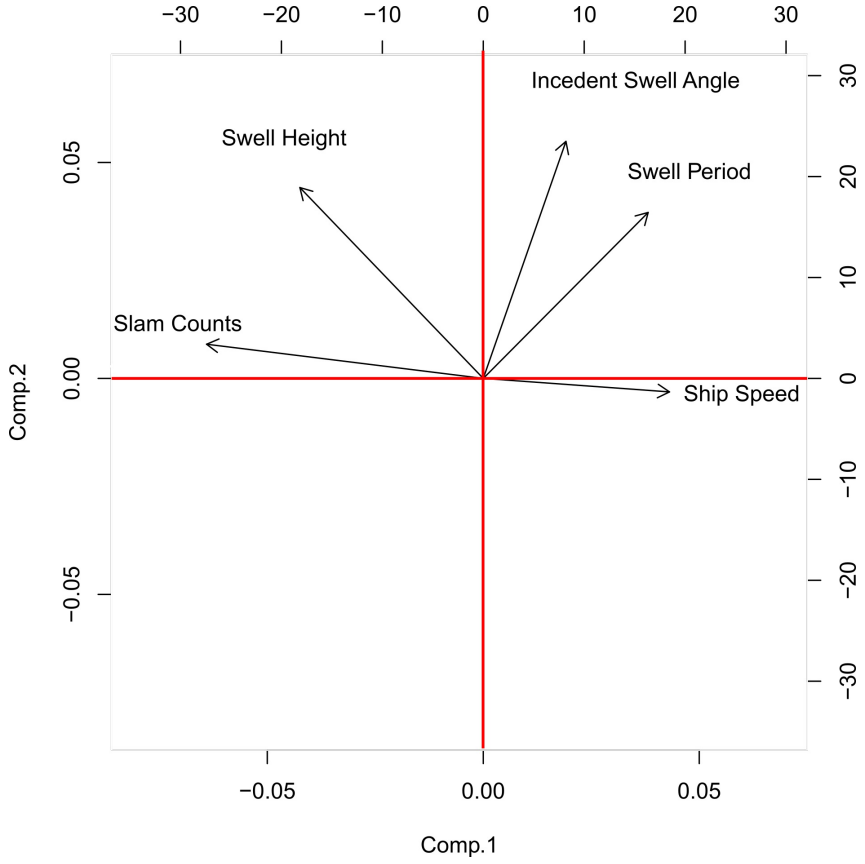

Figure 6.2: Principle component analysis for the multivariate data.

PCA the variables with the highest loadings in the components were slam counts and swell height (Table 6.2 and Figure 6.2). From this PCA it is clear that swell height has the greatest positive effect on the number of slams that were counted out of all the variables. Ship speed on the other hand can be seen to have the greatest negative effect on the slam count as well.

Table 6.1: The standard deviation, proportion of variance and cumulative proportion of all principal components in the PCA.

	Comp 1	**Comp 2**	**Comp 3**	**Comp 4**	**Comp 5**
Standard deviation	1.294	1.066	0.952	0.897	0.689
Proportion of variance	0.335	0.227	0.182	0.161	0.095
Cumulative proportion	0.335	0.562	0.744	0.905	1.000

From the results of the PCA above it can be seen that there is no significantly large relationship between any two variables. The variables seem to be closely

Stellenbosch University https://scholar.sun.ac.za

Table 6.2: The variable loadings for the first four principal components that explain more than 90% of the variability.

	Comp 1	**Comp 2**	**Comp 3**	**Comp 4**
Slam Count	-0.654	0.098	0.109	-0.023
H_{swell}	-0.434	0.548	0.188	0.509
v_{ship}	0.440	-0.039	0.734	0.419
T_{swell}	0.389	0.476	-0.579	0.379
$\phi_{incident}$	0.195	0.680	0.280	-0.648

related to one another. Based on the deductions made in Subsection 6.2.1 and the PCA information, there exists relationships between all of the variables that best describe slamming. The results show that there is not any one variable that dominates the causality of slam counts. For this reason it would be of interest to investigate a model that combines the variables to best explain the variance in slam counts specifically.

In order to determine which combination of these variables best explains the slam count a generalised linear model (GLM) was used. A GLM combines multiple independent variables in varying combinations in order to best model a dependent variable. It then selects the best linear combination of these variables by ranking the various variable combination models against one another (Nelder & Wedderburn, 1972). A test for co-linear variables was conducted for the GLM. It was found that there are no significant linear relationships between any of these environmental and operational variables.

The GLM looks at the effect that all the measured variables had on the slam counts. The GLM was done using a Gaussian distribution. The independent variables used were; H_{swell}, v_{ship}, $\phi_{incident}$ and T_{swell}. Fifteen models with various combinations of measured variables were run. A second order Akaike's information criterion (AIC) was used to select the model which best explains the slams counted for the same period of time. This criterion evaluates the relative performance of multiple statistical models. This allows a model to be selected based on its performance against these other models (Konishi & Kitagawa, 1996). A null model was also included to determine if the number of slams were a true reflection of the variables measured.

From the AIC values it is clear that the interaction between all the independent

Stellenbosch University https://scholar.sun.ac.za

Table 6.3: The GLM model of all environmental and operational variables influencing slam counts. Logliks (log likelihood), K (number of parameters), W_i (Akaike weight value), Delta AIC (the model AIC value).

Models	**Logliks**	K	W_i	**Delta AIC**	**AIC**
$H_{swell} + v_{ship} + \phi_{incident} + T_{swell}$	11530	6	0.82	0.00	11542
$H_{swell} + v_{ship} + T_{swell}$	11535	5	0.18	3.05	11545
$v_{ship} + \phi_{incident} + T_{swell}$	11793	5	1.24E-31	141.93	11684
$H_{swell} + T_{swell}$	11684	4	2.40E-33	149.82	11692
$H_{swell} + v_{ship} + \phi_{incident}$	11697	5	1.14E-36	165.14	11707
$H_{swell} + v_{ship}$	11714	4	7.69E-40	179.73	11722
$v_{ship} + T_{swell}$	11794	4	3.60E-57	259.54	11802
$H_{swell} + \phi_{incident} + T_{swell}$	11674	5	2.14E-57	260.59	11803
$H_{swell} + \phi_{incident}$	11841	4	1.62E-67	307.19	11849
H_{swell}	11866	3	1.69E-72	330.13	11872
$v_{ship} + \phi_{incident}$	11942	4	2.04E-89	408.04	11950
v_{ship}	11950	3	1.24E-90	413.64	11956
$\phi_{incident} + T_{swell}$	11959	4	3.93E-93	425.15	11967
T_{swell}	11963	3	1.76E-93	426.75	11969
$\phi_{incident}$	12109	3	2.80E-125	573.19	12115
$nullmodel$	12123	2	8.15E-128	584.87	12127

variables influences the number of slam counts the most (Table 6.3). The second model of best fit explaining the number of slam counts was H_{swell}, v_{ship} and T_{swell}. When the model of best fit is broken down, it is also clear that all the variables besides v_{ship} had a significant effect on slam counts (Table 6.4), significance being a p-value < 0.001. This model has an R^2 value of 0.3, this is not a very good fit for the data. This points to the likelihood that the relationship between slam counts and these variables is not necessarily linear.

Table 6.4: Summary of results of GLM model of best fit influencing slam counts ($H_{swell} + v_{ship} + \phi_{incident} + T_{swell}$)

	Standard error	**t-value**	**p-value**
Intercept	1.479	13.297	<0.001
H_{swell}	0.122	16.849	<0.001
v_{ship}	0.036	-12.247	<0.001
$\phi_{incident}$	0.002	-2.246	0.024
T_{swell}	0.142	-13.224	<0.001

Form these results it is clear that slamming events cannot be explained by one variable. It is better to use all the environmental and operational variables when

Stellenbosch University https://scholar.sun.ac.za

explaining slamming frequency, even then it remains difficult. Certain variables can be influencing slam counts during certain points in time. It is therefore important to look at a specific slamming event under certain conditions to determine the influence of environmental variables on those slamming events.

The discussion of the results above demonstrates that the slamming phenomenon is a complex one. The relationship between variables and the slam counts show that for certain times there is a positive linear relationship, where at other times there is a negative linear relationship for the same variables. This makes the prediction of slamming counts using environmental and operational variables not so simple, and would require more intensive study.

Stellenbosch University https://scholar.sun.ac.za

Chapter 7

Conclusion and future work

The data from this project will form part of the global pool of information gathered on wave slamming and how the SAAII experiences these events dependent on the environmental and operational variables. Conclusions and deductions from the project will help to understand the correlation between sea state information and crew operational patterns with the frequency of slamming events. This research is the starting point in developing more autonomous methods for the detection and counting of slamming events. This could also aid future categorising and quantifying slamming of events as well as the forces and structural responses they induce.

The aims set in the beginning of this project were in order to develop the process of autonomously counting slamming events in full-scale vibration data on the SAAII. The first aim, detection of wave slamming events in full-scale vibration data, needed to answer a few questions: what the characteristics of the slamming signal were, as well as how to best represent them for the detection of an event? These questions were answered by looking into literature for cases where people have characterised a slamming signal. This was based on its local impulsive feature as well as inducing a global response in a structure.

This aim was achieved by using the broad band frequency characteristic of an impulse and statistical thresholding. A higher frequency band (11.5 Hz) of the signal was analysed for sensors along the length of the vessel. This could confirm the propagation of large vibrations through the structure using a threshold as a

Stellenbosch University https://scholar.sun.ac.za

pass criteria. The time intervals with a breach in threshold were then compared across sensors along the length the vessel to answer the global response question. The detection of slams were considered successful given that the algorithm was capable of detecting slams to a degree of 70% certainty.

The second aim, counting slamming events over a period of time and comparing them with environmental and operational variables around the vessel, was achieved by using a binary classifier for each time interval investigated. If all six sensor registered a disturbance at the same time it was considered a slam. These events were summed in order to give a tally of slams experienced over a certain time. The environmental and operational variables were compared with the slam counts in order to determine which combination of variables can best explain the counts. A general linear model then also provided an understanding of the relationships between slamming events and the input variables of the vessel for a given time.

In considering the potential shortcomings of the thesis, the thresholding of the algorithm needs to be discussed. The threshold, as it stands, was determined based on the distribution of the peak values for each interval. For a larger data sets the distribution would tend towards normal (McKillup, 2012), making the motivation of using the MAD irrelevant. In this case the mean and standard deviation would be more applicable. Another method to consider for thresholding would have been a receiver operator curve (ROC). This curve plots TPR against the false positive rate (FPR) for all points in the data set. A threshold point can then be selected based on the highest possible TPR with the lowest possible FPR. As eluded to in the literature review, neural networks could also form part of a future detection algorithm. It would threshold itself during the supervised stage of learning, by adjusting the weights between nodes using the back propagation of errors.

When completing the manual counts of the case studies, a single point in time was chosen to represent a slamming event that typically spans multiple seconds. The algorithm attempted to account for this by using time intervals to describe the data. As was seen in the evaluation of the algorithm, in Section 5.5, the time interval selected does have an influence on the results. For the future of this algorithm the time interval selected must be reconsidered, possibly with an expo-

Stellenbosch University https://scholar.sun.ac.za

nential weighting of time interval values to make the separation between peaks more distinct. This would reduce the number of FPs detected by the algorithm while not influencing the TPs.

The environmental data for this thesis was collected subjectively. The swell height, absolute swell angle and the swell period, were observed by either crew members or SAWS personnel every three to four hours. For future study it would to beneficial to record this information more accurately and at a higher resolution. As discussed in the literature review, a device such as the WaMoS II could achieve this. Seeing the relationships that exist between the environmental and operational variables, future work could incorporate these variables in the detecting of events. This could add to the vibration thresholding in making a decision to detect a slam or not.

The results presented above show that an autonomous algorithm for the detection and counting of slamming events is possible. It also shows that the development of a statistical predictive model is also possible, though highly complex. This would need more study and work as the relationships between the slam counts and input variables are not necessarily linear.

Stellenbosch University https://scholar.sun.ac.za

Appendix A

Sensors used for data collection

A.1 Sensor calibration values

Table A.1: Sensitivity calibration values for typical sensor set-up used during measurements.

Location	**Type**	**Model no.**	**SN**	**Sensitivity** (mV/m/s^2)
Bow, port	DC	3711B1110G	LW6309	20.00
Bow, middle	DC	3711B1110G	LW8390	20.39
Bow, stb	DC	3711B1110G	LW9811	20.36
Chef's cabin	ICP	333B32	38400	10.03
Chef's cabin	ICP	333B32	38401	10.20
Cargo hold, fwd, port	ICP	333B32	49493	9.96
Cargo hold, fwd, stb	ICP	333B32	49495	10.05
Cargo hold, aft, port	DC	3711B1110G	49498	10.25
Cargo hold, aft, stb	DC	3711B1110G	49500	10.31
Fresh water room	ICP	333B32	49501	10.44
Engine store room	ICP	333B32	49502	10.36
Stern truster, port	ICP	333B32	50900	10.43
Stern truster, stb	ICP	333B32	18863	10.72
Steering gear, port	DC	3711B1110G	LW6302	20.25
Sterring gear, stb	DC	3711B1110G	LW6303	20.19
Sterring gear, stb	DC	3711B1110G	LW6304	20.22
Sterring gear, stb	DC	3711B1110G	LW6305	20.13

Stellenbosch University https://scholar.sun.ac.za

A.2 Sensor drift check procedure

Table A.2: Equipment used for sensors drift check.

Equipment:
1 x LMS SCADAS
All sensors to be checked
All signal conditioners to be checked
All coaxial cables ot be checked
LMS Test.Express 13A Measurement software
Laptop computer
SVANTEK SV111 Vibration Calibrator

Procedure for checking sensors for signal drift, in the laboratory before vessel instrumentation took place;

- Connect coaxial cable to SCADAS and sensor to coaxial cable.
- Secure sensor to calibrator's shaker platform.
- Enter sensor's sensitivity into the measurement software.
- Start calibrator vibration (this machine was calibrated to vibrate at a r.m.s. of 1 m/s^2 for 15.92, 79.58, 159.2, 636.6 Hz respectively.)
- A recording from the sensor was then taken over a 10 second time period, the desired result was that the r.m.s. recorded by the sensor over that time was also 1 m/s^2
- These recordings are repeated for all four frequencies the calibrator can achieve.
- An error of 2% was accepted for the 15.92 and 79.58 Hz frequencies, while and error of 5% was accepted for the 159.2 and 636.6 Hz frequencies. The measurement frequency range required for the SAAII was not this high.
- Coaxial cable and sensor combinations that passed this check were used for the measurement.

Stellenbosch University https://scholar.sun.ac.za

- In the case of a failed check, the coaxial cable was replaced and the check was run again. Failing that the sensor would be rejected and not used for the measurement voyage before being recalibrated and checked by a third party.

Stellenbosch University https://scholar.sun.ac.za

Appendix B

Contributing data distributions

B.1 Broad overview plots

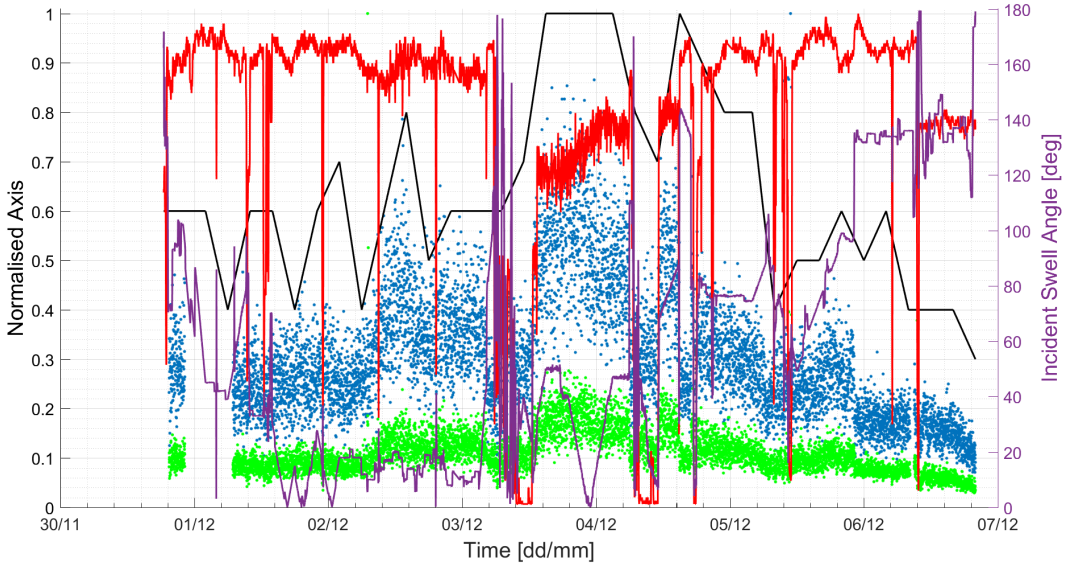

Figure B.1: r.m.s. data spanning the first leg of the Antarctic relief cruise 2016/2017; ● bow r.m.s., ● stern r.m.s., — swell height, — ship speed, — incident swell angle.

Stellenbosch University https://scholar.sun.ac.za

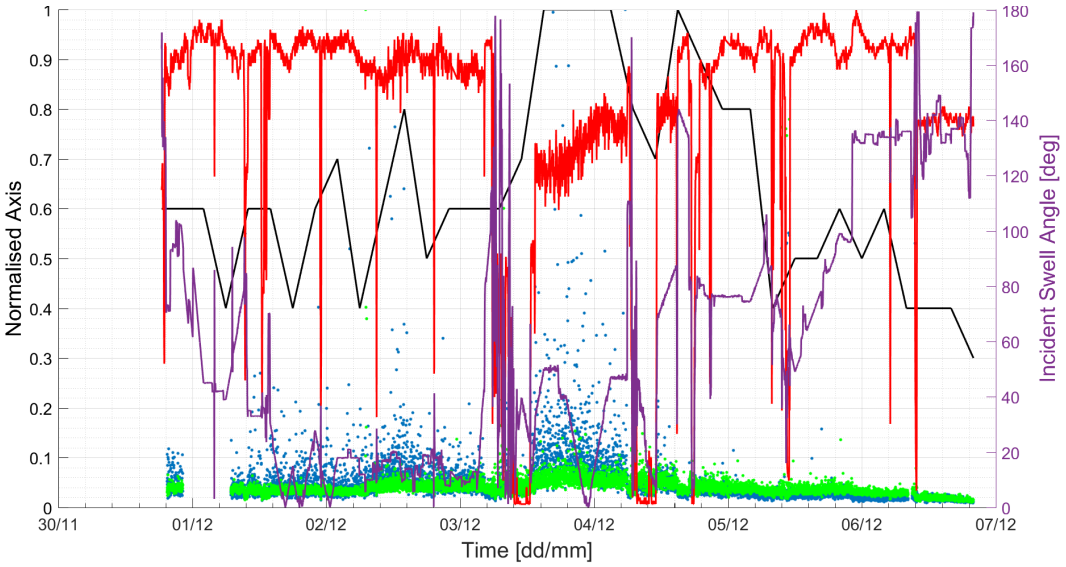

Figure B.2: Absolute peak data spanning the first leg of the Antarctic relief cruise 2016/2017; ● bow peaks, ● stern peaks, — swell height, — ship speed, — incident swell angle.

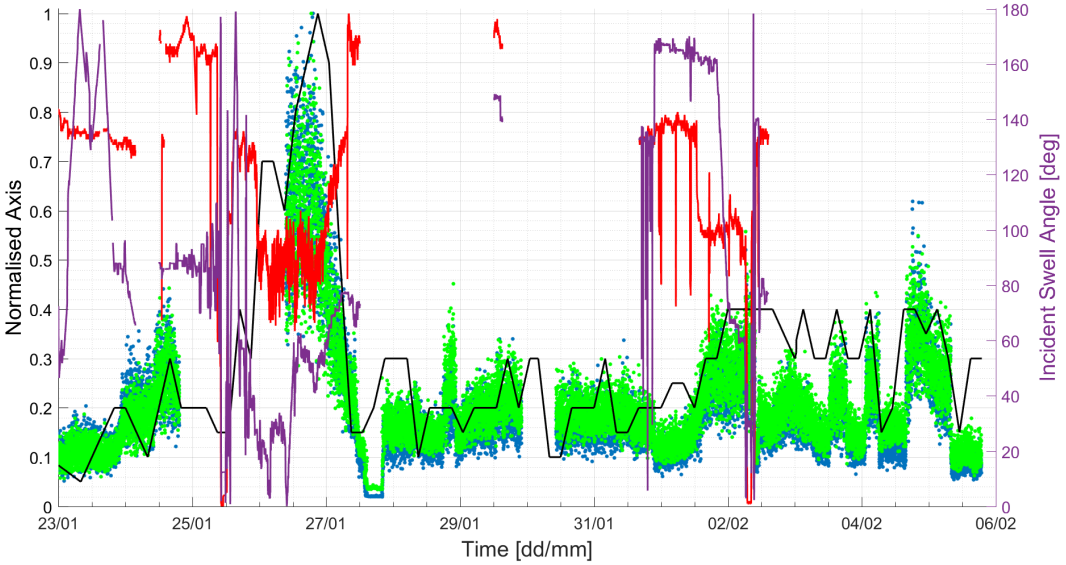

Figure B.3: r.m.s. data spanning the second leg of the Antarctic relief cruise 2016/2017; ● bow r.m.s., ● stern r.m.s., — swell height, — ship speed, — incident swell angle.

Stellenbosch University https://scholar.sun.ac.za

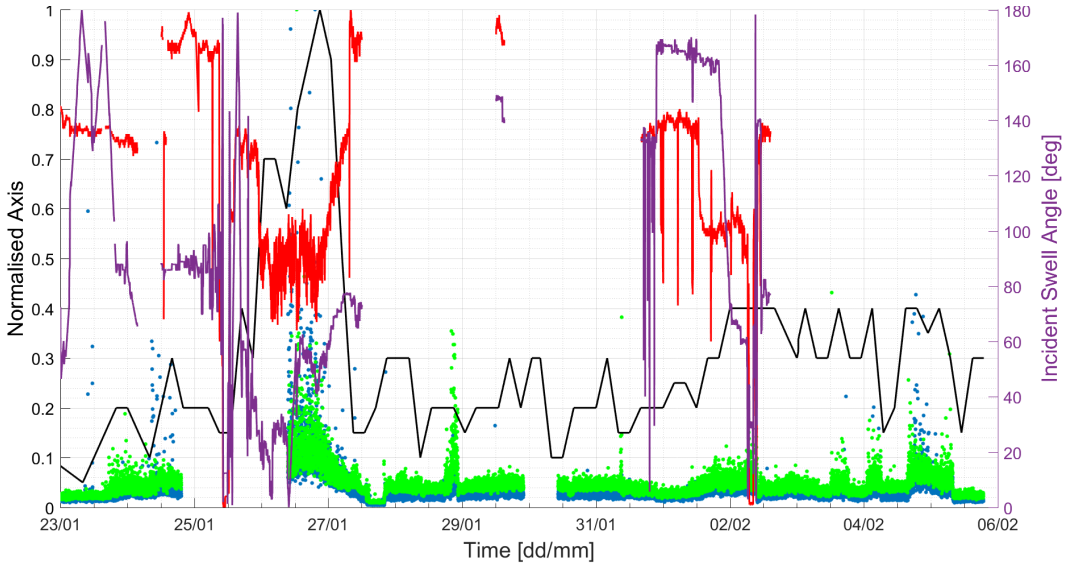

Figure B.4: Absolute peak data spanning the second leg of the Antarctic relief cruise 2016/2017; ● bow peaks, ● stern peaks, — swell height, — ship speed, — incident swell angle.

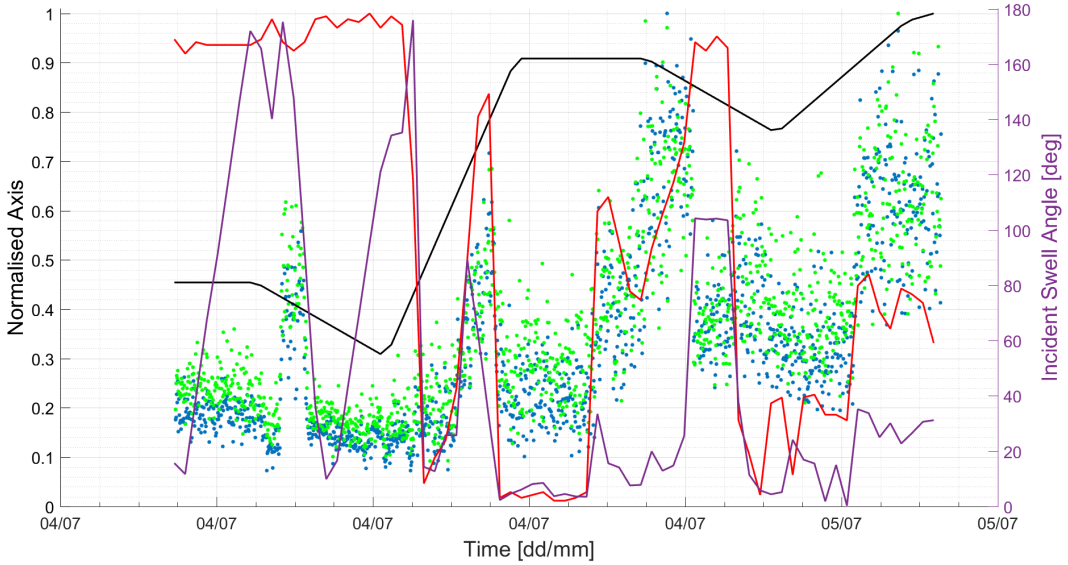

Figure B.5: r.m.s. data spanning the second leg of the Winter cruise 2017; ● bow r.m.s., ● stern r.m.s., — swell height, — ship speed, — incident swell angle.

Stellenbosch University https://scholar.sun.ac.za

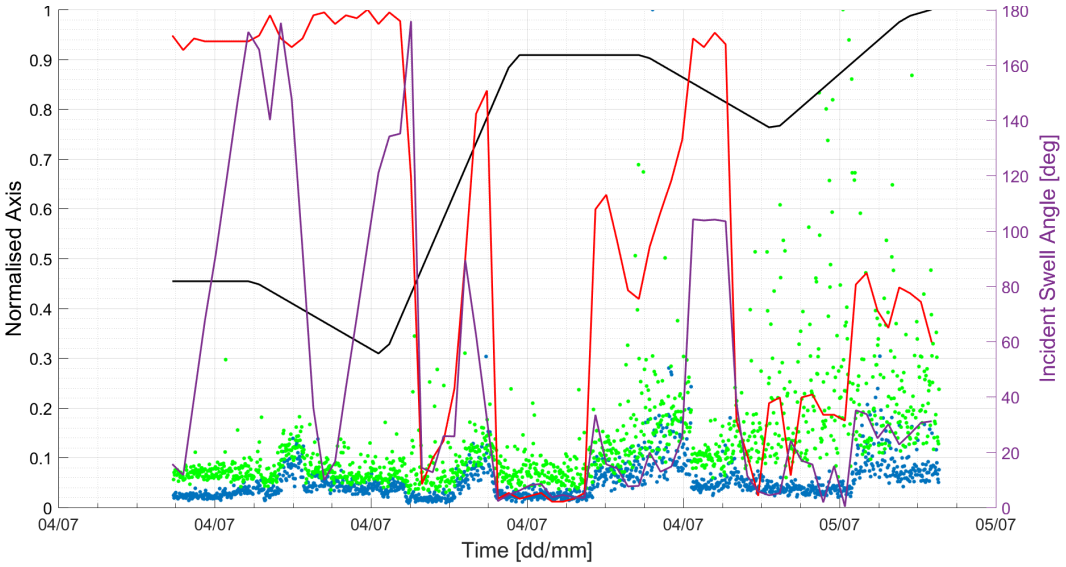

Figure B.6: Absolute peak data spanning the second leg of the Winter cruise 2017; ● bow r.m.s., ● stern r.m.s., — swell height, — ship speed, — incident swell angle.

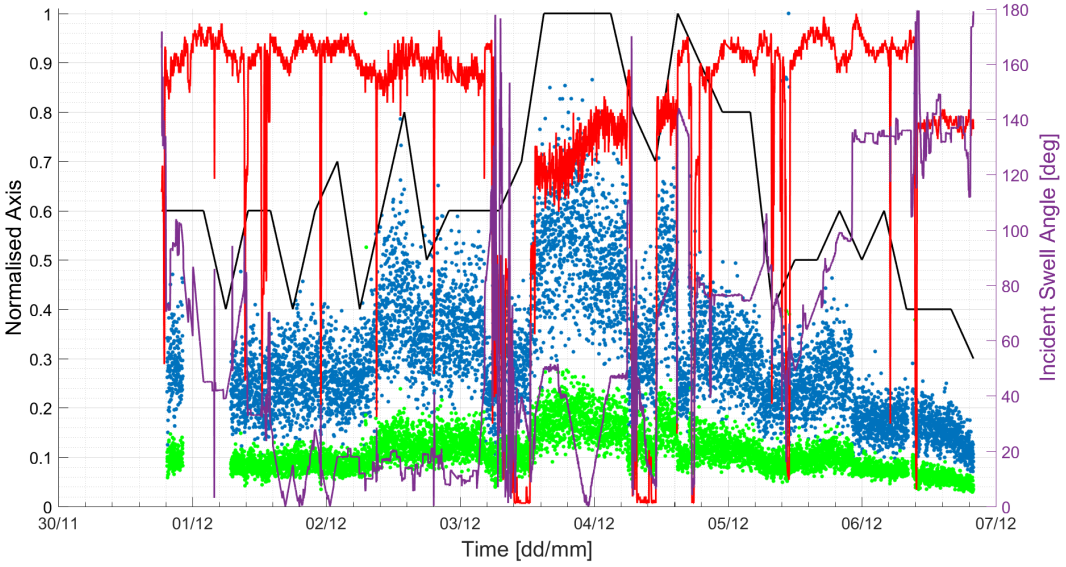

Figure B.7: r.m.s. data spanning the third leg of the Winter cruise 2017; ● bow r.m.s., ● stern r.m.s., — swell height, — ship speed, — incident swell angle.

Stellenbosch University https://scholar.sun.ac.za

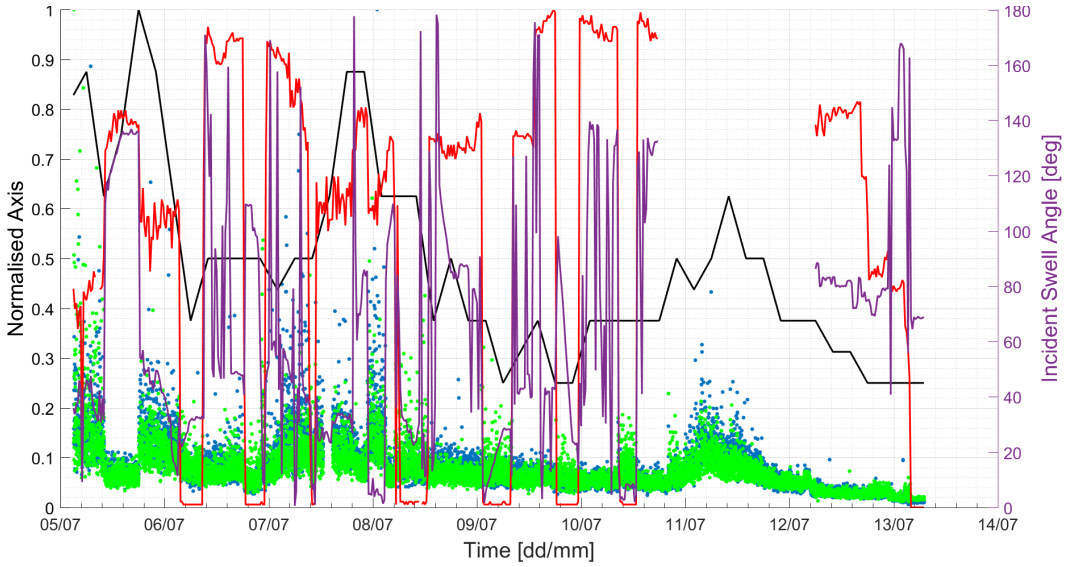

Figure B.8: Absolute peak data spanning the first leg of the Winter cruise 2017; ● bow r.m.s., ● stern r.m.s., — swell height, — ship speed, — incident swell angle.

B.2 Data distributions

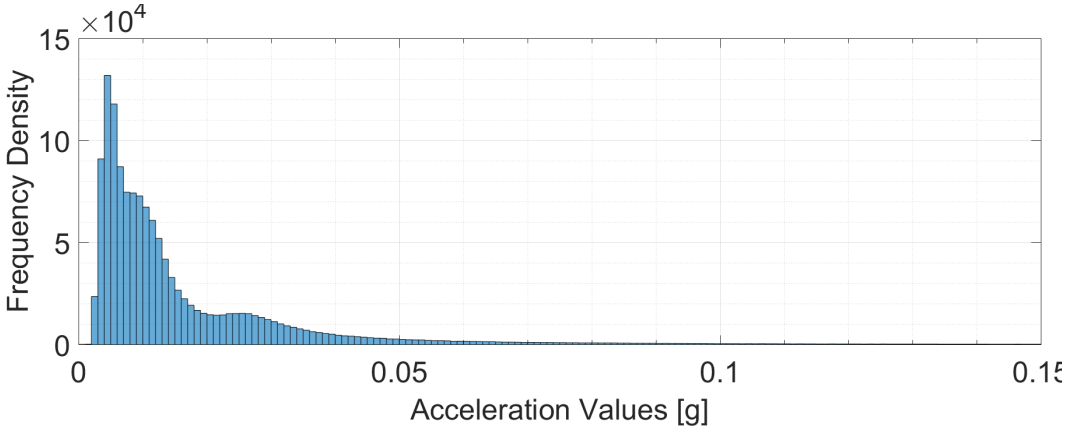

Figure B.9: Histogram of forward cargo hold time domain peak values across two voyages.

Stellenbosch University https://scholar.sun.ac.za

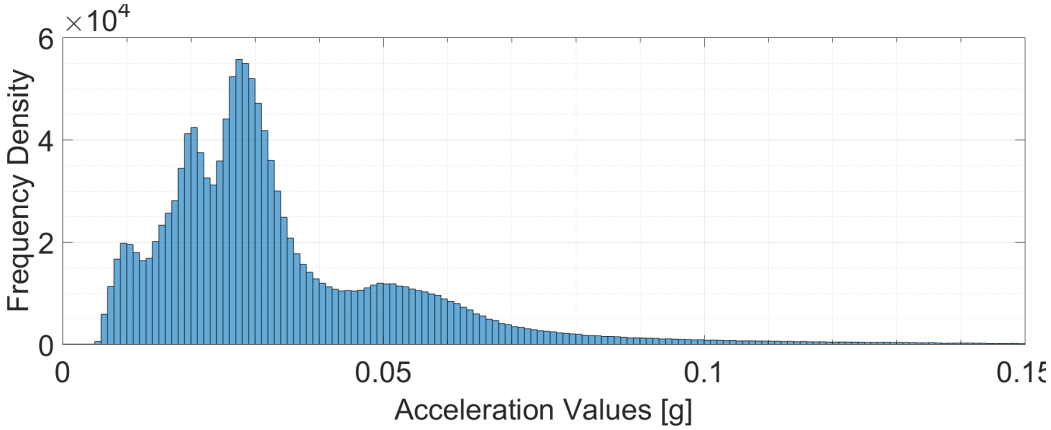

Figure B.10: Histogram of aft cargo hold time domain peak values across two voyages.

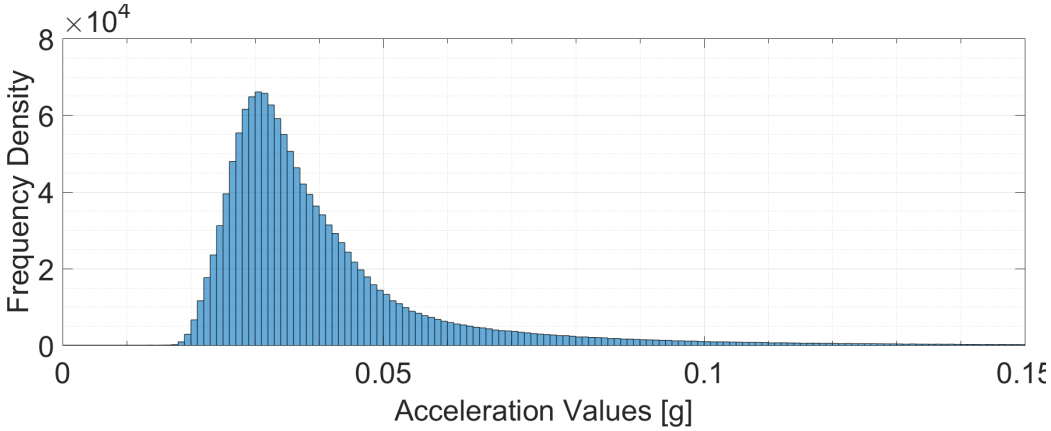

Figure B.11: Histogram of engine store room time domain peak values across two voyages.

Stellenbosch University https://scholar.sun.ac.za

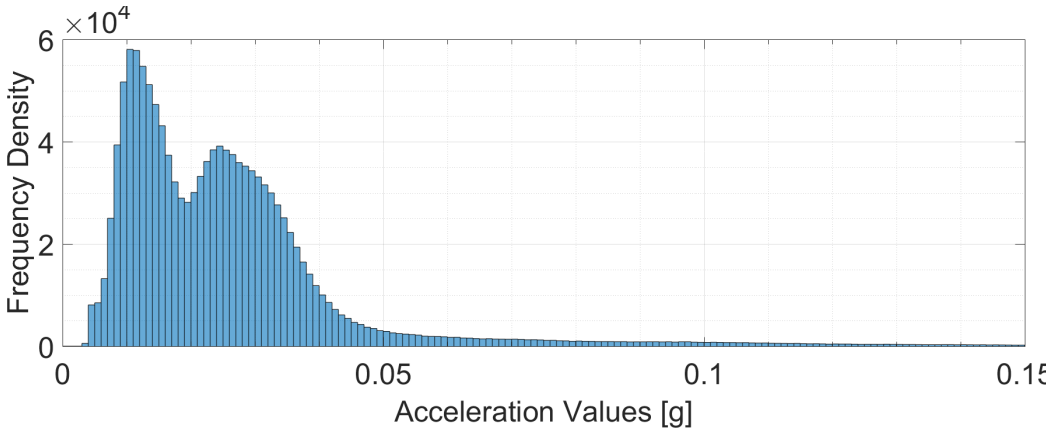

Figure B.12: Histogram of stern thruster room time domain peak values across two voyages.

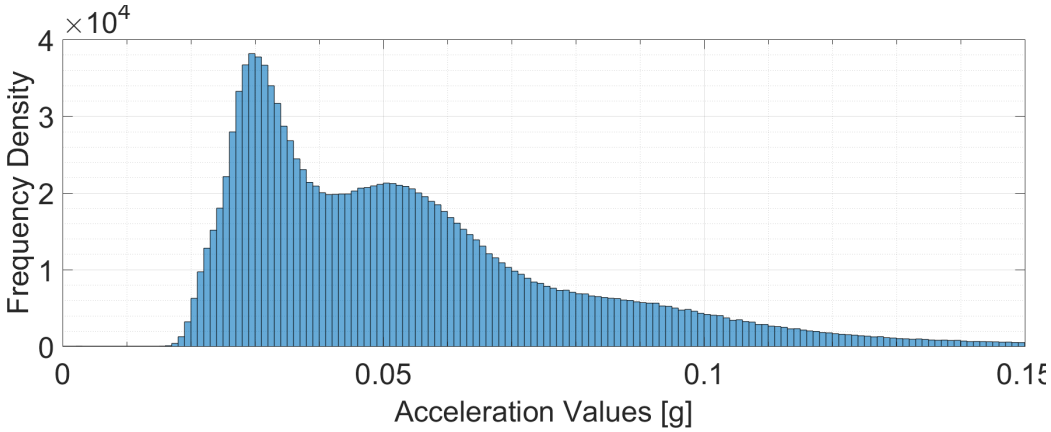

Figure B.13: Histogram of steering gear room time domain peak values across two voyages.

Stellenbosch University https://scholar.sun.ac.za

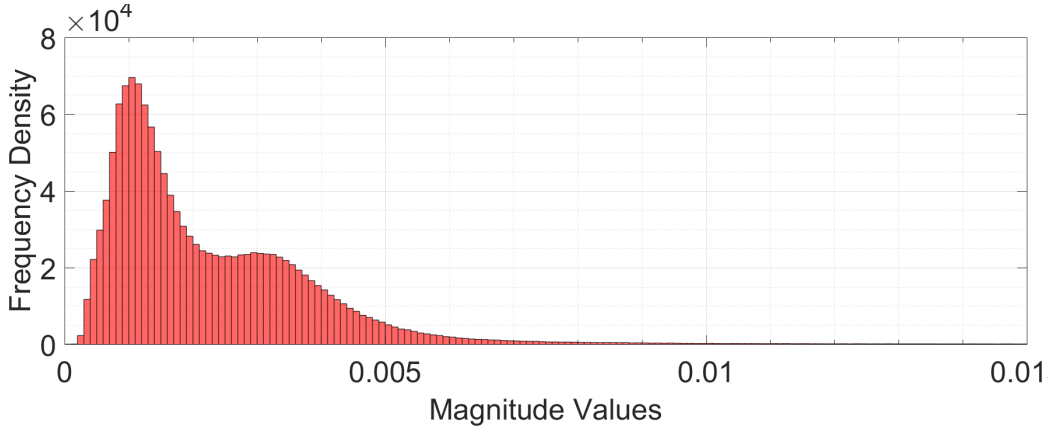

Figure B.14: Histogram of forward cargo hold frequency domain peak values across two voyages.

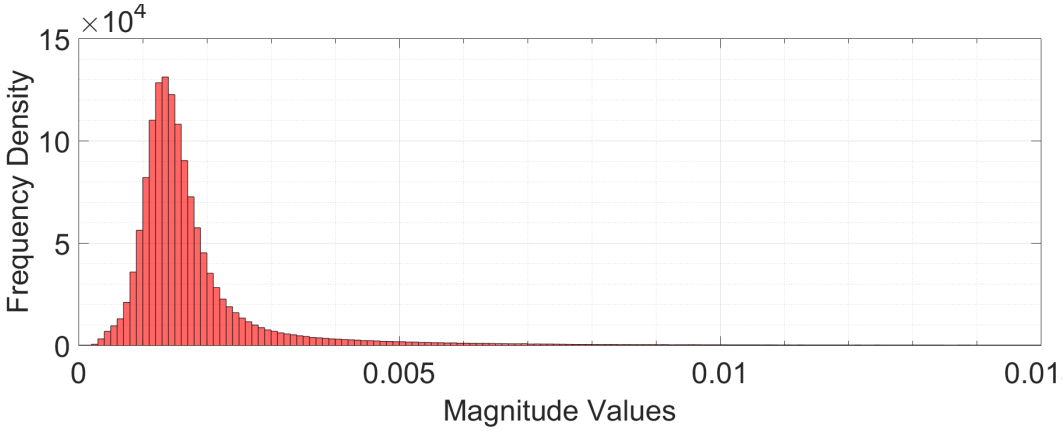

Figure B.15: Histogram of aft cargo hold frequency domain peak values across two voyages.

Stellenbosch University https://scholar.sun.ac.za

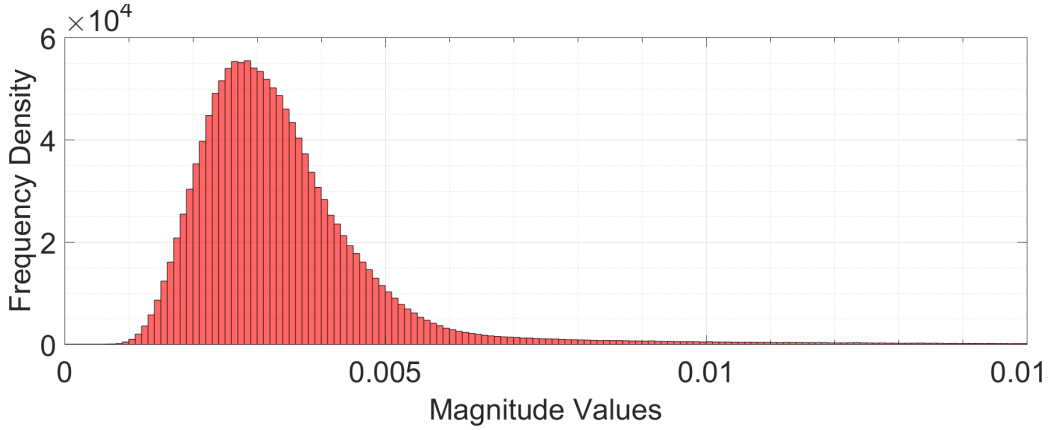

Figure B.16: Histogram of engine store room frequency domain peak values across two voyages.

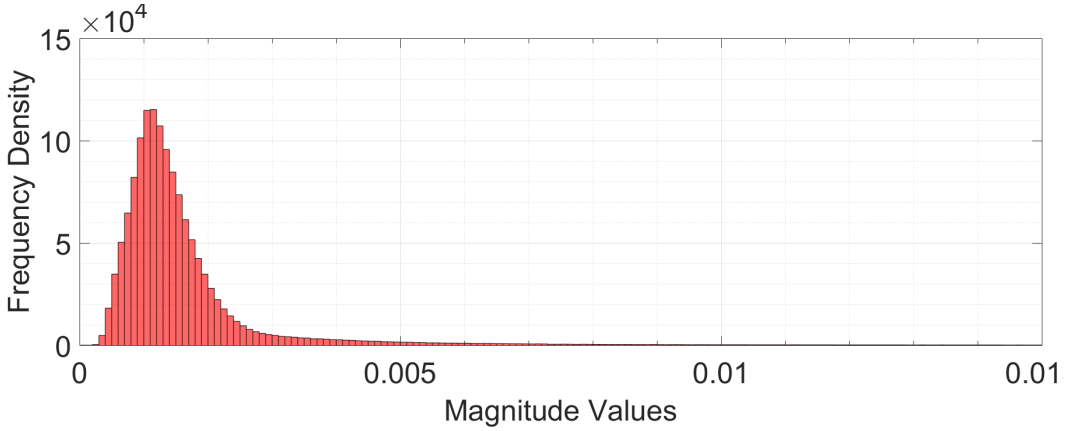

Figure B.17: Histogram of stern thruster room frequency domain peak values across two voyages.

Stellenbosch University https://scholar.sun.ac.za

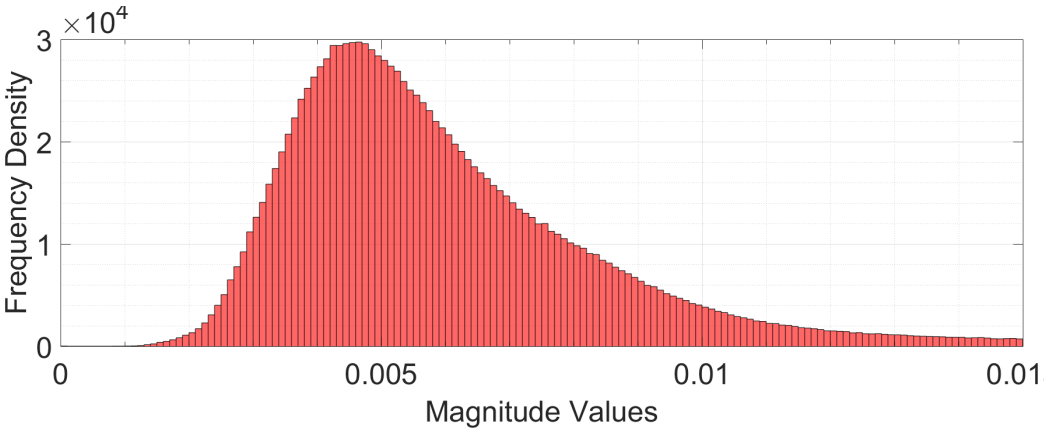

Figure B.18: Histogram of steering gear room frequency domain peak values across two voyages.

Stellenbosch University https://scholar.sun.ac.za

Appendix C

Case studies

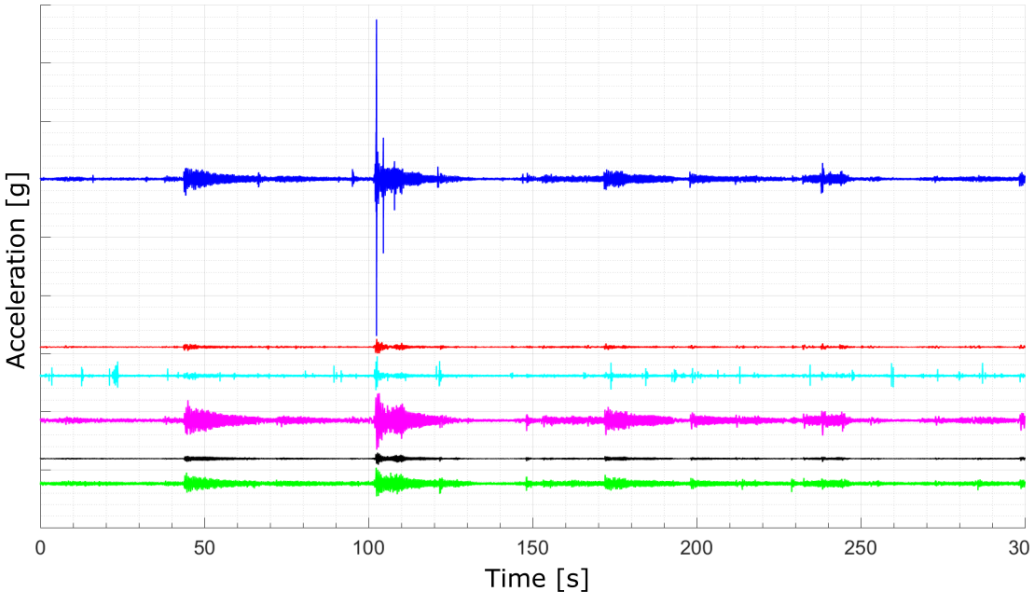

Figure C.1: Filtered case study 1 from 26/01/2017; bow cargo hold fwd cargo hold aft fresh water room stern thruster room stern.

Stellenbosch University https://scholar.sun.ac.za

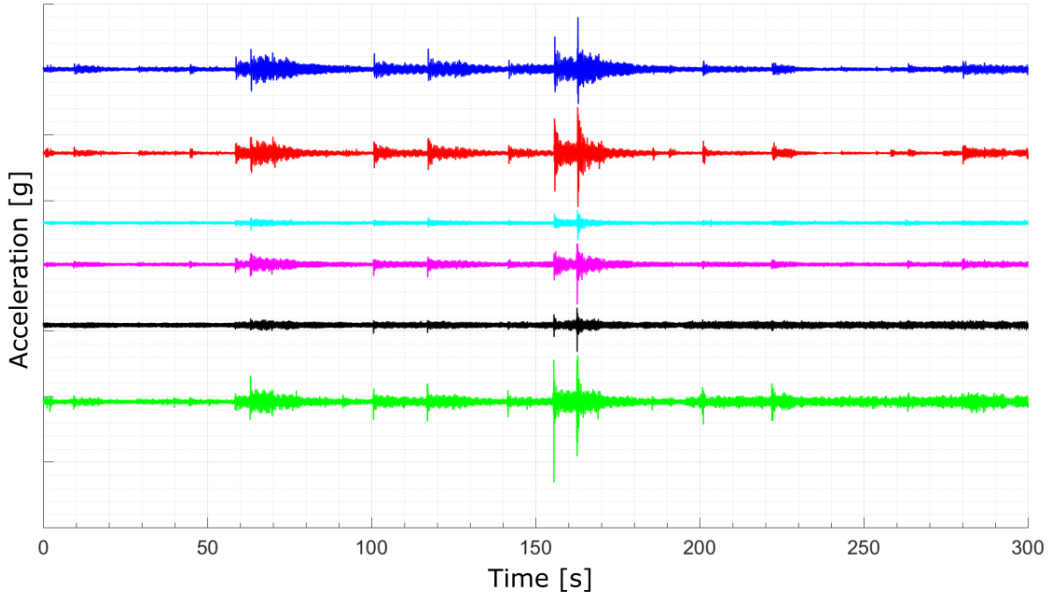

Figure C.2: Filtered case study 2 from 28/01/2017; bow cargo hold fwd cargo hold aft fresh water room stern thruster room stern.

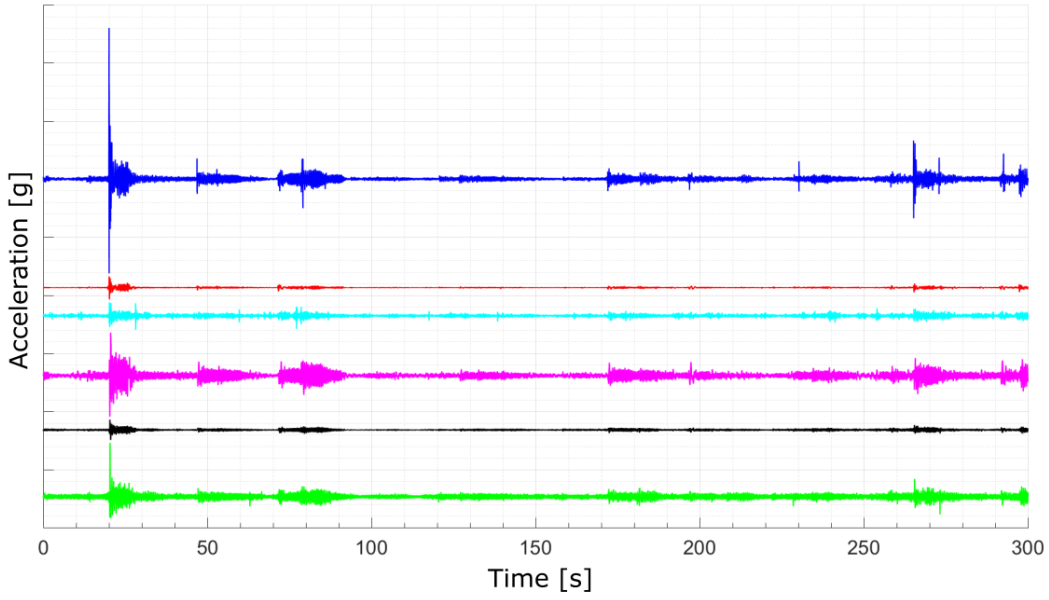

Figure C.3: Filtered case study 4 from 02/07/2017; bow cargo hold fwd cargo hold aft fresh water room stern thruster room stern.

Stellenbosch University https://scholar.sun.ac.za

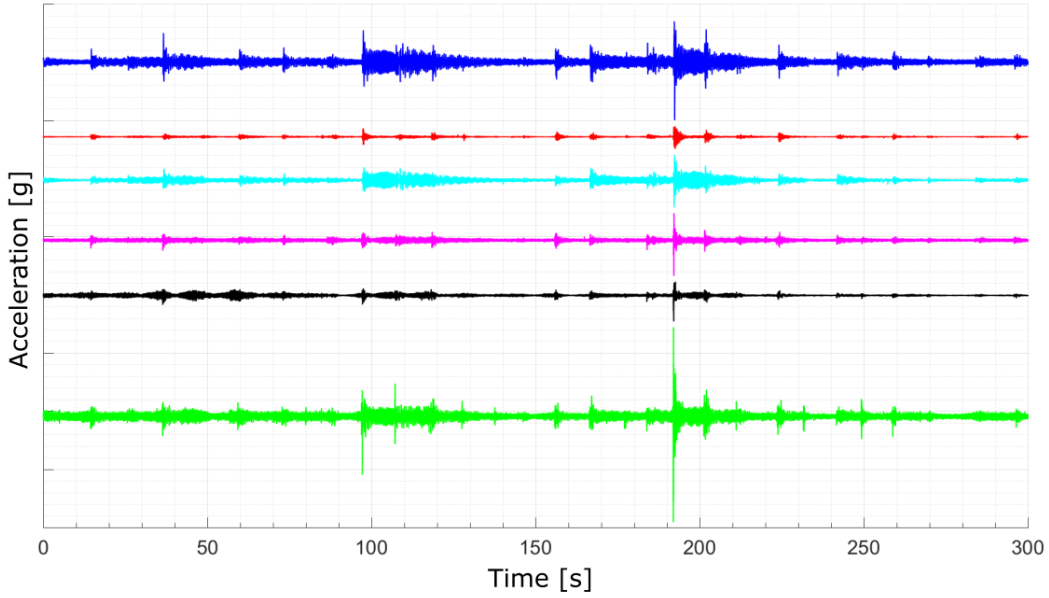

Figure C.4: Filtered case study 4 from 28/06/2017; bow cargo hold fwd cargo hold aft fresh water room stern thruster room stern.

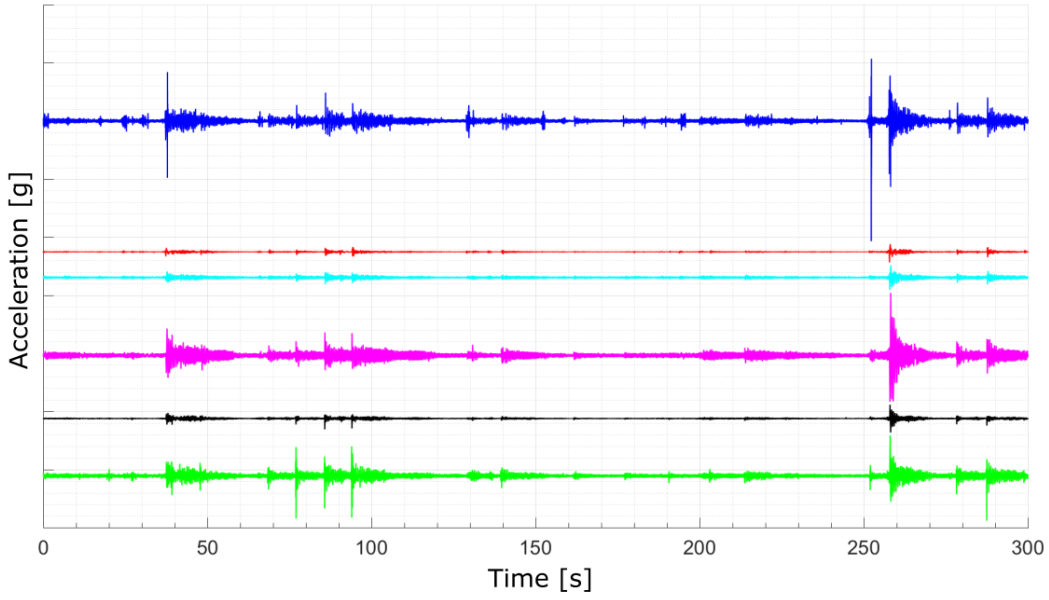

Figure C.5: Filtered case study 5 from 05/07/2017; bow cargo hold fwd cargo hold aft fresh water room stern thruster room stern.

Stellenbosch University https://scholar.sun.ac.za

Appendix D

Winter cruise voyage

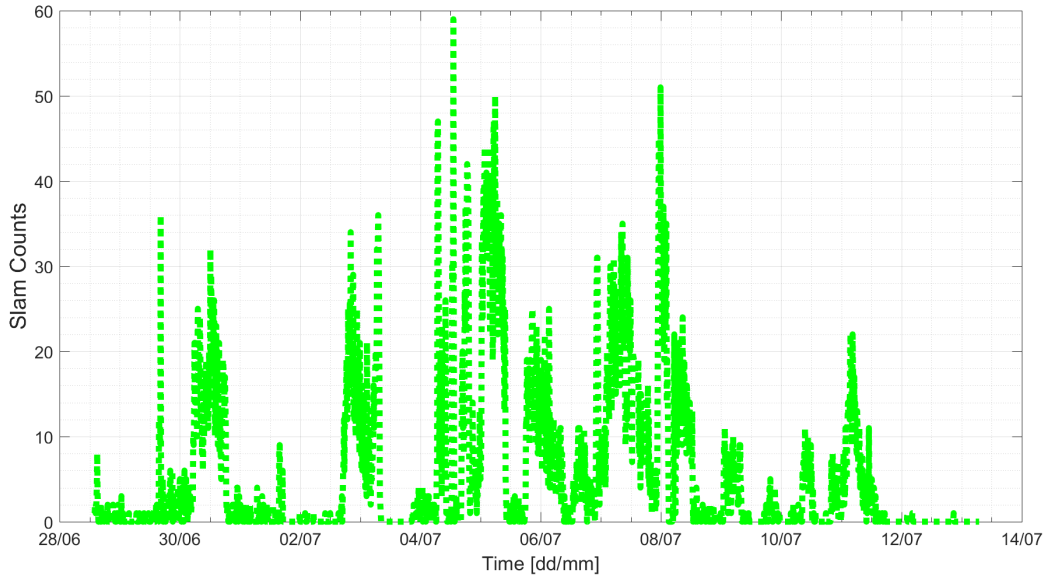

Figure D.1: Result of slamming count over the full Winter cruise 2017 voyage.

Stellenbosch University https://scholar.sun.ac.za

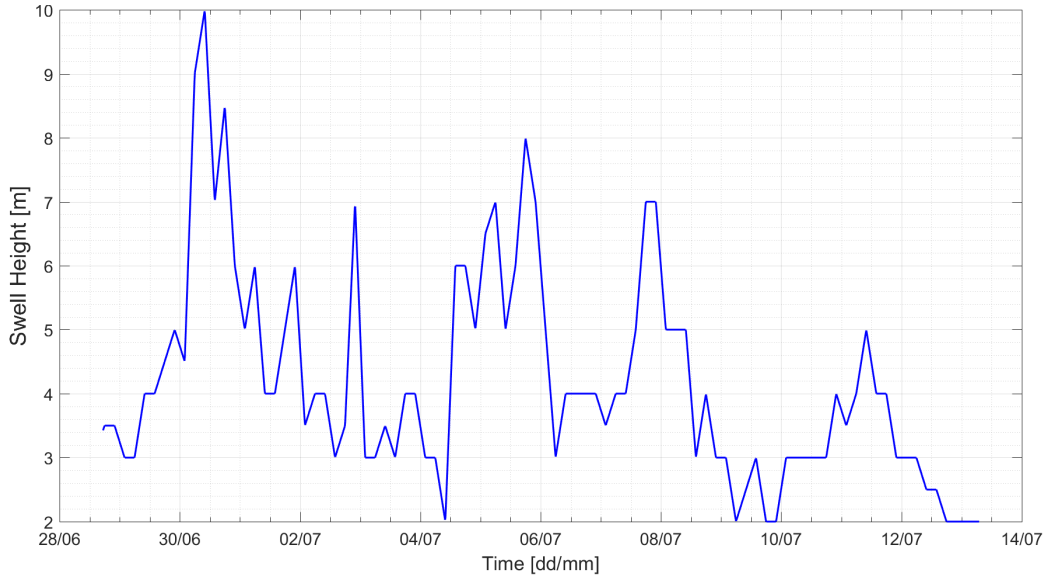

Figure D.2: Swell heights over the full Winter cruise 2017 voyage.

Figure D.3: Ship speeds over the full Winter cruise 2017 voyage.

Stellenbosch University https://scholar.sun.ac.za

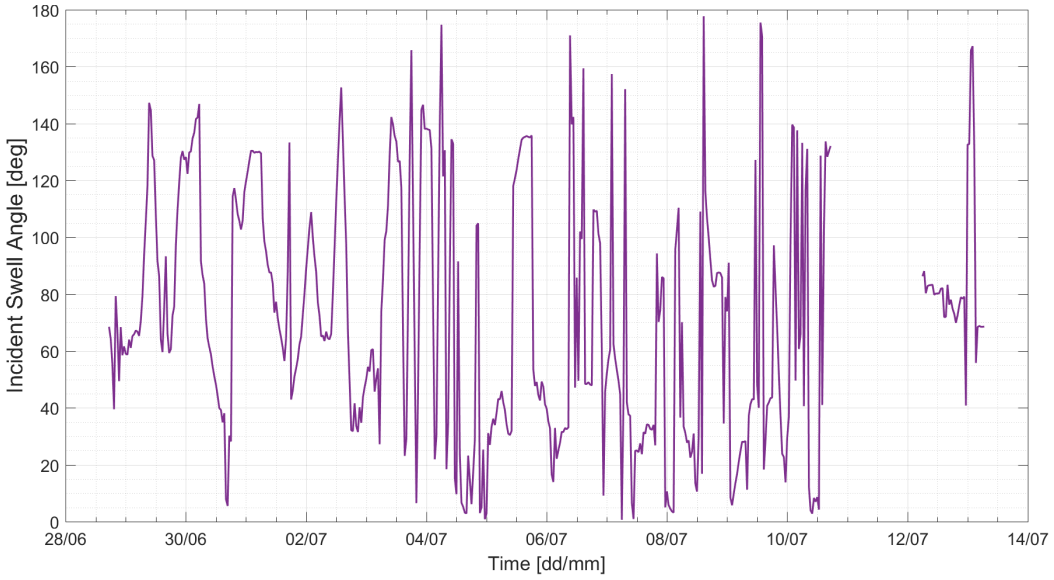

Figure D.4: Incident swell angles over the full Winter cruise 2017 voyage.

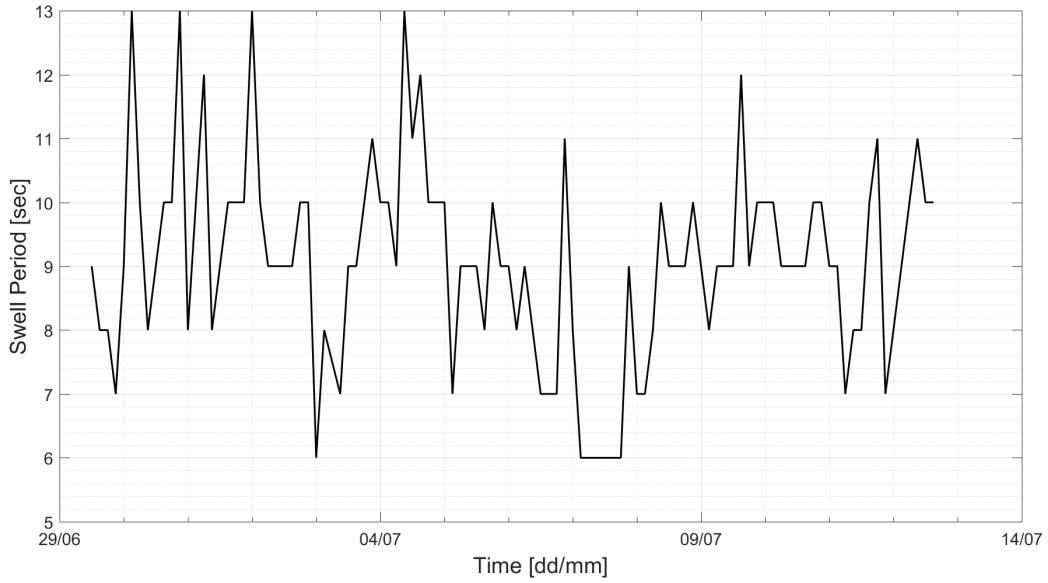

Figure D.5: Swell periods over the full Winter cruise 2017 voyage.

Stellenbosch University https://scholar.sun.ac.za

List of References

Aalberts, P.J. and Nieuwenhuijs, M.W. (2006). Full scale wave and whipping induced hull girder loads. In: *Proceedings of the 4th International Conference on Hydroelasticity in Marine Technology*. 10-14 September, Wuxi.

Aertssen, G. (1968). Laboring of ship in rough seas with special emphasis on the fast ship. In: *Proceedings of the SNAME Diamond Jubilee International Meeting*, pp. 10.1–10.16. New York NY.

Barnett, V. and Lewis, T. (1994). *Outliers in Statistical Data, Wiley Series in Probability and Mathematical Statistics: Applied Probability and Statistics*. Wiley and Sons.

Battjes, J. and Groenendijk, H. (2000). Wave height distributions on shallow foreshores. *Coastal Engineering*, vol. 40, pp. 161–182.

Bledsoe, M., Bussemaker, O. and Cummins, W. (1961). Seakeeping trails on three dutch destroyers. In: *Proceedings of the SNAME Spring Meeting*. 26-28 May, Washington DC.

Brandt, A. (2011). *Noise and Vibration Analysis: Signal Analysis and Experimental Procedures*. Wiley and Sons.

Brown, G.S. (1977). The average impulse response of a rough surface and its applications. *IEEE Transactions on Antennas and Propagation*, vol. 25, no. 1, pp. 67–74.

Carrasco, R., Streßer, M. and Horstmann, J. (2017). A simple method for retrieving significant wave height from dopplerized x-band radar. *Ocean Science*, vol. 13, pp. 95–103.

Stellenbosch University https://scholar.sun.ac.za

Dessi, D. (2014). Whipping-based criterion for the identification of slamming events. *International Journal of Naval Architecture and Ocean Engineering*, vol. 6, pp. 1082–1095.

Dessi, D. and Ciappi, E. (2013). Slamming clustering on fast ships: From impact dynamics to global response analysis. *Ocean Engineering*, vol. 62, pp. 110–122.

Det Norske Veritas (2017). S.a. agulhas ii dnv gl vessel register [online]. *Available: http://vesselregister.dnvgl.com/VesselRegister/vesseldetails.html?vesselid=30528 [2017, May 17]*.

Faltinsen, O. (1996). Slamming. In: *Proceedings of the Colloquium for Ship and Offshore Hydrodynamics in Advances in ship and offshore hyrodynamics*. Institut fur Schiffbau der Universitat Hamberg, Germany.

Haward, B.M., Lewis, C.H. and Griffin, M.J. (2009). Motions and crew responses on an offshore oil production and storage vessel. *Applied Ergonomics*, vol. 40, no. 5, pp. 904–914.

Haykin, S. (1994). *Neural Networks. A Comprehensive Foundation*. New York, Macmillan College Publishing Company.

Huber, P. (1981). *Robust Statistics*. New York: John Wiley.

Kapsenberg, G.K. (2011). Slamming of ships: where are we now? *Philosophical Transactions: Mathematical, Physical, and Engineering Sciences*, vol. 369, pp. 2892–2919.

Karn, U. (2016). A quick introduction to neural networks [online]. *Available: https://ujjwalkarn.me/2016/08/09/quick-intro-neural-networks/ [2017, March 5]*.

Konishi, S. and Kitagawa, G. (1996). Generalized information criteria in model selection. *Biometrika*, vol. 83, pp. 875–890.

Krogstad, H., Barstow, S., Haug, O., Marknussen, P., Ueland, G. and Rodriguez, I. (1998). Smart-800: Remotely sensed wave spectra from a moored buoy. *Proceed. Oceanology 98*.

Leys, C., Ley, C., Klein, O., Bernard, P. and Licata, L. (2013). Detecting outliers: Do

Stellenbosch University https://scholar.sun.ac.za

not use standard deviation around the mean, use absolute deviation around the median. *Journal of Experimental Social Psychology*, vol. 49, pp. 764–766.

Lloyd, A. and Andrew, R. (1977). Criteria for ship speed in rough weather. In: *Proceedings of the 18th American Towing Tank Conference*. 23-25 August, Annapolis MD: Naval Academy.

M.A.I.B (2008). Report on the investigation of the structural failure of msc napoli, english channel on 18 january 2007. Tech. Rep., Marine Accident Investigation Branch.

Mantri, H. (2013). How do you explain back propagation algorithm to a beginner in neural network? [online]. *Available: https://www.quora.com/How-do-you-explain-back-propagation-algorithm-to-a-beginner-in-neural-network/answer/Hemanth-Kumar-Mantri [2017, March 5]*.

McKillup, S. (2012). *Statistics Explained: An Introductory Guide for Life Scientists*. Cambridge University Press.

MIROS (2009). Wave monitoring [online]. *Available: http://www.miros.no/products/wave-monitoring/ [2017, February 16]*.

Natural Earth (2018). Vector and raster map data [online]. *Available: https://www.naturalearthdata.com/downloads/ [2018, July 20]*.

Nelder, J.A. and Wedderburn, R.W.M. (1972). Generalized linear models. *Journal of the Royal Statistical Society.*, vol. 135, pp. 370–384.

Nieto-Borge, C., Reichert, K. and Dittmer, J. (1999). Use of nautical radar as a wave monitoring instrument. *Coastal Engineering*, vol. 37, pp. 331–342.

OceanWaveS (2006). Wamos ii wave monitoring system operating manual and installation guide. *OceanWaveS GmbH, Germany*.

O.C.I.M.F. (2014). Offshore vessel operations in ice and/or severe sub-zero temperatures. Tech. Rep., Oil Companies International Marine Forum.

Omenzetter, P., Brownjohn, J.M.W. and Moyo, P. (2003). Identification of unusual events in multi-channel bridge monitoring data. *Mechanical Systems and Signal Processing*, vol. 18, pp. 409–430.

Stellenbosch University https://scholar.sun.ac.za

Omer, H. (2016). *The Impact of Wave Slamming Vibration on Human Factor and Equipment on the S . A . Agulhas II Polar Supply and Research Vessel.* Masters Thesis. Stellenbosch: Stellenbosch University.

Pimentel, M.A.F., Clifton, D.A., Clifton, L. and Tarassenko, L. (2014). A review of novelty detection. *Signal Processing*, vol. 99, pp. 215–249.

Polar Class (2011). *Requirements concerning Polar Class*, vol. 2011. International Association of Classification Societies (IACS).

Reichert, K., Hessner, K., Nieto-Borge, J.C. and Dittmer, J. (1999). Wamos ii : A radar based wave and current monitoring system. In: *Proceedings of the ISOPE'99*, vol. 3. May, Brest.

Rufenach, C.L. and Alpers, W.R. (1978). Measurement of ocean wave heights using the geos 3 altimeter. *Journal of Geophysical Research Atmospheres*, vol. 83, no. 10, pp. 5011–5018.

Scharroo, R., Bonekamp, H., Ponsard, C., Parisot, F., Von Engeln, A., Tahtadjiev, M., De Vriendt, K. and Montagner, F. (2016). Jason continuity of services: Continuing the jason altimeter data records as copernicus sentinel-6. *Ocean Science*, vol. 12, no. 2, pp. 471–479.

Soal, K. (2014). *Vibration response of the polar supply and research vessel the S.A. Agulhas II in Antarctica and the Southern Ocean.* Masters Thesis. Stellenbosch: Stellenbosch University.

Suominen, M., Karhunen, J., Bekker, A., Kujala, P., Elo, M., von Bock und Polach, R., Enlund, H. and Saarinen, S. (2013). Full-scale measurements on board psrv s.a. agulhas ii in the baltic sea. In: *Proceedings of the 22nd International Conference on Port and Ocean Engineering under Arctic Conditions*. 9-13 June, Espoo.

Suominen, M. and Kujala, P. (2014). Variation in short-term ice-induced load amplitudes on a ship's hull and related probability distributions. *Cold Regions Science and Technology*, vol. 106, pp. 131–140.

Thornhill, E.M. and Stredulinksky, D.C. (2010). Real time local sea state measurements using wave radar and ship motions. *SNAME annual meeting*, vol. 118, pp. 248–268.

Stellenbosch University https://scholar.sun.ac.za

Tuitman, J. (2010). *Hydro-elastic response of ship structures to slamming induced whipping*. Ph.D. thesis, Delft: Delft University of Technology.

von Karman, T. (1929). The impact on seaplane floats during landing. Tech. Rep., NACA Technical Note No.321.

Warnsinck, W. and Saint Denis, M. (1957). Dutch destoryer trials. In: *Proceedings of Symposium on the Behaviour of Ships in a Seaway*. 7-10 September, Wageningen.

Wheaton, J., Kano, C., Diamant, P. and Bailey, F. (1970). Analysis of slamming data from the ss wolverine state. ship structure committee report. Tech. Rep., US Coast Guard Headquarters.

Worden, K., Manson, G. and Allman, D. (2003). Experimental validation of a structural health monitoring methodology: Part ii. novelty detection on a gnat aircraft. *Journal of Sound and Vibration*, vol. 259, no. 2, pp. 323–343.

Worden, K., Manson, G. and Fieller, N. (2000). Damage detection using outlier analysis. *Journal of Sound and Vibration*, vol. 229, no. 3, pp. 647–667.

Yang, W. and Ren, X. (2004). Detecting impulses in mechanical signals by wavelets. *Eurasip Journal on Applied Signal Processing*, vol. 8, pp. 1156–1162.

Young, I., Rosenthal, W. and Ziemer, F. (1985). A three-dimensional analysis of marine radar images for the determination of ocean wave directionality and surface currents. *Journal of Geophysical Research Atmospheres*, vol. 90, pp. 1049–1059.